COLLECTIVE BEHAVIOR AND TASK PERSISTIFICATION IN LAZY AND MINIMALIST COLLECTIVES

A Dissertation
Presented to
The Academic Faculty

By

Bahnisikha Dutta

In Partial Fulfillment
of the Requirements for the Degree
Doctor of Philosophy in the
School of Electrical and Computer Engineering

Georgia Institute of Technology

May 2021

COLLECTIVE BEHAVIOR AND TASK PERSISTIFICATION IN LAZY AND MINIMALIST COLLECTIVES

Thesis Committee:

Dr. Dana Randall, Advisor
School of Computer Science
Georgia Institute of Technology

Dr. Magnus Egerstedt, Co-advisor
School of Electrical and Computer Engineering
Georgia Institute of Technology

Dr. Seth Hutchinson
School of Interactive Computing
Georgia Institute of Technology

Dr. Ayanna Howard
School of Electrical and Computer Engineering
Georgia Institute of Technology

Dr Matthieu Bloch
School of Electrical and Computer Engineering
Georgia Institute of Technology

Dr. Andrea Richa
School of Computing, Informatics, and Decision systems Engineering
Arizona State University

Date Approved: April 28, 2021

”At the heart of science is an essential balance between two seemingly contradictory attitudes an openness to new ideas, no matter how bizarre or counterintuitive they may be, and the most ruthless skeptical scrutiny of all ideas, old and new. This is how deep truths are winnowed from deep nonsense.”

Carl Sagan

To Mom, Dad, Bobo, and Ghonge.

ACKNOWLEDGEMENTS

There is a saying in Sanskrit “Karmanye Vadhikaraste, Ma phaleshou kada chana” which painly put means “Perform your duty diligently but do not have any expectation of the fruits and don’t give up on your job”. This saying was very inconsequential and meant very little to me when I first learnt about this, but the past 7 years was a true testament of how meaningful this statement is. I have had a rather unconventional PhD trajectory and I would like to first acknowledge the unwavering love and support of my parents for 7 long years where I had left my home saying I would be back in 2 years with a Master’s degree. The last few years of my PhD was extremely challenging given that we had a full blown pandemic and my father was taken seriously ill. My partner stood by me as a pillar during these trying times and hold my pieces together as I kept marching towards finishing this thesis. If there is a man behind every woman’s success, he is mine. Except for being each others emotional support, we also have had numerous scientific and technological debates and discussions and I have learnt a great deal from him. Next, I would like to thank my advisor Dr Dana Randall and my co-advisor Dr Magnus Egerstedt for taking me under their tutelage and supporting me in every possible way. I appreciate all the honest and frank feedback that I have received from Dr Egerstedt and I am grateful to Dr Randall for her unwavering support during some tumultuous times. I was an unconventional student for them as the intersection of our ideas and expertise was interesting but minimal. I would also like to thank my committee members Dr Seth Hutchinson, Dr Ayanna Howard, Dr Mathieu Blocch and Dr Andrea Richa for agreeing to be on my committee and meeting with all the administrative requirements, on very short notices most of the time. I would like to acknowledge the useful feedback I received from them during my proposal and defense presentation. All their advise made a huge impact on me and helped me get my ideas more focused and greatly improved my contributions towards this thesis and would definitely help me with my future endeavors. During my stay at Georgia Tech, I had the pleasure

of working with Dr Daniel Goldman during my Master's degree in Bioengineering and I would extend my gratitude to him for letting me work with amazing peers and providing an excellent learning environment. I would like to thank all of my past and present lab members especially Enes Aydin, Yasemin Aydin, Jennifer Rieser, Feifei Qian, Christain Hubicki, Vadim Linevich, JSP, Jeff Aguilar, Will Savoie, Daria Monaenkova, and Veronica Paez.

My thesis heavily depends on high throughput computation and analysis. I am forever grateful to the Open Science Grid (OSG) initiative which is making computational resources easily accessible to all researchers across United States at no cost. In the era of open source that we live in, such initiatives really help break barriers caused by monetary and infrastructural limitations. I am extremely grateful to my partner, Sudarshan Ghonge for introducing me to the Open Science Grid (OSG) and giving me a headstart in learning how to use the resources. I acknowledge Carrie Brown for helping me set up my OSG account and aiding me whenever I faced any technical issues. A huge shoutout to Tim Cartwright who was my OSG school mentor. Tim is a wonderful mentor and he followed up with me regularly to get updates on how I was using the cluster and if I needed any extra facilities to help me with my research demands. He provided all the necessary resources to me to finish up my summer school project which later helped me reduce the runtimes of my research simulations even further.

Finally, I am forever grateful to all the wonderful friends I made during my stay here in Atlanta who were always present to pick me up during my worst and to pick on me when I was at my best. It wont be fair to name a few of them but I can't help but mention the remarkable companionship I received from Hemaa selvakumar, Rohini Mopuri, Mayank Agrawal, Bhavesh Khamesra, Shanshank Markande and all the members of ASHA-GT. Thanks to Alvin Lee for introducing me to some pretty amazing board games, Louis for the bizzarest gifts, Anish Mukherjee for being the only known face in the United States when we set foot here, Anthony for being my first guy housemate, taking me to the gym

for the first time and playing carrom with me almost regularly. My life here at Tech would not have been remotely as enjoyable without you guys. Being actively involved with the philanthropic events of ASHA- GT (a student organization that fundraises for the education of underprivileged women and children of India) taught me life lessons that no literary document could have taught me. My site visit to a remote village in India as an ASHA volunteer still remains one of the most cherished moments of my past 5 years. The real value of education is felt only when you can impart some where it is needed the most and watching those kids learn and the realisation that my efforts however tiny aided that made all the turmoils of striving for a good education worth it. I will also cherish my time spent volunteering at the Atlanta Humane Society.

The year of 2020 changed many lives and mine was no different. My father was taken seriously ill several times (ironically not due to COVID). My career trajectory also changed significantly due to practical obligations. During this trying time, I made a strange companion 'Plants' who by far have proven to be the best therapy available in the market. My mom is an avid gardener and growing up, I always helped her with her projects. I myself, started gardening with a small patio garden when I first moved to the United States. It all started with a small 'Polka Dot' plant and now several years later I am a proud owner of ~ 300 plants. It was only last year although that they really became a companion from being just a hobby and I can't put into words how much they have helped me cope with the stress and anxiety and pushed me to keep moving forward. I am extremely grateful to the friends I made through the local and national plant clubs, especially 'Atlanta Plant Club' and I can already tell some of these relationships are going to be lifelong ones.

TABLE OF CONTENTS

LIST OF TABLES

LIST OF FIGURES

SUMMARY

When individuals in a collective system are constrained in terms of sensing, memory, computation, or power reserves, the design of algorithms to control them becomes challenging. These individual limitations can be due to multiple reasons like the shrinking size of each agent for bulk manufacturing efficiency or enforced simplicity to attain cost efficiency. Whereas, in some areas like nano-medicine, the nature of the task itself warrants such simplicity. This thesis presents algorithms inspired by biological and statistical physics models to achieve useful collective behavior through simple local physical interactions and, minimalist approaches to persistify tasks for long durations in collectives with limited capabilities and energy reserves. The first part of the thesis presents a system of vibration-driven robots that embodies the features of simplicity described above. A combination of theory, experiment, and simulation is used to study dynamic aggregation behavior in these robots facilitated via short-range physical attraction potentials between agents. Collectives in a dynamically aggregated state are shown to be capable of transporting objects over relatively long distances in a finite arena. In the rest of the thesis, two different, yet complementary systems are studied and elaborated to highlight the usefulness of distributed inactivity and activity modulation in aiding persistification of tasks in collectives incapable of implementing complicated algorithms to incorporate regular energy replenishing cycles. To summarize, an approach to achieving dynamic aggregation and related tasks like object transport in a constrained brushbot system is described. Two different artificial and biological collective systems are explored to reveal strategies through which tasks can be persistified without requiring complicated computations, sensing, and memory.

CHAPTER 1
INTRODUCTION

Self-organizing collective behaviors are witnessed in nature at many scales and extents of sophistication. Shoals of fish aggregating to intimidate predators [1], active versions of gels[2], liquid crystals [3], fire ants forming rafts to survive floods [4], and bacteria forming biofilms to share nutrients when they are metabolically stressed [5, 6] are a few examples. Fully comprehending how these ensembles of driven entities cooperate and self organize to form beautiful patterns and perform useful tasks, how they are controlled, how they sense others and the environment, and what information is exchanged in between agents to accomplish the collective goal, is a substantial challenge. Our knowledge about this has, however, increased over the last couple of decades, owing to an increase in research on collective behavior across several disciplines. This can be attributed to the availability of tools for conducting laboratory experiments, better computational methods, resources, and techniques for analyzing large data sets reflecting inter-agent interactions, etc. One particular discipline that has benefited a lot from these studies and has numerous existing and potential applications is swarm robotics.

Swarm robotics, as a discipline, aims at unraveling approaches for the control and coordination of a large number of robots to accomplish useful collective behavior. Inspired by natural systems, researchers have made strides in recent decades towards enabling ensembles of simple, independent units to cooperatively accomplish complex tasks [7]. Owing to their robustness, flexibility, and scalability, these swarms are particularly interesting when compared to single, monolithic robots for dynamic and unpredictable task domains such as space exploration or disaster management where risk minimization is paramount [8]. A particular challenge in swarm robotics, however, is deciding the complexity surrounding design and mass manufacturing of independent robot units without compromising the col-

lective functionality. With continued progress in the semiconductor industry that enables a large number of circuitry to fit in relatively small chips, combined with technological advances in control theory, motorized machinery, etc., researchers have been successful in overcoming this challenge by being able to produce highly functional computational units at small scales that can accomplish complex collective tasks [9, 10, 11].

However, there is a limit to the computational capabilities attainable per unit area of a robot chip and recent forecasts on the saturation of Moore's law suggest that the per unit area component density of a chip will plateau in a few years [12]. This poses a significant challenge for approaches to collective robotics platforms that rely heavily on the sensing or communication capabilities of individual robots to achieve their goals. This issue becomes more pronounced as we consider the area of micro- and nano- robotics that has seen a recent boost owing to numerous potent applications including bio-medicine [13]. These small-scale systems are incapable of traditional computation and require new machinery to implement distributed protocols for collective behavior [14].

Fortunately, we find many biological and physical collective systems in nature at various scales (e.g. ants, termites, bacteria, colloids, etc.) that can guide further research in this area. Owing to the phenomenon of emergence, some of these collectives can accomplish complex behavior and dynamics despite of being composed of small units with low to no computational capabilities. The term "emergence" was coined by the philosopher G.H. Lewes in 1875 [15] and has since been used in various fields to refer to any observable outcome that is greater than the sum of its parts [16, 17]. The collective intelligence in natural swarm systems is usually, not proportional to the sum of the intelligence of individual entities. Instead, it is several orders of magnitude more, and an outcome of simple but smart repetitive local rules or interactions. On a separate note, while centralized, connected system functionality depends heavily on ensuring each component is sophisticated and robust, decentralized and distributed collectives can function well with simpler redundant constituents [18]. Additionally, many of the natural decentralized collectives are adept at

performing tasks persistently for long durations of time [19, 20, 21]. Keeping this in mind, the proposed line of research is expected to provide us with simple, novel tools for swarm manipulation and control while reducing the complexities of individual entities, and to do so persistently.

The objective of this thesis is to develop a series of computational and experimental studies for collective/modular robotic systems that are sensing and communication constrained, and probe the effect of distributed inactivity in such systems by leveraging ideas and principles from statistical physics and active matter. Towards this goal, we explore principles of achieving collective aggregation that can leverage fundamental physics of interactions and thus, can be utilized across many scales. To develop these principles, we take a three-pronged approach: a theoretical abstraction based on a self-organizing particle system, an experimental robot system inspired by this, and a physical simulation platform to support and extend the experimental results. We develop a system of minimalistic analog robots that can utilize mechanics and physical dynamics to accomplish goals. This robotic testbed is used as an experimental tool to study and analyze distributed stochastic algorithms for collective aggregation behavior, which are in turn inspired by studies on statistical physics algorithms. We support our findings with grid-based particle and physics-based simulations for higher population sizes which is unachievable with our robotic testbed.

We consider the problems of dynamic aggregation, dispersion, and collective transport. Dynamic aggregation is defined as the collective behavior where entities aggregate without the specificity of an aggregation site and remain motile in the aggregated form. Aggregation is a prerequisite for many other collective tasks like object transport and manipulation, information transfer, etc., and constitutes a widely studied collective behavior. In biological collectives, aggregation can aid more fundamental physiological processes like thermoregulation, collective food processing, etc. Hence, this particular collective behaviour is an important one to study and serves as a good starting platform to explore our algorithms and findings. Inspired by the phase transition in a statistical physics model called the ‘Fixed

Magnetization Ising Model'[22], our theoretical algorithm predicts a sharp transition from dispersed to aggregated states as attraction bias between neighboring agents increases. This is mirrored in our robotic studies where a parameter representing local interparticle attraction is increased to transition the robots from a dispersed phase to a dense and compact aggregated state. These results point to a fruitful interplay between algorithm design and active matter physics that can result in new non-equilibrium physics and principles for programming collectives without the need for complex algorithms or capabilities. This study led to the following publication: *S. Li*, B. Dutta*[1], S. Cannon, J. J. Daymude, R. Avinery, E. Aydin, A. W. Richa, D. I. Goldman, and D. Randall, "Programming active cohesive granular matter with mechanically induced phase changes", 2021. arXiv:2009.05710 [cond-mat.soft]. (Accepted by Science Advances)*

The next goal of this thesis is to explore task persistification in constrained systems. We probe the effects of selective inactivity on the long-term autonomy of tasks in robot simulations. We assign fixed lifetimes to robots and study if we can achieve task persistification through strategies where robots hibernate intermittently. In particular, we develop a strategy of selective and periodic inactivity to achieve persistence of dynamic aggregation in the above system where each individual hibernates periodically based on a bias. We show the usefulness of prolonged dynamic aggregation achieved via this selective, periodic hibernation through a collective "debris removal" task where the robotic system is commissioned with keeping a fixed area clean of debris. This approach of selective inactivity is inspired by biophysical collective systems that exhibit the usefulness of distributed inactivity. The findings from this study are reported in the following article: *B. Dutta, D. Randall, M. Egerstedt, "Task persistification with distributed inactivity in robot swarms" (submitted to 2021 IEEE/RSJ International Conference on Intelligent Robots and Systems, IROS 2021).*

In the penultimate section of the thesis, we study one such biological system. We explore how fire ants distribute their workload while collectively excavating their nests, and

[1] * marked authors contributed equally

show the benefits of distributed individual laziness while carrying out a collective task, like excavation, in a confined environment. Fire ants are great excavators, often rebuilding their nests several times in short periods due to heavy rainfalls and other environmental factors. We present laboratory experiments with fire ants to show how they distribute workload and implement other strategies like selective retreats, to efficiently excavate their nests. We support our observations with statistical data analysis, simulations, and robotic experiments. This research is published in the following article: *J. Aguilar, D. Monaenkova, V. Linevich, W. Savoie, B. Dutta, H. S. Kuan, M. Betterton, M. Goodisman, and D. Goldman, "Collective clog control: Optimizing traffic flow in confined biological and robophysical excavation," Science, vol. 361, no. 6403, pp. 672677, 2018.*

The outline of this thesis is as explained below. In chapter 2, we present a literature review of research in the broader area of collective behavior from the perspective of three distinct disciplines with a special focus on collective aggregation. We then, provide a comprehensive account of the task persistification literature in robotics. We highlight the need for simpler algorithms for persistifying tasks as individual agents are forced to work with limited capabilities in constrained environments. In chapter 3, we present our experiments, theory, and simulations for collective dynamic aggregation. We elaborate on the designs of the robots, simulation details, and theoretical findings and conclude with the demonstration of some application-specific tasks. Chapter 4 is dedicated to describing the effects of distributed inactivity on the collective aggregation dynamics of robots and how it can be selectively and periodically tuned to achieve task persistification. Chapter 5 extends and complements the idea of task persistence mediated by selective distributed inactivity by providing experimental data and analysis on fire ant excavation system. Chapter 6 concludes the thesis by providing a summary of the main findings of the thesis and highlighting some potential future directions.

CHAPTER 2
LITERATURE REVIEW

Many approaches have addressed the challenging task of designing and controlling collective robotic behavior. As a result, several taxonomies have emerged from these approaches. For the scope of this review, we classify these approaches into three categories: bio-inspired approaches, multi-agent robotics, and active matter studies. Although there is some overlap in the ideologies in these areas, we highlight the differences in these approaches, and how studies have harnessed specific attributes from each of these to produce robust collective behavior in artificial swarms.

2.1 A biologist's bird's eye view on collectives

Bio-inspired approaches in swarm robotics (see, e.g., [23] and the references therein) mimic phenomena observed in nature. Biological swarming systems in various scales are capable of harnessing simple local interaction rules into complex emergent tasks and behavior. Many algorithms of collective behavior have been derived from biological systems. Some of these representative research studies pertinent to swarm self-aggregation are explained below. However, with notable exceptions, these studies tend to lack the backing of formal analysis and proofs that yield a full understanding of the underlying dynamics. Consequently, most bio-inspired collective robotics studies are phenomenological. A typical methodology for a bio-inspired collective robots study can be divided into the following steps [23]:

- Laboratory experimentation with model biological systems to find key components of collective behavior

- Abstraction and analysis of the key components into mathematical models and simulation studies
- Construction of robotic setup and translation of the model into robotic algorithms

Aggregation in nature has several uses. For example: it is used for safety, foraging, interactions, and information exchange in many biological systems like that of social insects. It is often also fundamental for any collective to aggregate in order to accomplish other tasks crucial to survival and existence like self-defense [24], thermo-regulation in bees [25], and flood escape by the formation of rafts in fire ants [4]. Some model organisms that have inspired aggregation algorithms are slime mold [26], bees [27], cockroaches [28], c.elegans [29], etc. Some of these algorithms rely on long-range cues like light gradient [30] or thermal gradient in addition to short-range attractions whereas some other methods are based on probabilistic finite state machines (PFSM) which translate to robots randomly exploring the domain until they meet neighbors and stochastically decide whether or not to join the aggregate [31]. In each of these specified models, parameters like the probability of joining the aggregate are quantified by rigorous analysis of the biological system that inspired the algorithm. For example, in [32], probabilistic estimation of individual parameters of cockroaches like dynamics of motion, interaction time distribution, etc are experimentally quantified. These parameters are then used for both simulation and robotic experiments. Similarly, [33] proposes a population dynamics model, and a robot simulator based on studies of social German cockroaches that qualitatively and quantitatively show that single aggregate formation requires a minimal mobility or sensing threshold. These studies thus pave the way for bio-inspired collective behavior algorithms, which form a subset of multi-agent algorithms. However, these studies have a distinct flavor: the phenomenological methodology described above, that distinguishes them from the other multi-agent studies.

2.2 Multi-agent swarm engineering: A control perspective

Multi-agent swarm engineering comprises of a broad umbrella of approaches that relies on tools from control theory, graph theory, probabilistic methods, etc. In some studies, swarms are modeled using networks with robots as nodes that communicate over the network's edges (see [34] for a comprehensive review). Such approaches can leverage the wealth of graph theory literature to map convergence of collective outcomes onto various graph measures, often yielding strong algorithmic guarantees. In [35], the authors present a good review of structural taxonomies for multi-agent algorithms and tabulated the reach and maturity of these algorithms in terms of applications. They identify 10 branches based on mathematical structures of the algorithm, namely artificial potential functions, distributed feedback control, geometric algorithms, state machines and behavior composition, bio-inspired algorithms, density-based control, distributed optimization algorithms, local optimization algorithms for global behavior, and centralized optimization algorithms. These algorithms were further classified to link studies that have utilized these mathematical approaches to applications like pattern formation, area coverage, collective transport, etc. A few of these algorithms have been used in the context of aggregation. We covered a subset of these studies (the bio-inspired algorithms) in the previous section. Among the rest, consensus algorithms are the most widely used distributed algorithms where each agent acquires its neighbor's state (position for aggregation) and averages its state with neighbors [36]. Numerous studies look into the convergence of consensus algorithms under various graph structures and constraints[37, 38, 39].

Several other review papers outline this relatively broad field of swarm engineering with the help of relevant taxonomies, for example: [40] reviews the field in terms of methods and collective behavior, [41] classifies the literature by swarm and communication properties, and [42] presents a review of swarm tasks.

Highly analogous to approaches above, distributed computing models robots as simple,

homogeneous units in an effort to understand which behaviors are theoretically possible under a given set of limitations on sensing, communication, or computational power [43, 44, 45]. Both of these approaches often rely critically on robots computing and communicating complex state information, requiring relatively sophisticated hardware that can be prohibitive at small scales.

A variety of terrestrial swarm robotic testbeds have tested one or more of the aforementioned methodologies in achieving collective tasks. A few of those are tabulated below in Table 2.1 showing their cost, hardware requirements, and power reserves. While this list is not exhaustive, it provides a good sample set to highlight the cost, sensing and power resources, and scalability of the state-of-the-art robotic testbeds. Almost all of these robots depend on one or more sensors for task execution and have a finite battery life.

Table 2.1: **Comparisons of swarm robotics test-beds**

Robot	Cost ($)	Scalable operation	Sensing	Locomotion	Size (cm)	Battery(h)
Alice [46]	30	None	Distance	Wheel, $1cm/s$	2	3.5-10
Kilobot [9]	10	Charge, power, program	Distance, ambient light	Vibration, 1 cm/s	3	3-24
Formica [47]	15	None	Ambient light	Wheel	3	1.5
Jasmine [48]	90	Charge	Distance, bearing, light colour	Wheel	3	1-2
E-puck [11]	450	None	Camera, distance, bearing, IR proximity, acc, encoders	Wheel, 13 cm/s	7.5	110
R-one [49]	150	None	Visible light, accel/gyro, IR sensors, encoders	Wheel, 30 cm/s	10	6
Droplets [50]	25	Charge	Distance, bearing, ambient light, RGB colour	Vibration	4.4	–
iRobot [51]	–	Charge, power, program	Camera, distance, bearing, bump	Wheel, $50cm/s$	12.7	3
Swarm-Bot [52]	–	None	Camera, distance, bearing, proximity, accel/gyro	Treel	17	4-7
GRITSBot [53]	50	Charge, power, program	Range, Bearing, Wi-Fi, GPS	Wheel, $25cm/s$	3	1-5
Khepra-III	2750	none	Distance, Bearing, IR	Wheel, $50cm/s$	13	1-8

2.3 Active matter to programmable matter

As individuals are simplified to maximize cost efficiency and are miniaturized [54] to overcome thermodynamic limits of computing [55], each of the above methodologies comes with some inherent tradeoffs that make it less suitable for useful applications. Traditional robotic functions of movement, communication, and computation become very limited, as do the power reserves used to drive these functions [14]. Thus, the protocols used to control these systems must both respect these strict limitations and scale with the size of the swarm while achieving the desired task, motivating a search for highly simplified, distributed algorithms.

Fueled by this quest, researchers have started looking into fundamental physical systems driven out of equilibrium using statistical physics tools to facilitate collective robotics research. Dynamic self-assembly into complex architectures is one of the key attributes of these systems and forms a major area of ongoing active matter research. This is a relatively new way to look at macroscopic swarm robotics problems under constraints. However, these tools have been used for nearly a decade to study collective behavior in both natural and man-made micro/nanoscale active matter systems.

One can find a plethora of comprehensive review articles in this domain. Based on the propulsion mechanisms, active matter is broadly classified into two subgroups: active colloids and microswimmers. Active colloids utilize self phoretic mechanism to propel themselves whereas swimmers depend on molecular rotational machineries like helical flagella for propulsion. An extensive list of experimentally realized active matter systems is provided in [56] along with propulsion mechanism and speed. This information is summarized in Figure 2.1 and helps us identify the mechanism, scales, and ranges at which these systems work.

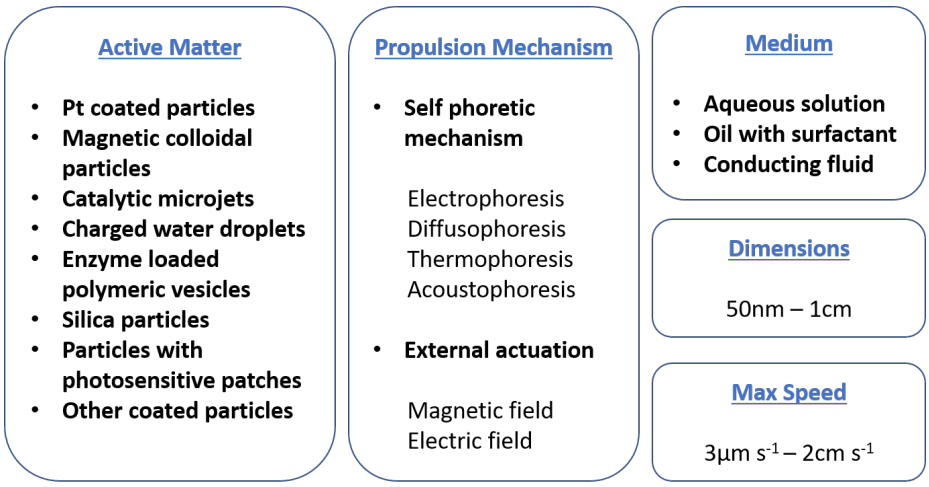

Figure 2.1: **Examples of experimentally realized artificial active matter**

Regardless of the propulsion mechanism, these systems exhibit an array of interesting emergent collective behavior ranging from steady-state patterns like bands/lanes [57, 58] to dynamic structures like pulsating rings/ rotating vortices [59]. For an extensive review of such behavior in active colloids, we refer to [60] where the authors formally review single particle to collective dynamics highlighting avenues for further research. A similar review [61] elaborates the physics behind the individual and collective dynamics of swimmers. Microswimmer collective dynamics are more evolved and complex than their active colloidal counterparts and in this study, we will limit ourselves to drawing formal connections between macroscopic swarm robotics systems and the latter.

It is important to understand that while the motion of passive colloidal particles is a result of thermal fluctuations alone, active colloids exhibit active swimming in addition to thermal fluctuations. Thus, most equilibrium theoretical tools based on energy minimization and entropy maximization cannot be directly applied to these systems. Direct numerical modeling is thus the preferred research approach, along with a few lesser popular continuum and kinetic approaches [62]. However, recently, connections between collective features of such self-propelled systems and well-studied equilibrium models are being drawn [63, 64, 65]. A great formal insight into such connections and their shortcomings can be found in [66].

A minimalistic model for active particle dynamics is an active brownian particle [56, 60] whose stochastic equations of motion are as follows:

$$\begin{cases} \dot{x} &= v\cos\varphi + \sqrt{2D_{\mathrm{T}}}\,\xi_x \\ \dot{y} &= v\sin\varphi + \sqrt{2D_{\mathrm{T}}}\,\xi_y \\ \dot{\varphi} &= \sqrt{2D_{\mathrm{R}}}\,\xi_\varphi \end{cases} \tag{2.1}$$

where (x, y, ϕ) represent the positional state, v is the self-propulsion speed, $\xi_{x,y}$ denote the noise components, and $D_R; D_T$ are the thermal rotational and diffusional coefficients respectively.

In Chapter 3, we study a robotic system whose dynamics can be explained by an extension of active brownian particles called chiral active brownian particles. The dynamical equations of such a system is represented by an additional rotational drive term as shown below:

$$\begin{cases} \dot{x} &= v\cos\varphi + \sqrt{2D_{\mathrm{T}}}\,\xi_x \\ \dot{y} &= v\sin\varphi + \sqrt{2D_{\mathrm{T}}}\,\xi_y \\ \dot{\varphi} &= \omega + \sqrt{2D_{\mathrm{R}}}\,\xi_\varphi \end{cases} \tag{2.2}$$

This robotic system with inter-particle attraction is critically analyzed for aggregation dynamics theoretically, computationally and experimentally, and the findings are reported in Chapter 3. Therein, we explore the problem of *dynamic free aggregation*, where robots gather together without preference for a specific aggregation site and are motile in aggregate form.

In summary, some approaches to aggregation problems in the literature rely on external fields to actuate robot collectives, using global, coordinated guidance to achieve their goals [67, 68, 69]. Some works take inspiration from emergent behavior in biological systems but lack rigorous mathematical foundations explaining the generality and limitations of the resulting algorithms. Other approaches rely on some form of long-range sensing. For

example, the authors equip robots with speakers and microphones that can be used to infer relative position and distance between members of the swarm in [31]. In another study, the authors mimic biological stigmergy which is indirect communication through an active environment by allowing robots to emit signals that propagate throughout their surroundings to attract other robots [70, 71]. More recent results indicate that robots can aggregate reliably [72], achieve distributed consensus [73], and perform spatial coverage [74] without computation or communication, using only a binary line-of-sight sensor. Our focus, instead, is on self-actuated systems that are highly resource-limited and utilize strictly local interactions between robots to induce macroscale behaviors. This thesis takes a stab at approaching this by offloading emergent computation on mechanics.

2.4 Task persistification

Energy-aware swarm robotics policies are designed to aid long-term autonomous applications. Most of these approaches typically rely on designing smart algorithms to incorporate repeated charging routines to recharge robot batteries without affecting the overall system trajectories and outcomes. For example, in [75] the authors work toward a heuristic algorithm to help a multi-robot system cover targets or tasks persistently by adjusting target-specific costs based on detours to charging stations. Another study divides a team of robots into "task" and "delivery" robots, where delivery robots are routed to provide energy resources to task robots based on delivery requests. The authors pose this as a vehicle routing problem with time windows and solve the scheduling problem using mixed integer quadratic programs [76]. Similarly, [77] formulate an optimization problem leveraging control barrier functions with energy constraints over persistified tasks, and demonstrate the application of the devised algorithm on a set of wheeled, mobile robots in the Robotarium, which is an open-source experimental platform [10].

Although these studies are significant milestones towards energy aware swarming policies, we wish to focus on systems that lack the basic intelligence necessary to perform any

of the above-discussed algorithms. Here we take inspiration from some studies on biophysical systems for simpler strategies of efficient long-term behavior. For example, [78] illustrates the usefulness of uneven workload distribution in the foraging behavior of bees. This disproportionate share of workload in eusocial insect societies is associated with the term "elitism" and is prevalent across other organisms [78, 19]. Similarly, some recent work on monodisperse mixtures of isometric active and passive colloidal particles show that binary mixtures can phase separate from an initial disorganized configuration with minimal presence of active particles [79]. With these relevant findings in place, we propose to explore the effects of distributed inactivity in collective systems under constraints. We hypothesize that bouts of lazziness in collective systems may be quintessential to enhancing task efficiencies and persistence.

CHAPTER 3
DYNAMIC COLLECTIVE AGGREGATION

We first develop a distributed stochastic algorithm for a *self-organizing particle system (SOPS)* on a discrete lattice to achieve aggregation. We show that there is a phase change in the system from dispersed (behaving like a gas) to aggregated (behaving like a solid) as a parameter representing attractive pairwise interactions is varied. Next, we design physical robots to replicate features of the SOPS algorithm to test whether simple relaxations of the theoretical model retain the dominant collective behavior. These *BOBbots* (or *behaving, organizing, buzzing robots*) use physical ferromagnetic attraction to implement a close variant of the algorithm without any computation, communication, proximity sensing, or persistent memory whatsoever. Finally, we use physical simulations of the robotic system to explore whether the predicted behavior persists in significantly larger collectives. We conclude with some tasks and other relevant findings related to this phase change.

3.1 Simulations of SOPS showing phase change

The SOPS consists of particles that exist on the nodes of a triangular lattice, with at most one particle per node. The original algorithm for aggregation is inspired by the "Fixed magnetization Ising model for ferromagnetism"[22] and the moves can be described as follows. Particles on the lattice can move stochastically on a bounded region along lattice edges favoring positions with more particle neighbors according to a bias parameter $\lambda > 1$ (Fig. 3.1 A). Each particle can only assess the number of particles occupying adjacent lattice nodes (when required) and does not have access to any global information such as a coordinate system or the total number of particles. The pseudocode for this theoretical SOPS algorithm for aggregation and dispersion is presented in Algorithm 1.

One can express this sequence of random particle activations and the resulting random

Algorithm 1 Markov chain $\mathcal{M}$ for aggregation and dispersion in SOPS

Beginning at any configuration of N particles, fix a $\lambda > 1$ and repeat:

1: Choose a particle P uniformly at random; let ℓ be its location.
2: Choose a neighboring location ℓ' and $q \in (0, 1)$ each uniformly at random.
3: **if** ℓ' is unoccupied **then**
4: Let n be the number of neighbors P has in location ℓ, and let n' be the number of neighbors it would have in location ℓ'.
5: **if** $q < \lambda^{n'-n}$ **then** P moves to ℓ'.
6: **else** P remains at ℓ.

particle moves as a Markov chain. This Markov chain can be carefully analyzed to provide bounds on λ that proves a transition from dispersed states to aggregated states when λ is increased. A previous study looked at the same problem in the SOPS but with the difference that particle configurations were restricted to be connected components and proved bounds on λ that separated dispersed and aggregated states.[80, 81] Following similar techniques our explorations proved a transition point $\lambda > 5.566$ above which the system evolves to aggregated states[82].[1] The theoretical analysis also suggested that compact connected components are formed in the aggregated states where the perimeter(P_{MC}) of the largest component should scale as $\mathcal{O}(\sqrt{N_{MC}})$ where N_{MC} is the size of the component.

We ran discrete particle simulations for the algorithm defined in algorithm 1 for different numbers of particles and different values of λ. The plots from these simulations give a strong indication that this aggregation algorithm indeed undergoes a phase transition around the theoretical transition point of $\lambda \sim 5.566$ where the macroscopic behavior of the system suddenly changes from dispersion to aggregation. (Fig. 3.1 C–D).

[1] The theoretical analysis were done in collaboration with former graduate student, Sarah Cannon.

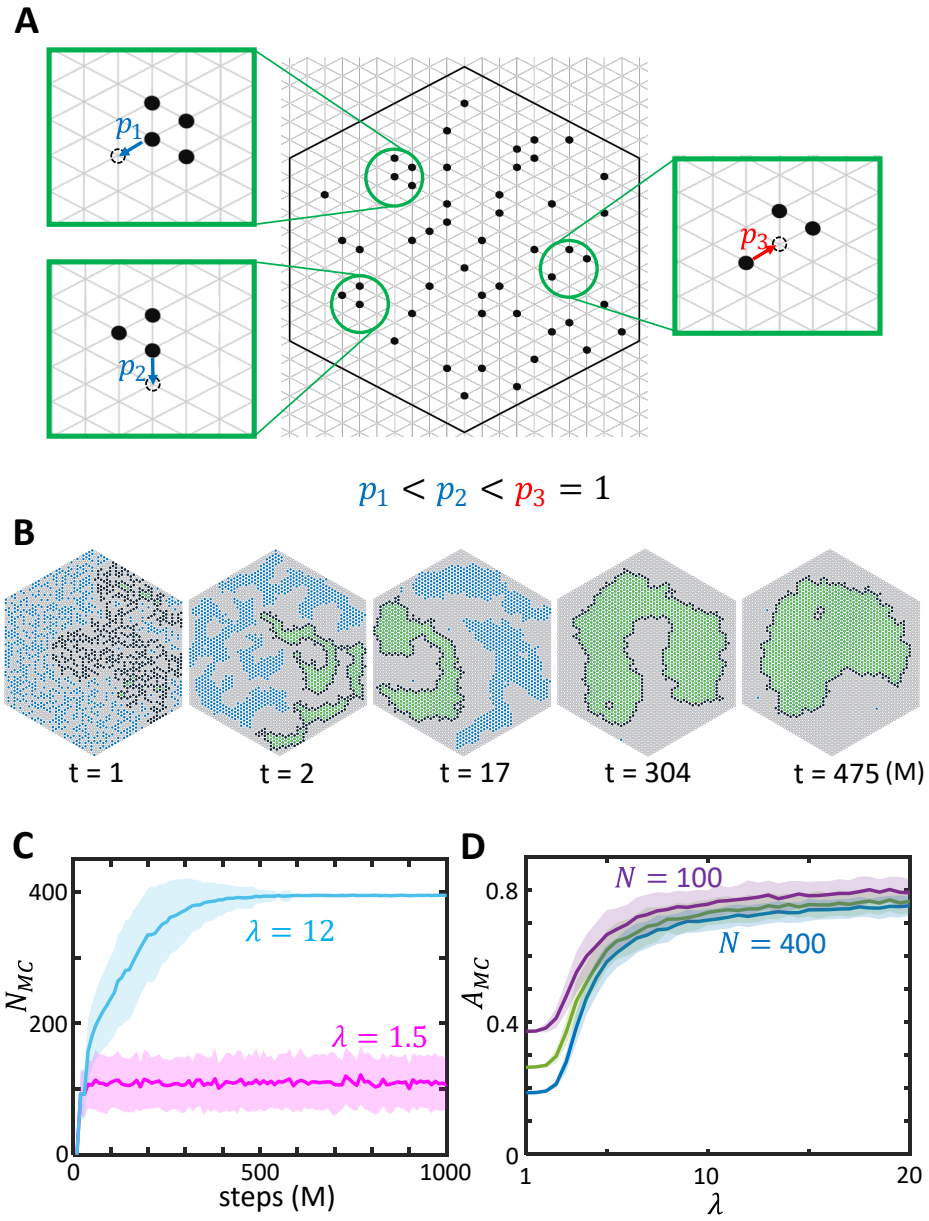

Figure 3.1: **The theoretical self-organizing particle system (SOPS).** (**A**) A particle moves from a node where it has n neighbors to a node where it would have n' with probability $\min\{\lambda^{n'-n}, 1\}$, where $\lambda > 1$. Thus, moves that decrease the number of neighbors are made with proportionately smaller probability (e.g., in the left insets, $p_1 = \lambda^{-3} < \lambda^{-2} = p_2$), while moves that increase or maintain the number of neighbors are made with probability 1 (e.g., in the right inset, $p_3 = 1$). (**B**) Time evolution of a sample simulated SOPS with 1377 particles for $\lambda = 7.5$ showing progressive aggregation. The bulk of the largest connected component is shown in green and its periphery is shown in black. (**C**) Time evolution of N_{MC}, the size of the largest connected component, showing dispersion for $\lambda = 1.5$ and aggregation for $\lambda = 12$. (**D**) Phase change in λ-space for the aggregation metric $A_{MC} = N_{MC}/(k_0 P_{MC}\sqrt{N})$, where k_0 is a scaling constant, P_{MC} is the number of robots on the periphery of the largest component, and N is the total number of robots. This phase change is qualitatively invariant to the system's size.

3.2 Theory to practice: a physical embodiment of aggregation and dispersion

The SOPS model demonstrates that agents can achieve self-organizing aggregation merely by moving randomly, preferring positions with more neighbors. Although this simple distributed, stochastic algorithm requires minimal computational capabilities compared to others in the literature, physical robots would seemingly still need to perform computation and sensing to implement its rules. Here, we introduce a slight variant of the SOPS algorithm that maintains the same provable behavior, but can be implemented by a system of robots lacking any computation, communication, sensing, and persistent memory.

First, we modify the transition probabilities of the SOPS algorithm so that particles no longer explore potential moves before taking them, as this is physically difficult for rudimentary robots to achieve. The original transition probabilities are expressed as a ratio between the weights of the current and proposed system configurations, as required by the celebrated Metropolis-Hastings algorithm [83]. Instead of moving from a node with n neighbors to one with n' neighbors with the original probability $\min\{\lambda^{n'-n}, 1\}$, the modified algorithm makes such a move with probability λ^{-n}. This potentially reduces the probabilities of some moves by a constant (at most λ^5), but importantly does not change the algorithm's stationary distribution.

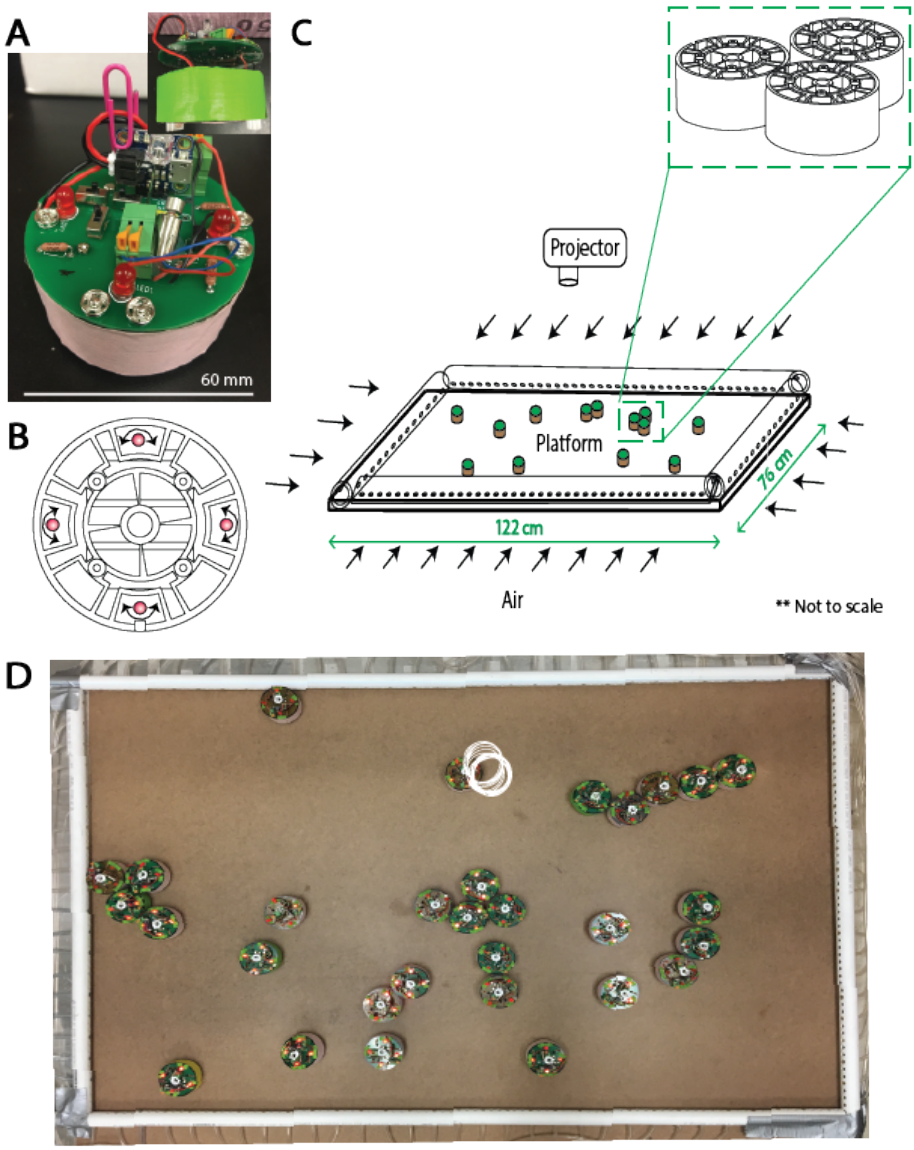

Figure 3.2: **BOBbot and experimental arena design.** (**A**) Oblique view of a BOBbot showing the main electro-mechanical components. Inset: Layered view. (**B**) Horizontal cross-section of the BOBbot showing the loose magnets (red circles) in four alternating slots, the configuration used in this study. (**C**) Schematic of experimental setup. Inset: Diagram representation of three BOBbots interacting. (**D**) The experimental platform, with white track lines showing a sample BOBbot trajectory.

Next, we introduce a collective of *BOBbots* (Fig 3.2 A) whose design *physically embodies* the modified aggregation algorithm, capturing its salient features while replacing all sensing, communication, and probabilistic computation with physical morphology and

interactions. Each BOBbot has a cylindrical chassis with a base of elastic "brushes" that are physically coupled to an off-center eccentric rotating mass vibration motor (ERM). The vibrations caused by the rotation of the ERM are converted into locomotion by the brushes. Due to asymmetry in this propulsion mechanism, the BOBbots traverse predominantly circular trajectories that are randomized through their initial conditions but — unlike the SOPS particles — are inherently deterministic with some noise.

Analogous to the modified transition probabilities in the aggregation algorithm that discourage particles from moving away from positions where they have many neighbors, each BOBbot has loose magnets housed in shells around its periphery that always reorient to be attractive to nearby BOBbots (Fig 3.2 B). The probability that a BOBbot detaches from its neighbors is negatively correlated with the attractive force from the number of engaged magnets, suggesting it should approximate the movement probabilities given by the algorithm which scales inversely and geometrically with the number of neighbors. We subsequently verify this assertion experimentally. The strength of the magnets determines whether the system aggregates or disperses at long times (analogous to λ in the algorithm), though the magnets must always be weak enough to allow the BOBbots some probability of detachment.

3.3 Experiments and simulations

We investigate the degree to which collectives of BOBbots aggregate as a function of their peripheral magnet strength ${F_M}^2$ in both robotic experiments and physics-based discrete element method (DEM) simulations. The experimental protocol begins with placing magnets of a particular strength F_M into the BOBbots' peripheral slots. The BOBbots are positioned randomly in a rectangular arena (Fig. 3.2 C–D) and are then actuated uniformly for a fixed time during which several aggregation metrics are tracked . These trials are conducted for several F_M values with repetition.

[2]For convenience, F_M is normalized by the gravity of Earth $g = 9.81$ m/s^2 when using the unit of gram.

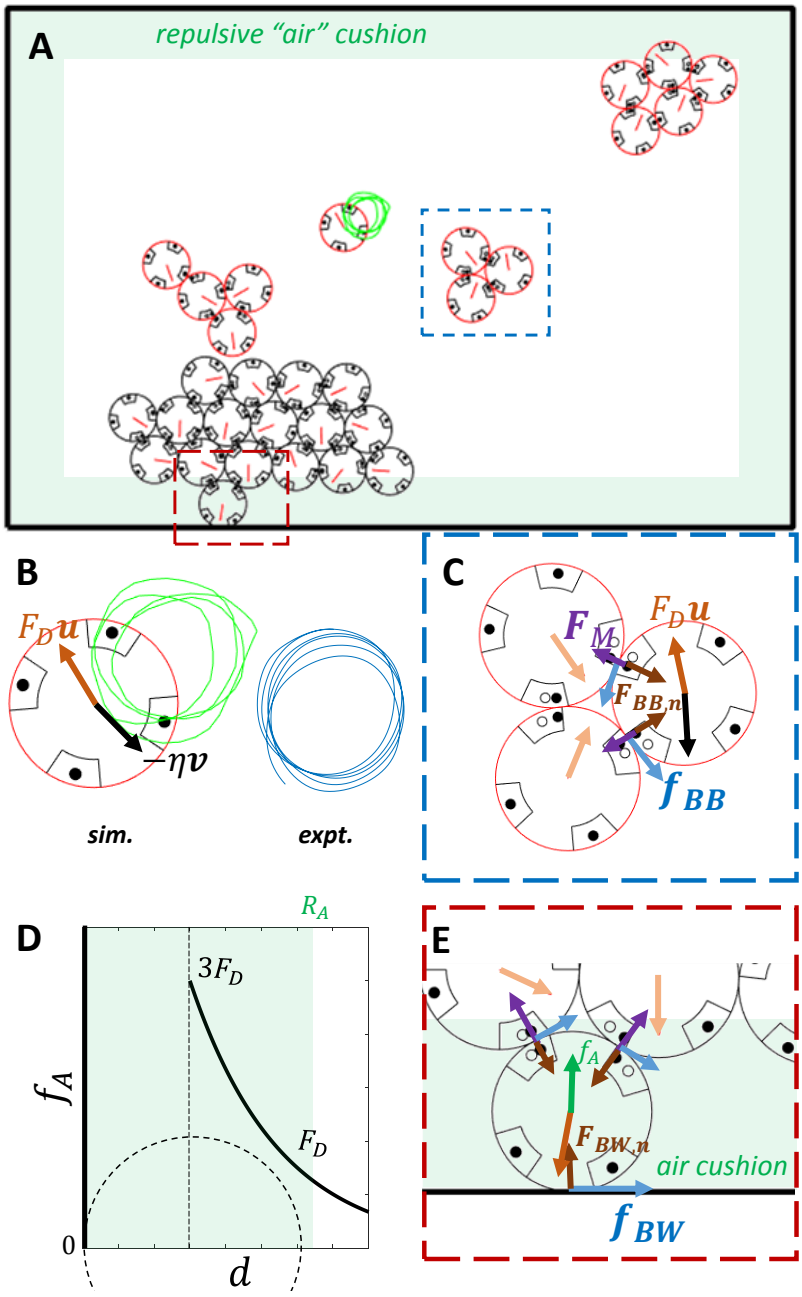

Figure 3.3: **Discrete element method simulation setup.** (**A**) Illustration of the simulation platform with a sample simulated trajectory in green. (**B**) Simulated and experimental individual trajectories. A freely moving BOBbot is driven by a translational drive $F_D\hat{u}$ and dragged by a damping $-\eta$v. (**C**) The inter-BOBbot interactions: attraction between magnetic beads F_M, inter-BOBbot friction f_{BB}, and sterical exclusion $F_{BB,n}$. (**D**) The airflow profile near the boundary, pushing with a maximum strength of $f_A = 3F_D$ when the BOBbot is touching the boundary and decaying exponentially such that $f_A = F_D$ when the BOBbot is distance R_A away. (**E**) BOBbot-boundary interactions: airflow repulsion f_A, BOBbot-boundary friction f_{BW}, and normal force $F_{BW,n}$.

Mitigating the effects of the fixed boundary in both experiments and simulations is

a significant design challenge. Often, robots will crawl along the boundary or persist in corners, affecting the overall analysis of system dynamics. To address these issues, uniform airflow is employed to gently repel BOBbots away from the boundary (Fig. 3.2 C), and similar effects are implemented in simulation.

We complement our robotic experiments with physics-based DEM simulations (Fig. 3.3) to study BOBbot system dynamics with larger numbers of robots and a more comprehensive sweep of the F_M-parameter space. The motion of an individual BOBbot is modeled as a set of over-damped Langevin-type equations governing both its translation and rotation subject to diffusion and drift, as seen in [84]. The dynamical equations are:

$$\begin{cases} m\ddot{\vec{r}} &= F_D\hat{u} - \eta\dot{\vec{r}} + \vec{F}_{env}(\vec{r},\varphi) + \vec{\xi}(t) \\ I\ddot{\varphi} &= \tau_D - \eta_\varphi\dot{\varphi} + \tau_{env}(\vec{r},\varphi) + \xi_\varphi(t) \end{cases} \tag{3.1}$$

where $\vec{r}$ is the BOBbot's position vector and φ is its orientation vector. The BOBbot's drive has magnitude F_D and is assumed to align with the heading $\hat{u} = (\cos\varphi, \sin\varphi)^T$. The drag force $-\eta\dot{\vec{r}}$ is antiparallel to the velocity, balancing the drive when no other BOBbots are around (Fig. 3.3 B). When a BOBbot is in contact with other BOBbots, the environmental forces $\vec{F}_{env}$ include the magnetic attraction F_M, inter-BOBbot friction f_{BB}, and sterical exclusion $F_{BB,n}$ (Fig. 3.3 C). When a BOBbot is near or in contact with the boundary, these environmental forces also include the airflow repulsion f_A, BOBbot-boundary friction f_{BW}, and normal force $F_{BW,n}$ (Fig. 3.3 D–E). Noise is added to the translational motion as $\vec{\xi}(t)$, where t represents time. The rotational motion and torques are modeled analogously.[3]

[3]The simulation code was written and calibrated in collaboration with CRAB Lab member, Shengkai Li

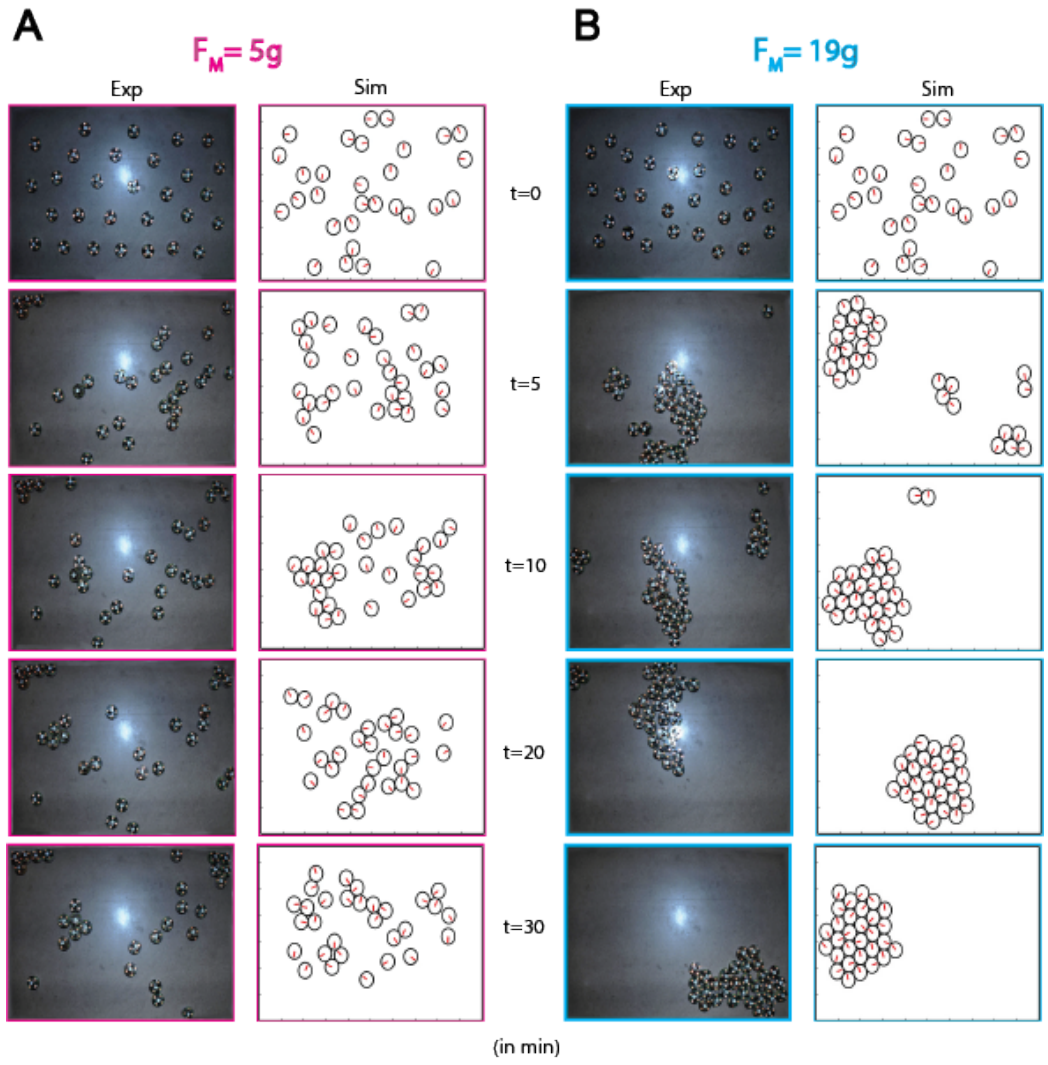

Figure 3.4: **Dispersion and aggregation in experiment and simulation.** Time evolution snapshots of both experiment and simulation for a system of 30 BOBbots with different magnet strengths: (**A**) $F_M = 5$ g, where we see dispersion, and (**B**) $F_M = 19$ g, where we see aggregation.

To model the attractive force between two BOBbots, recall that a physical BOBbot houses its loose magnets in four orthogonal slots in its periphery, resulting in a patchy magnetic interaction as the magnets move freely in their slots. The simulated BOBbots have these same slots, each housing a uniformly magnetized sphere with exponential decay. Attraction between two simulated BOBbots is calculated based on the strength of these magnetic spheres and the minimum physical separation between any interacting pair, which depends on the relative position and orientation of the two BOBbots. We validate

our simulations using experiments with physical BOBbots designed to isolate individual physical parameters.

As predicted by the SOPS theory, the BOBbot collectives remain dispersed with weaker magnets and aggregate when the magnets are sufficiently strong in both experiment and simulation (Fig. 3.4). As a first characterization of collective aggregation, we consider the number of BOBbots in the largest connected component, denoted by N_{MC}. Tracking N_{MC} in systems of 30 BOBbots indicates, both in experiment and simulation, that the largest connected component grows in size over time when equipped with stronger magnets ($F_M = 19$ g), while those with weak magnets ($F_M = 5$ g) never form sizable components (Fig. 3.5 A–B).

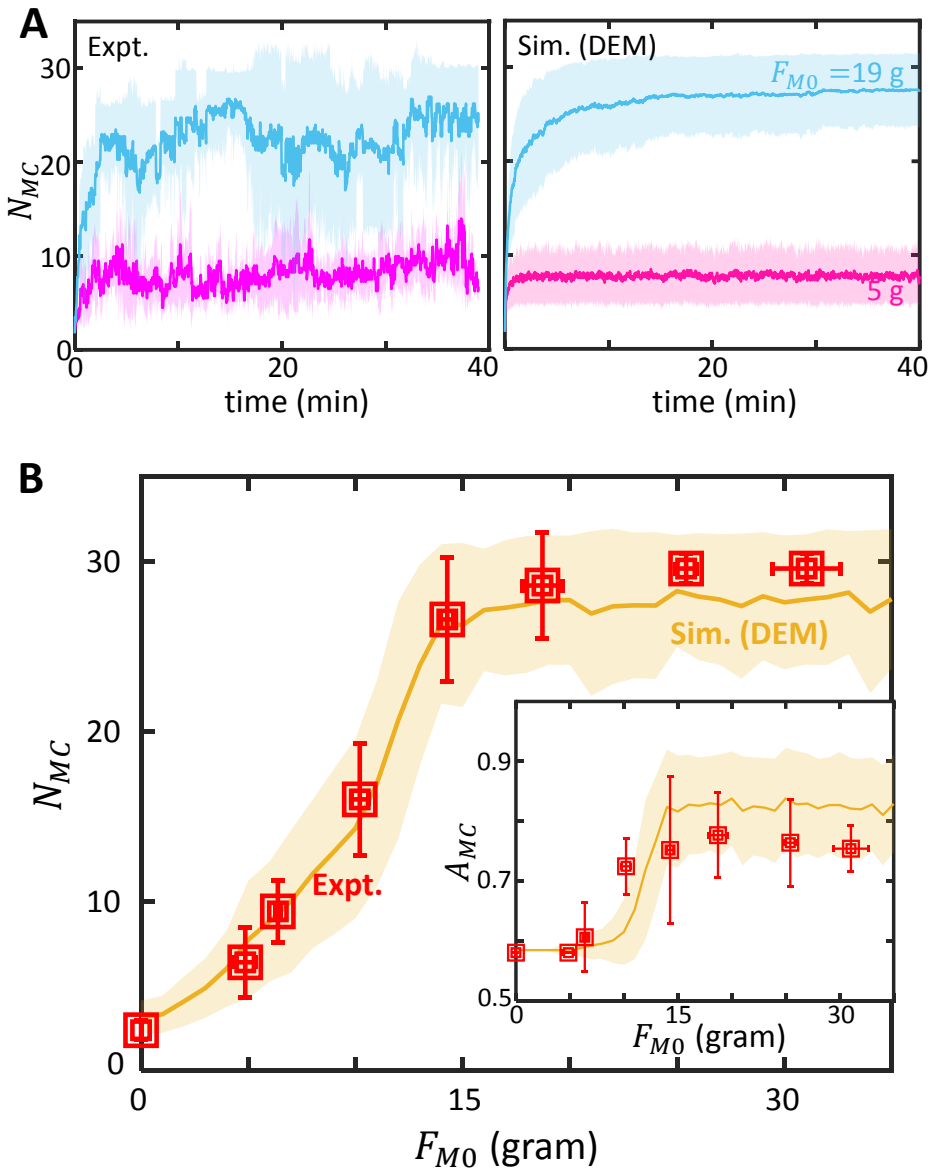

Figure 3.5: **The aggregation-dispersion phase change.** (**A**) Time evolutions of the size of the largest component N_{MC} in experiment and DEM simulation for a system of 30 BOBbots with $F_M = 5$ g (magenta) and $F_M = 19$ g (cyan). (**B**) Phase plot for a system of 30 BOBbots showing an increase in N_{MC} as the magnet strength F_M increases. The yellow plotline shows the mean and standard deviation of N_{MC} in the 150 simulation runs for each magnetic strength F_M between 1–35 g, with a step size of 1 g. Experimental data is shown in red with error bars showing the variation of the largest cluster size N_{MC} and the uncertainty of F_M due to empirical measurement. Inset: Phase plot showing the aggregation metric A_{MC} for the same BOBbot systems. A sharp phase change is apparent just after $F_M = 10$ g.

The SOPS theory further predicts that the largest connected component should not only be large but also compact, occupying a densely packed region. To capture both component

size and density, we track $A_{MC} = N_{MC}/(k_0 P_{MC}\sqrt{N})$, where k_0 is a scaling constant, P_{MC} is the number of BOBbots on the periphery of the largest component, and N is the total number of BOBbots. The scaling constant k_0 is defined such that $A_{MC} = 1$ when the system is optimally aggregated, as in the hexagonal packing. Using the DEM simulation, we sweep the space of magnetic strengths F_M with fine resolution in the range 0–35 g. We observe a phase change in both N_{MC} and A_{MC} that match well with the experimental data (Fig. 3.5 C).

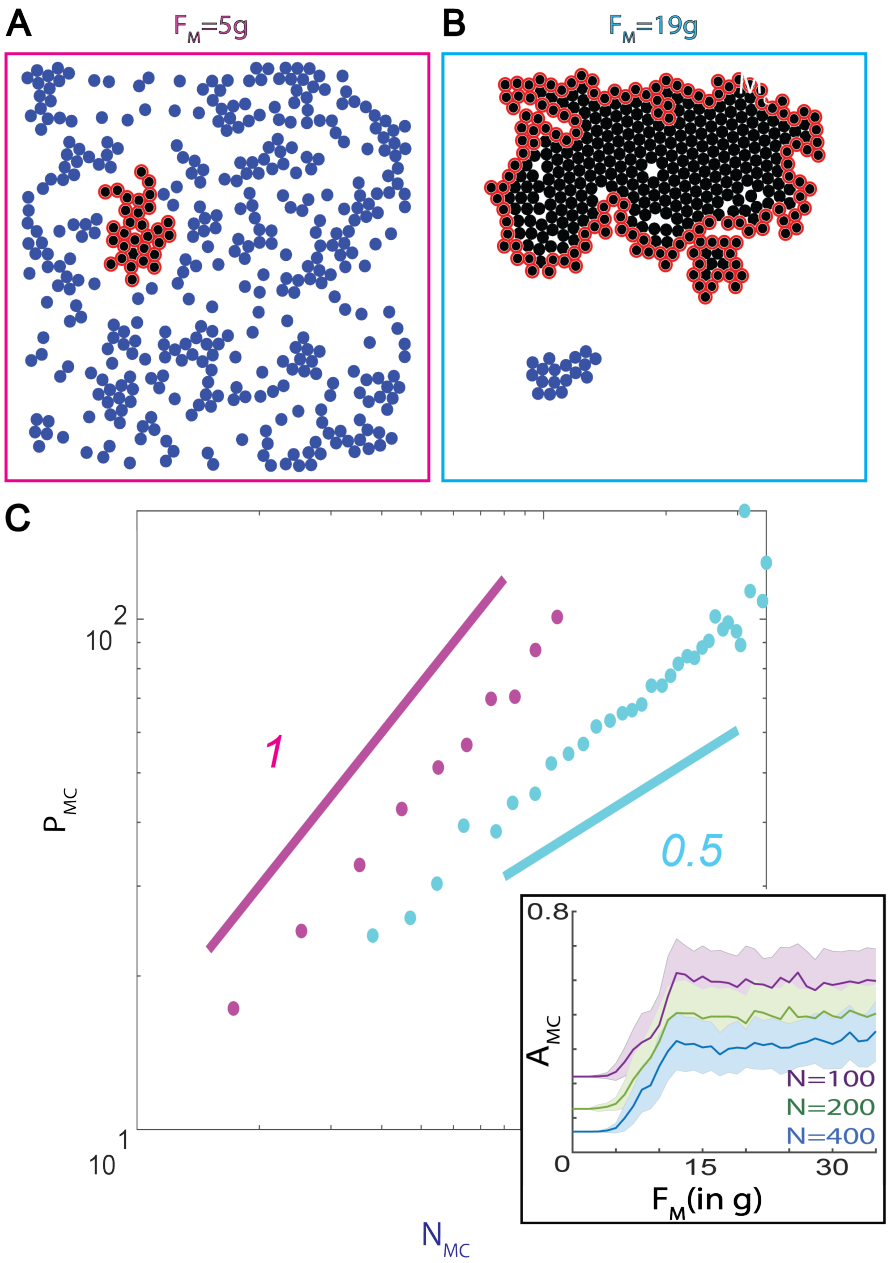

Figure 3.6: **Perimeter scaling.** Steady-state snapshots for a simulated system of 400 BOBbots showing (**A**) dispersion when $F_M = 5$ g and (**B**) aggregation when $F_M = 19$ g; BOBbots shown in black belong to the largest connected component; those outlined in red are on its periphery. (**C**) Log-log plot showing the scaling relationship between the largest component's size N_{MC} and perimeter P_{MC} is the number of BOBbots for simulated systems of 100–400 BOBbots with $F_M = 5$ g (magenta) and 19 g (cyan). Each data point uses an average over 20 simulations. Inset: Phase plot showing the aggregation metric A_{MC} for the same BOBbot system. A sharp phase change is apparent just after $F_M = 10$g.

The results from [81] that we apply to the SOPS algorithm for aggregation also suggest the following relationship between the largest component's size N_{MC} and perimeter

P_{MC}. In dispersed configurations, P_{MC} should scale linearly with N_{MC}, meaning that most BOBbots lie on the periphery of their components (Fig. 3.6 A). In aggregated configurations, however, P_{MC} should scale as $\mathcal{O}(\sqrt{N_{MC}})$, approximating the optimal circle packing where the majority of BOBbots lie in the interior of the component (Fig.3.6 B). We validate these scaling relationships in simulation for a variety of system sizes ranging from 100–400 BOBbots (Fig. 3.6C) and find that the theory's predictions hold.

3.4 Object transport in the aggregated phase

Collective transport can be viewed under several lenses spanning equilibrium phenomena, like collective charge transport in metals, and non-equilibrium phenomena, like trickling water droplets on an irregular surface carrying surface matter it interacts with [85, 86]. In most cases, transport manifests from an order-disorder transition as seen in cases like cooperative transport of food by ants [87]. Although fundamentally different than the above systems, we now show how the above phase change from disordered (dispersed) to ordered (aggregated) states can be harnessed for transport.

Collective transport relies heavily on conformism between carriers for concerted effort and alignment of forces. In our robotic system, by maintaining high F_M value, we ensure the attainment of aggregated states where robots connect physically and cumulatively reinforce forces on untethered random objects (e.g., a box or disk) placed in the arena (Fig. 3.7 A). While the additive effects of robotic forces can collectively overcome the static friction of the objects, their ability to stochastically attach and detach gives the collective an added functionality of reconfiguring around the object and achieving a good grasp on it. This reconfigurability also aids reorientation and the magnification of forces that lead to various types of superdiffusive transport[4] (Fig. 3.7 B, blue). On the contrary, systems with weak magnets collectively disperse, typically leading to diffusive and subdiffusive transport, with some slightly superdiffusive fringe cases (Fig. 3.7 B, magenta).

[4]Object transport over time t is *diffusive* if the mean-squared displacement $\langle r^2(t)\rangle \propto ct$, for some constant $c > 0$. Transport is *subdiffusive* (resp., *superdiffusive*) if $\langle r^2(t)\rangle \propto t^\alpha$, for some $\alpha < 1$ (resp., $\alpha > 1$).

The kinds of superdiffusive object transport observed in the BOBbot systems seem to be affected significantly by the preferential circular bias in each BOBbot's noisy motion. Compared to collective transport by more capable entities, our strictly limited and stochastic paradigm causes the orientation and position of each BOBbot relative to the object to have great influence over the resulting transport. These effects are an interesting area for further study. Moreover, while our system does not aim to achieve directed (destination-oriented) object transport due to the stochastic dynamics associated with each BOBbot, this could be achieved by adding some rudimentary control mechanism exploiting morphology and mechanics.

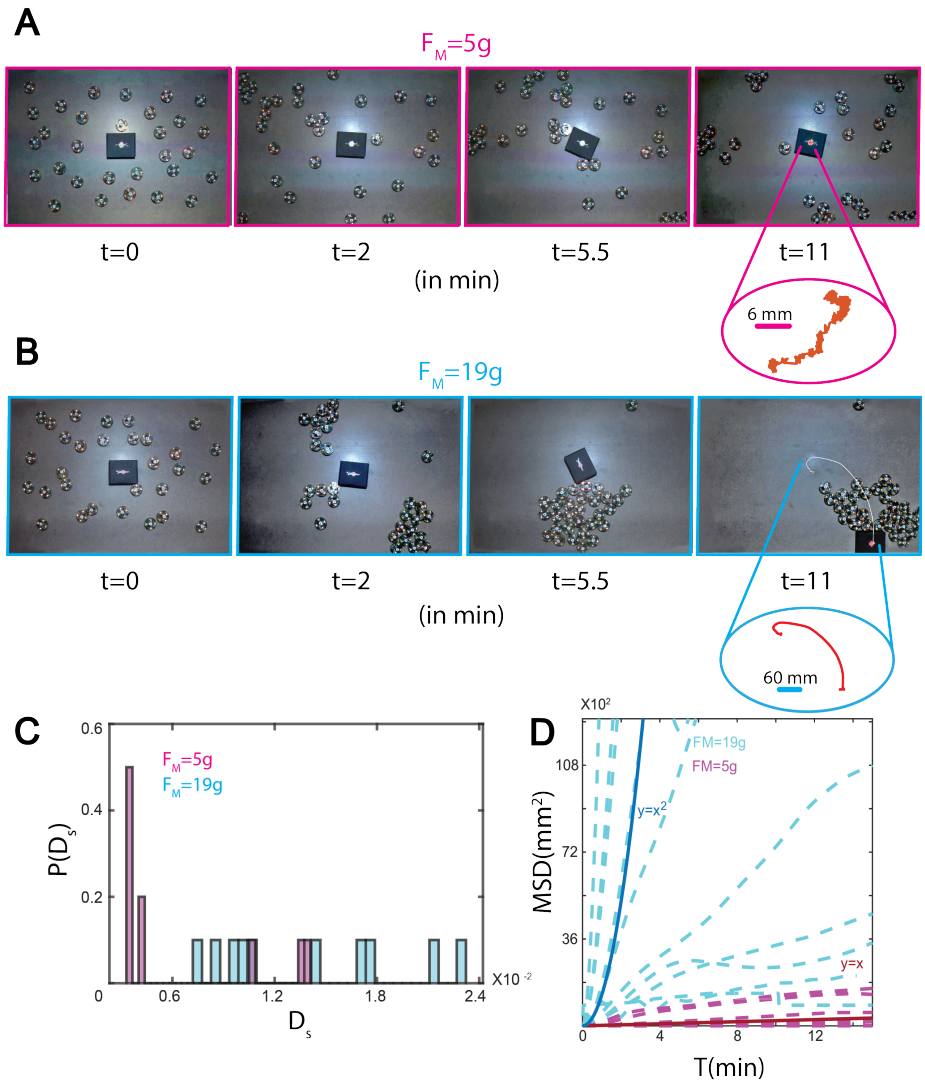

Figure 3.7: **Object transport using aggregation.** Time evolution snapshots of object transport by a system of 30 BOBbots magnet strength (**A**) $F_M = 5$g and (**B**) $F_M = 19$g. The outsets shows the object's complete trajectory (in red). (**C**) The probability density of trajectory lengths D_S for box transport over 10 trials for each of $F_M = 3$g (magenta) and $F_M = 19$g (blue) shows that dispersed collectives rarely move the object a significant distance. (**D**) Mean-squared displacement plot showing a mix of sub-diffusive to diffusive object movement with some superdiffusive outliers when $F_M = 5$g (magenta) and various types of superdiffusive transport for $F_M = 19$g (cyan). Each experimental trial (dotted line) was run for 15 minutes. Solid lines denote characteristic subdiffusive (magenta) and superdiffusive (cyan) trajectories.

3.5 Trade-off between velocity and magnetization

Similar to the Fixed magnetization Ising model that inspired our theoretical undertakings, we hypothesize that two parameters modulate the phase space of the robotic system, namely the velocity of each robot(v_0) and the inter-robot attractive forces (F_M). We posit that they have similar counteracting effects as the temperature and interaction energy of an Ising model respectively. To shine some light on this conjecture, we explore the entire phase space of the BOBbot system defined by these two parameters. This is experimentally done by using a display projector that projects slides with different gray intensities. The motor speed of each robot is proportional to the amount of light shone on the phototransistor on board. A detailed analysis of the relationship between the gray scale images to luminous intensity to velocity is provided in figure 3.8

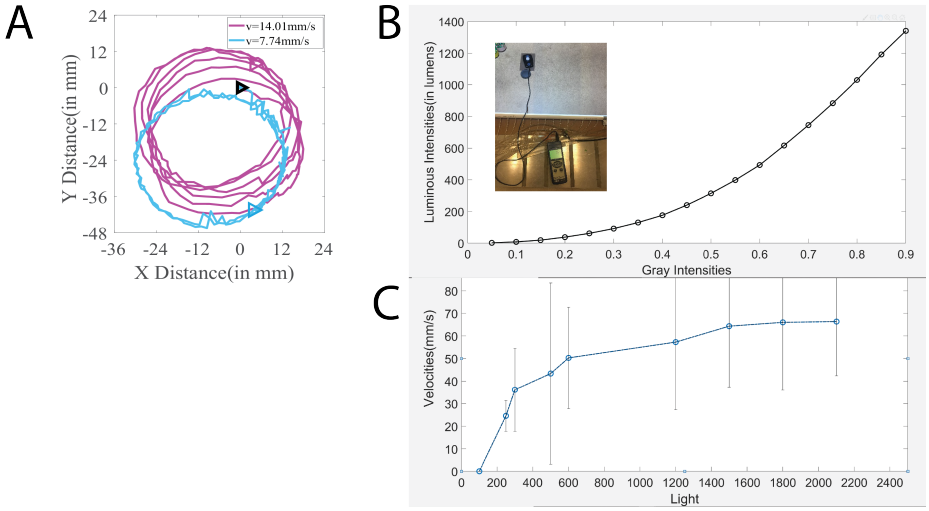

Figure 3.8: **Conversion of light to velocity.** (**A**) Example trajectories at two different saturated velocities ($v_0 = 0.14cm/s$ and $v_0 = 0.008cm/s$). (**B**) Luminous intensities as a function of grayscale values of an image with intensities scaled to the range 0 to 1(inset shows a light meter reading lumens. (**C**)Relationship between BOBbot saturated velocities(v_0) and Luminous intensities.

We run robotic aggregation experiments with different average saturated velocities (v_0) at different inter-particle magnetization (F_M). The results from these experiments are displayed in 3.9. Partially in unison with our hypothesis, we see a decrease in cluster sizes with an increase in average velocity as seen in 3.9A for the same magnetization value(F_M).

The relationship between velocity and max cluster size is, however non-monotonic (3.9B) and we observe a decrease in cluster sizes for a range of velocities both higher and lower than a threshold (v_t). We conjecture the decrease in cluster sizes below (v_t) to the fact that the chiral trajectories of the bots are bounded in space and thus statistically, the likelihood of each robot finding another is extremely low at velocities below a threshold in a finite time period. On the other hand, for high enough velocities, the clusters break more easily as they form at a given magnetization, thus explaining the downward trend for velocities higher than the threshold(v_t). Based on our experimental heuristics, the value of (v_t) is in the range $0.03 - 0.04cm/s$. We note that this value and the relationship observed is also a function of the saturated radius of curvatures of the trajectories made by the robots. In any case, further explorations need to be done to justify the observations of these systems. For the scope of this thesis, we limit our undertakings to a qualitative utilization of these findings in the following sections.

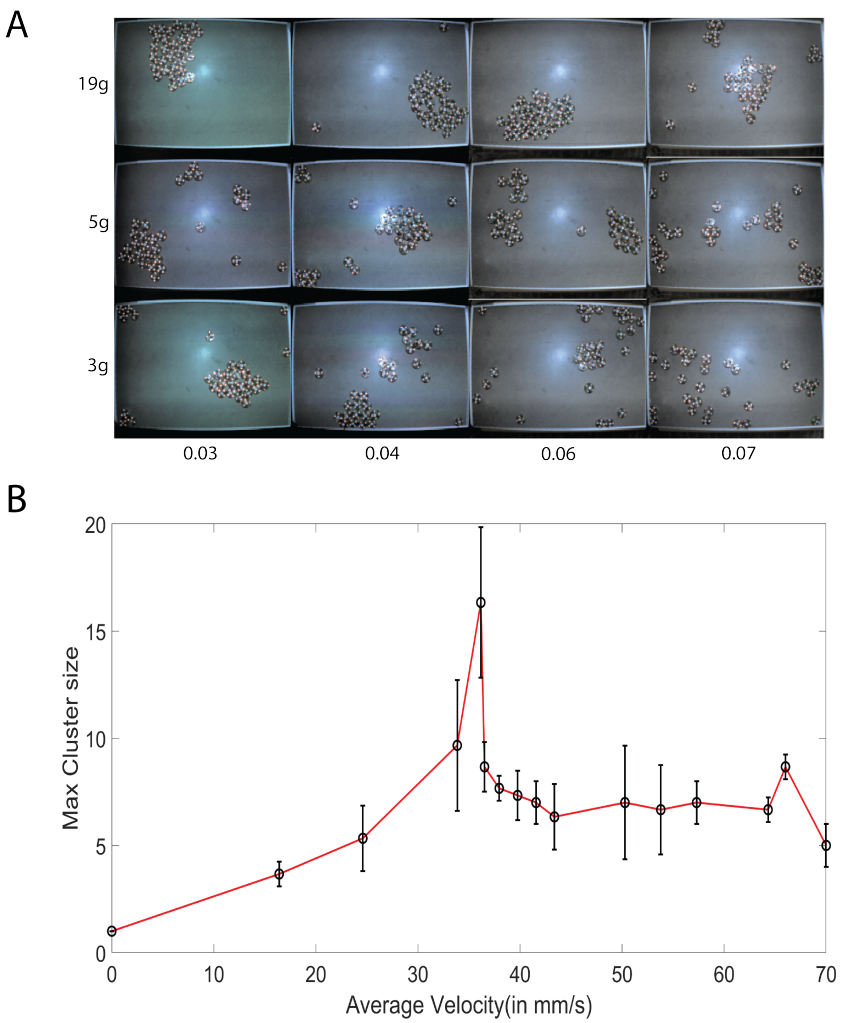

Figure 3.9: **Effects of changing average saturated velocities (v_0).** (**A**) Phase space of steady states at different velocity(v_0) and magnetization(F_M). (**B**) Max Cluster size at steady state is a non-monotonic function of BOBbot velocity (v_0).

3.6 Mechanical stress sensing to enhance aggregation

The span of this work has focused on collective behaviors that can be achieved without any robot computation, communication, proximity sensing, or persistent memory. Here, we study the effects of granting each BOBbot a very minimal sensing capability as a means to achieve aggregation even in the regime of weak magnet strengths.

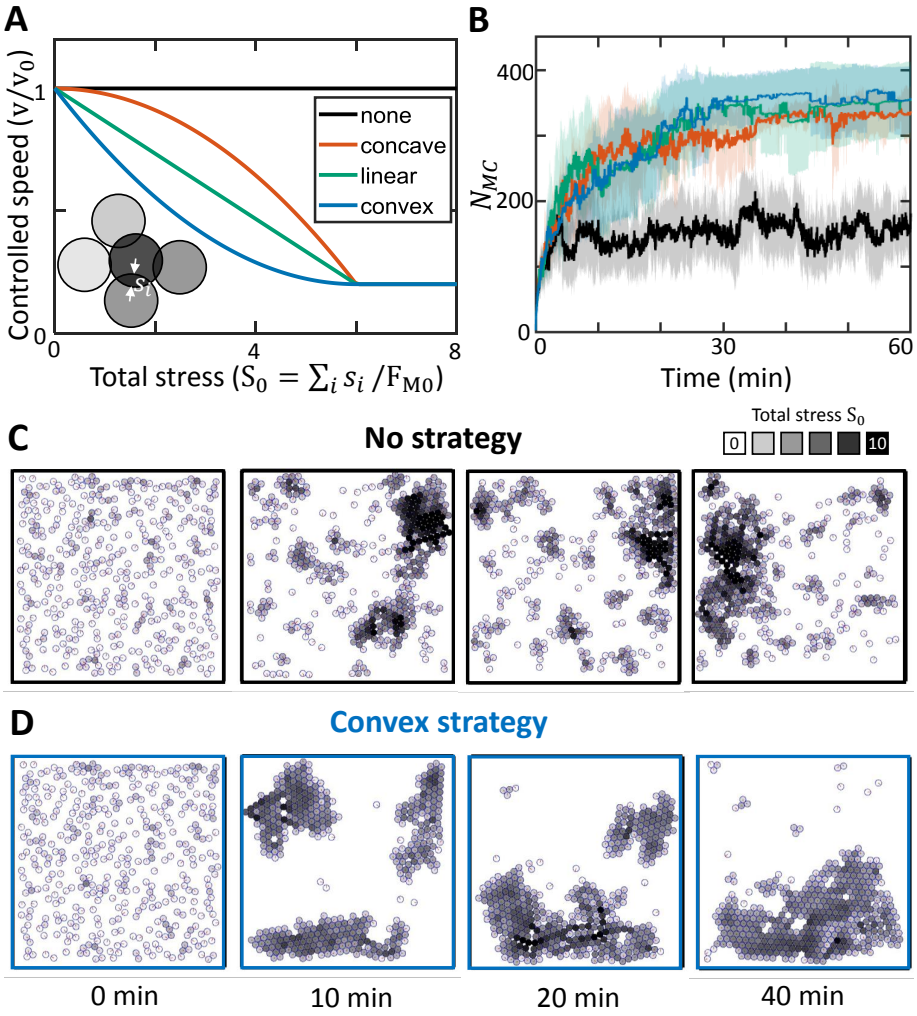

Figure 3.10: **Force sensing in simulation.** (**A**) Strategies for modulating simulated BOBbot velocities based on force sensing. The controlled speed v/v_0 is given by the BOBbot's current velocity v normalized by its initial velocity v_0. The normalized total stress on BOBbot j is $S_0(j) = \sum_{i \in I(j)} s_i / F_M$, where $I(j)$ is the set of BOBbots interacting with BOBbot j and s_i is the stress of BOBbot i on BOBbot j. (**B**) The size of the largest component N_{MC} over time for each of the force sensing strategies, averaged over 10 simulation runs of a 400 BOBbot system with $F_M = 7$ g. All force adaptive strategies significantly outperform the non-adaptive one, managing to aggregate even with weak magnets. (**C–D**) Time evolution snapshots for a simulated 30 BOBbot system using $F_M = 7$ g with no strategy and the convex strategy, respectively.

In simulations, we enable each BOBbot to reduce its driving velocity in proportion to the amount of mechanical stress it senses from its neighbors. Thus, as increasing numbers of neighbors aggregate around a given BOBbot, it experiences higher mechanical stress and slows its movement, making it less likely to escape from its current attachments.

Among the four functional relations between velocity and mechanical stress as shown

in Fig. 3.10 A, we observe that those utilizing this additional sensing capability produce significantly enhanced aggregation, even in the regime of weak magnets (Fig. 3.10 B–D). The simulation results suggest a promising future for controlling collectives of relatively incapable robots through minimal additional sensing.

To recapitulate, we build a theoretical and experimental model for dynamic aggregation with a foundation of principles from a statistical physics model. We see a phase change from dispersed to aggregated state across a single system parameter (F_M) which can act as a potential control knob for future explorations. We show a preliminary study to exhibit this potential in carrying out a collective task of object transport. We end the chapter with a slightly elaborate exploration of the phase space of the steady states produced by two competing system parameters v_0 and F_M and highlight how the trade-off between the two can produce interesting results with some additional rudimentary sensing. In the next chapter, we intend to study a similar system to figure out how the aggregation behavior and related tasks can be persistified over long time horizons.

CHAPTER 4
LAZY ROBOT COLLECTIVES

Robots are limited in their ability to persistently perform tasks based on the depletion times of their power reserves. Thus, any task that they perform is constrained in time or depends on the incorporation of functionally complex algorithms for energy management such as recharging cycles. The energy requirement of the collectives scales with the complexity of the task and environment, and centralized charging hardware such as solar cells often becomes impractical outside of controlled laboratory settings. Task persistification in robotic swarms is the ability of the collective to perform a task for a duration longer than the expected battery life of an individual in the swarm. In this chapter, we suggest an approach to persistification of tasks through distributed inactivity. Inspired by biological and physical counterparts that succeed in subverting this energy depletion challenge by utilizing distributed inactivity, we propose that individuals in artificial collective systems intermittently hibernate i.e., turn off their batteries to preserve energy. We benchmark the effectiveness using simulation studies of a modified brush-bot system, where individuals lack any computationally intensive sensing and processing capabilities as seen in the previous chapter. To illustrate the efficacy of the proposed framework, we demonstrate improvement in a debris clearing task with collectives incorporating activity modulation, in contrast to systems without hibernation.

Natural active matter systems such as insect swarms, birds, and fish can perform coordinated tasks continually for days, often building remarkable landmarks like gigantic termite mounds encompassing 30 meters in diameter [20] and deep subterranean fire ant nests [21]. Robotic swarms, on the other hand, are typically limited by their ability to perform long-duration tasks, as their run time is bounded by the batteries used to power them. Long-term autonomy in robotic swarms can help various applications such as environmental monitor-

ing and exploration, intra-warehouse transportation, and debris or rubble management, etc. As robots step out of conventional laboratory settings for such tasks, research to develop energy aware task driven algorithms have gained substantial interest in the recent decade [77, 75, 88, 89, 90, 76]. This line of inquiry has led to some advancements in developing energy aware control policies that account for the limited energy reserve of each robot and incorporate that information in the algorithm development process.

Most of these approaches, however, require some non trivial, memory intensive digital computation to be carried out by each robot that is dependent on microcontrollers or central processing units [77, 75, 88, 89, 90, 76]. We are interested in achieving task persistification in robots that are constrained in terms of memory and computation power with bounded energy reserves. This aligns with an area of multi-agent robotics that utilizes systems of individual robots inspired by rudimentary physical systems. These systems provide a major advantage in terms of scalability. This can be useful in micro-scale and high risk applications that require constant throughput; where bulkier, costlier, and smarter robots requiring the computation of complex state and environment information may be impractical [91, 92, 93].

Our objective is to explore methods by which a constrained system can attain long duration autonomy to fulfill tasks persistently where each robot has a fixed energy reserve. In particular, we are interested in testing distributed inactivity as a mechanism to attain long-term dynamic aggregation behavior in systems similar to the robotic system introduced in Chapter 3. As previously defined, dynamic aggregation is defined as the process by which robots accumulate and move together as one unit. This collective behavior has potential applications in area coverage, collective transport, and related tasks which utilize the collective strength of the cohort in motile form. We envision one such task, clearing debris in a confined arena, and we develop approaches to continuously sweep the arena clean of the debris through persistent dynamic aggregation.

A variety of natural systems exhibit heterogeneous activity levels and dynamic activity

modulation between agents [19, 78]. In the next chapter, we will study fire ants swarms that exhibit heterogeneity in activity during tunnel excavation for clog control and improved efficiency of transport of excavated materials. Additionally, lazy ants can increase their activity level when active nest mates are removed, to maintain a tunnel density that is optimal and leads to maximum excavation efficiency under the given constraints [19]. A complementary perspective is obtained from studies of mixtures of active and passive colloids which suggest that concentrations as low as 15% of active colloids can lead to phase separation in these mixtures [79]. Inspired by these findings, we investigate whether a small fraction of active individuals can sustain the task of dynamic aggregation in the system described in Chapter 3.

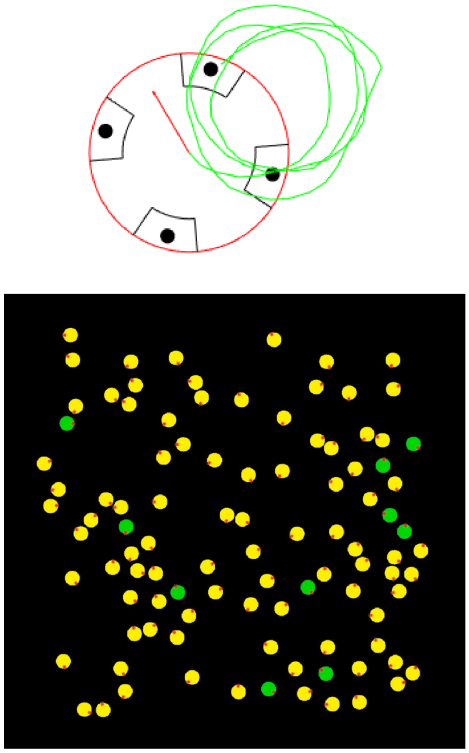

Figure 4.1: **Fixed inactive simulation setup for $\mathbf{p_A = 10\%}$, $\mathbf{N = 100}$ robots.** Green: active robots (trajectories are shown in upper panel); yellow: inactive robots)

We formalize the problem setup by presenting our experimental details and hypothesis. We wish to solve the problem of persistent dynamic aggregation for time periods of several orders of magnitude longer than the lifetimes of each individual robot. Towards this goal,

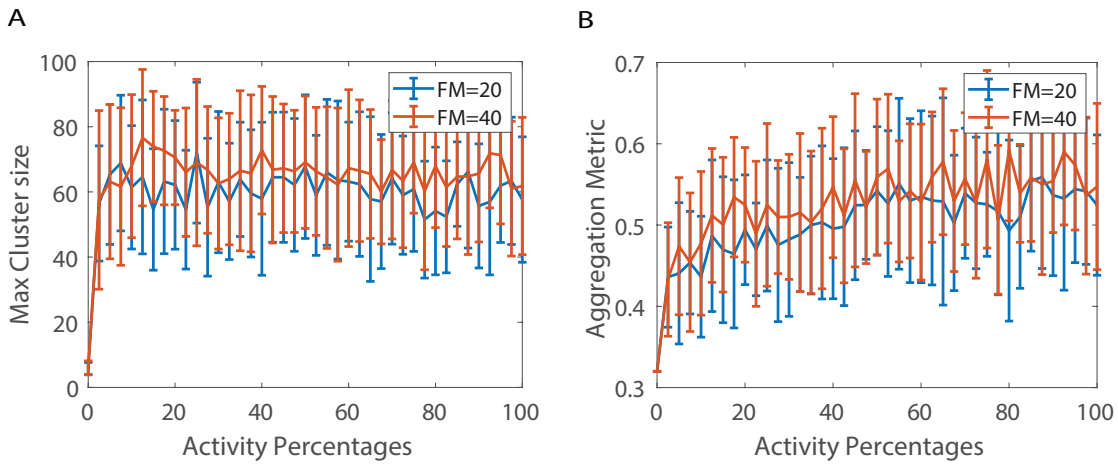

Figure 4.2: **Steady state aggregation efficiency as functions of activity percentage (p_A) for N = 100 robots.** A) Max cluster size (N_{MC}) B) Aggregation metric (A_M). Two different values of inter-robot interactions strengths are depicted: $F_M = 20g$ of force (blue) and $F_M = 40g$ of force (red). The central tendency plotted here is the mean value and the error bars depict one standard deviation.

we study a class of vibration-driven robots whose dynamics and features are similar to the system introduced in the previous chapter. We gather data on the simulation platform modeled after these types of robots to support our ideas of using distributed inactivity as a means to prolonging aggregation behavior in the robot swarms.

The overall dynamics of an active robot are described by the same set of equations as in Chapter 3

$$\begin{cases} m\ddot{\vec{r}} &= F_D\hat{u} - \eta\dot{\vec{r}} + \vec{F}_{env}(\vec{r},\varphi) + \vec{\xi}(t) \\ I\ddot{\varphi} &= \tau_D - \eta_\varphi\dot{\varphi} + \tau_{env}(\vec{r},\varphi) + \xi_\varphi(t) \end{cases} \tag{4.1}$$

where $\vec{r}$ is the robot's position vector and φ is its orientation vector. F_D is the translational drive, η is the translational drag coefficient. The environmental forces are represented by $\vec{F}_{env}$, which is a combination of the inter-robot attractive force F_M, the inter-robot frictional force f_{BB}, and the sterical exclusion force $F_{BB,n}$. $\vec{\xi}(t)$ is the translational noise term. The rotational motion and torques are modeled similarly. The translational drive direction and orientation are coupled.

An inactive robot is subject to only short range environmental forces, namely, attractive

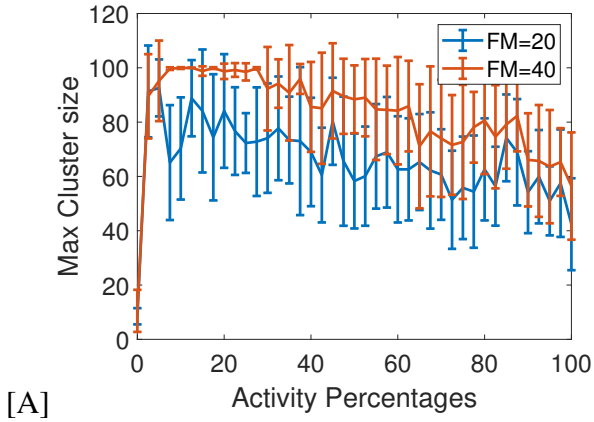

[A]

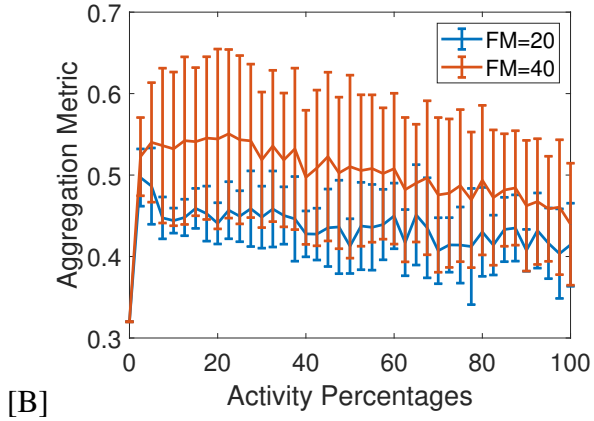

[B]

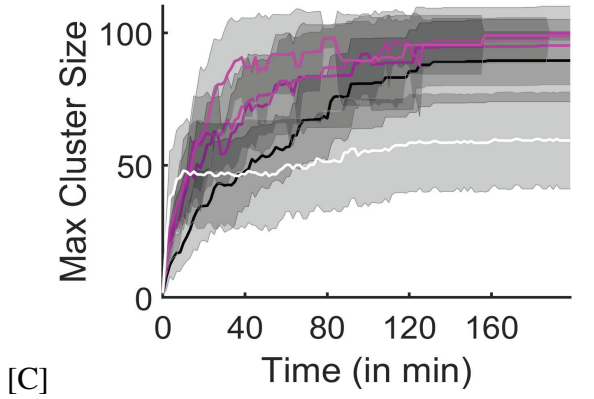

[C]

Figure 4.3: **Steady-state aggregation efficiency as functions of activity percentage ($\mathbf{p_A}$) in the case of temporal modulation of active identities for $\mathbf{N = 100}$ robots.** A) Max cluster size (N_{MC}) B) Aggregation metric (A_M) C) Time evolution to steady states for different activity percentages. (black: $p_A = 2.5\%$; white: $p_A = 100\%$; magenta: $p_A = 10-20\%$ and the shaded regions depict one standard deviation of variation). For Subfigures A) and B), the values of inter-robot interactions strengths as well as the error-bar scheme is the same as those in Figure 4.2. The system used here has the following attributes: L=20 minutes, T=200 minutes; t=1.67 minutes

forces exerted by other robots, boundary forces, and friction. The equations of motion for an inactive robot do not include drive and stochastic noise terms described in Equation 4.1

	Description	Value
m	Mass of the robot	0.060 kg
R_0	Radius of the robot	0.030 m
I	Moment of inertia	2.7e-5 kg·m^2
v_0	Saturated speed	60.0 mm/s
ω_0	Saturated angular velocity	2.40 rad/s
F_D	translational drive	0.06 N
τ_D	rotational drive (torque)	5.5e-4 N·m
η	translational drag coefficient	1.0 kg/s
η_φ	rotational drag coefficient	2.3e-4 N·m·s
F_{M0}	magnetic force on contact	20, 40 gf
d_0	magnetic force decay length	1.5 mm
μ	bot-bot friction coefficient	0.143
μ_W	bot-wall friction coefficient	0.143

Table 4.1: **List of parameters used in simulations.**

and reduce to:

$$\begin{cases} m\ddot{\vec{r}} &= \vec{F}_{env}(\vec{r},\varphi) - \eta\dot{\vec{r}} \\ I\ddot{\varphi} &= \tau_{env}(\vec{r},\varphi) - \eta_\varphi\dot{\varphi} \end{cases} \tag{4.2}$$

An inactive robot at rest will, therefore, not move and not rotate in the absence of other active neighbors and environmental factors.

Arena $\mathbf{A}$ is defined by a continuous 2D square space $\in x$. Any robots in close proximity to the boundary experience an inward exponentially decaying force which is highest at the boundary and reduces with distance away from the boundary as described before.

More details about the simulation parameters and constants are tabulated in Table 4.1. All simulations are performed with the help of high throughput computing clusters of the open science grid (OSG) [94, 95].

Similar to the previous chapter, the efficiency of aggregation is measured with two quantities at steady state: (a) "Max Cluster Size" N_{MC}, which is the number of robots in the biggest aggregate, and (b) "Aggregation Metric" A_M, which is defined as $N_{MC}/(k_0 P_{MC}\sqrt{N})$, where P_{MC} is the number of robots in the perimeter of the aggregate and k_0 is a scaling constant measured from the optimally compacted system configuration possible for the given

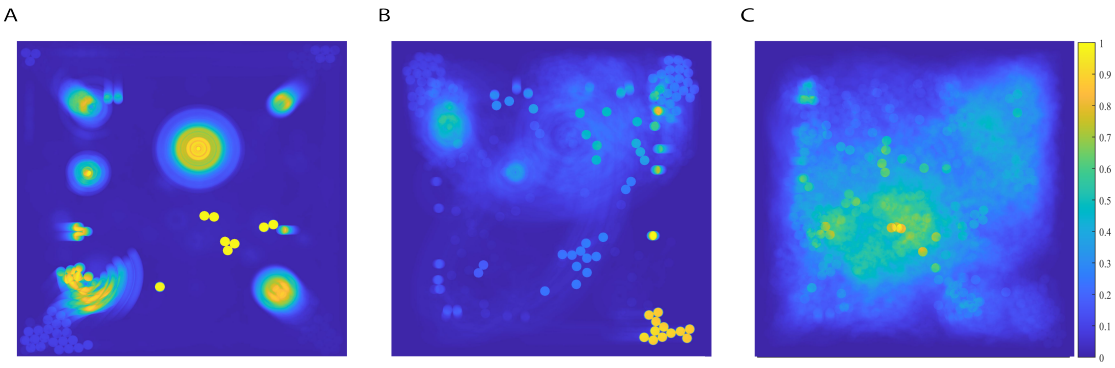

Figure 4.4: **Heat maps of area coverage at stationarity for N = 100 robots.** A) $p_A = 100\%$ system without temporal modulation B) $p_A = 10\%$ system without temporal modulation C) $p_A = 10\%$ system with temporal modulation. The value of pixels is scaled between 0 to 1 with 1 being the most visited pixel in the experiment shown. The inter-robot interaction magnet strength is $F_M = 20g$ of force.

system size N. While N_{MC} gives a measure of how much the collective aggregates, A_M gives a sense of how compact the aggregated clusters are. The compactness of aggregates is a useful quantity while considering tasks that require the collective physical strength of the cohort such as transporting objects, and hence is an important quantity to consider.

The purpose of the simulations reported in the following sections is three-fold. In the first set of simulations, we wish to explore how the system's aggregation behavior changes with different fractions of inactive robots. Our first hypothesis is as follows:

Hypothesis 1: Let us consider a system of N vibration-driven robots with unbounded energy, where the robot dynamics and features are as described above. For such a system confined in arena $\mathbf{A}$ at a fixed density ρ, and where p_A represents the percentage of active robots, the ability to dynamically aggregate at steady states is unaltered when the proportion of active robots $p_A \geq \epsilon$ where ϵ is a very small quantity specific to the system.

In the second set of simulations, we want to quantify and compare the effect of temporally modulating the identity of active individuals on dynamic aggregation efficiency. This leads us to our second hypothesis.

Hypothesis 2: For a system of N robots with a fixed energy reserve rendering a lifetime of L, confined in arena $\mathbf{A}$ at a fixed density ρ, we claim that for a given fraction of active

robots p_A, the ability to dynamically aggregate persistently is enhanced through temporal modulation of the identity of active individuals. We also claim that this holds if robots hibernate periodically in time such that the overall activity of the system on an average is $\sim$p$_A$ at any given time point.

Finally, we wish to test the efficacy of our approaches with a debris clearing task.

Hypothesis 3: For a system of N robots with a fixed energy reserve rendering a lifetime of L, confined in arena $\mathbf{A}$ at a fixed density ρ, we hypothesize that a system that maintains distributed inactivity fraction $p_A \geq \epsilon$, where ϵ is as defined in *Hypothesis 1*, and performs periodic activity modulation can clear debris more efficiently and persistently than a system where every robot is active at all times i.e., $p_A = 1$.

4.1 Fixed Inactivity effects

In this section, we present results from simulations with fixed percentages of active robots. These simulations are performed in arena $\mathbf{A}$ with a fixed population size (N), and each simulation is instantiated with a fixed percentage of active individuals p_A, where p_A is chosen to be between 0 to 100%. The active individuals are initialized at uniformly distributed random positions in the arena. The simulated robots are given an unlimited lifetime in this series of experimentation. The experiments at each p_A are carried out 10 times to get statistically significant results. Figure 4.1 shows a cartoon representation of the fixed inactivity setup.

In support of our posited *Hypothesis 1*, we find that a very small fraction of active individuals ($p_A \gtrsim 10\%$) can lead to efficient aggregation of the cohort, and the size of the biggest cluster at steady state (N_{MC}) saturates for the range ($p_A \gtrsim 10\% - 100\%$). This is shown in Figure 4.2 which shows the variation of N_{MC} and A_M as a function of p_A. In other words, its apparent that increasing the number of active robots beyond ($p_A \gtrsim 10\%$) in this particular system is redundant, and does not add any value in terms of the expected aggregation behavior of the collective. This validates our first hypothesis.

However, we also notice that the aggregation metric, which is a measure of how compact the aggregates are, increases by a small amount with more active robots. This is intuitive, as the inactive robots do not have the ability to rearrange and reshuffle actively to find the compact configurations. Therefore, the higher the number of inactive robots, the more likely it is that the clusters are stuck in non-compact local neighborhoods around the inactive robots.

For these findings to be useful in both achieving long-term aggregation dynamics and also to be able to form compact clusters, we hypothesize that modulation of the identity of the active individuals temporally will establish escape routes from unfavorable local minima, while also conserving the energy of the system globally.

4.2 Spatio-Temporal activity modulation

We test our second hypothesis which states that if robots hibernate periodically in time while keeping a fixed percentage of active robots alive at all times, long-term autonomy can be achieved in specific collective tasks in the described system. We design another set of experiments in which N robots with a fixed lifetime L are instantiated at randomized positions and orientations in the arena $\mathbf{A}$. A random number generator is used to choose the identity of the active robots for a given p_A and the identities are altered every t time units for a duration $T = f * t$ where f is chosen to be large enough to ensure $T >> L$.

As shown in Figure 4.3, we observe continued dynamic aggregation for longer durations, i.e., time frames much larger than each individual lifetime (L), with temporal activity modulation of a small p_A. In fact, we observe that the best performance is obtained in the $p_A \sim 10\% - 20\%$ range. This can be partially attributed to the fact that $p_A \sim 10\% - 20\%$ systems have lower effective average velocities and thus, form larger clusters than a $p_A = 100\%$ system for a given attractive force F_m as shown in chapter 3. Additionally, such a temporal modulation of the activity of a small proportion of robots also helps the system escape local minima caused by the inherent idiosyncrasies of the robots

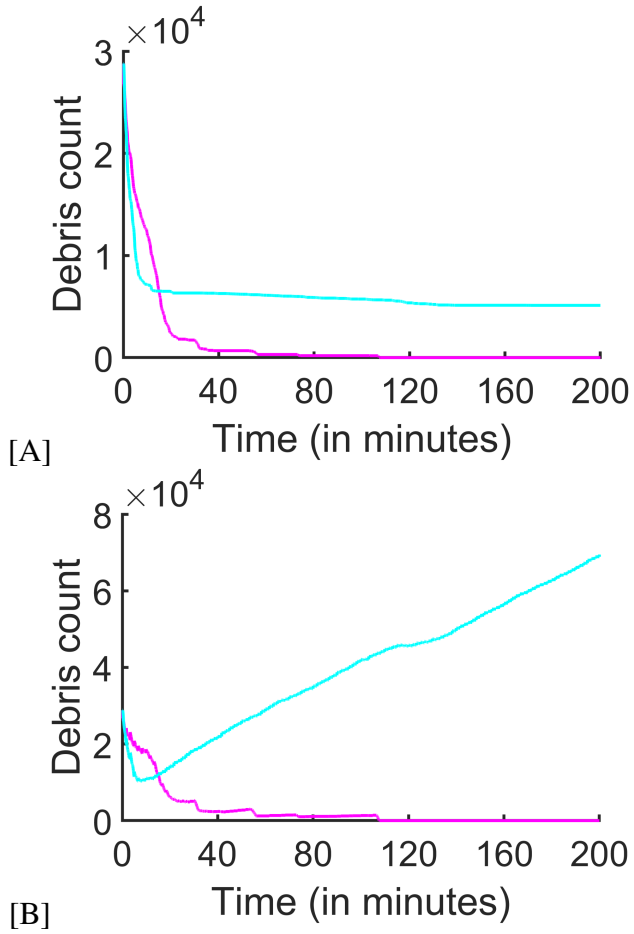

Figure 4.5: **Debris removal as a function of time for N = 100 robots.** $p_A = 100\%$ system without temporal modulation (cyan) and $p_A = 10\%$ system with temporal modulation (magenta). A) with fixed debris concentration B) with recurring debris at every t_R=100 seconds. The inter-robot interaction magnet strength is $F_M = 20g$ of force. The representative systems used here has the following attributes: L=20 minutes, T=200 minutes; t=1.67 minutes

such as the chiral trajectories. Thus, not only do the $p_A \sim 10\% - 20\%$ systems perform better in terms of persistence, but these systems also traversed larger areas with larger aggregates compared to other values of p_A. This is shown in Figure 4.4 with the help of heat maps of area coverage at stationarity.

For a team of robots to be able to utilize the benefits of temporal activity modulation in a decentralized fashion, each robot would need to choose its inactivity without any user input. We chose a simple tweak to our algorithm to make our experiments decentralized. At every active identity alteration event at t time units, each robot makes a probabilistic

determination of its activity state with p_A being the probability that it is active, all the while keeping all other experimental details consistent with the discussions above. The analysis of the data from this distributed algorithm shows results similar to the ones obtained without the decentralized setting.

The above results support our second hypothesis and show that under the constraints of limited energy, we can persistify dynamic aggregation by periodically switching robots to be inactive while maintaining a small population of active robots at all times.

4.3 Improved area coverage with activity modulation

We can demonstrate the practical usability of the above findings in this section by empirically showing the efficacy of distributed activity modulation in a task that would benefit from long-term autonomy. Towards this end, we chose a debris clearing task that would require persistence, specifically in the presence of evolving debris count. We compare the efficiency of two separate setups: a) temporal activity modulation, and b) no-inactivity i.e., all robots are active. Finite sized particles are randomly distributed all around the arena at initiation. The goal of each robotic system is to remove as many particles as it can by hovering over the particles like a collective robotic vacuum cleaning system. The particles are then removed based on the number of times a particular area is visited by any robot.

We observe, once again, that the $p_A \sim 10\% - 20\%$ system with temporal modulation outperforms an all-active system ($p_A = 100\%$) in terms of debris removal efficiency and magnitude as shown in Figure 4.5A. The experiments are repeated in a variation of the same setup where debris particles are introduced randomly in the arena at regular time intervals while the initial conditions are maintained to be the same. In this setup, we obtain similar results and the $p_A \sim 10\% - 20\%$ systems are able to keep up with evolving debris content and maintain a clean arena uniformly, and for longer durations of time in comparison to the $p_A = 100\%$ system. These results are depicted in Figure 4.5B which shows the amount of debris "cleaned" by the robots as a function of time.

In summary, these explorations show that under the constraints of limited energy, long-term autonomy is attained for a task that requires surveying large spatial areas persistently. This is achieved through distributed inactivity in the system coupled with periodic modulation of the identity of the active individuals. This works for instantaneous active percentages of as small as $p \sim 10\% - 20\%$ and these systems outperform systems where the entire population of robots are tasked to clean at once ($p_A = 100\%$), even when debris gets re-introduced in the arena periodically.

CHAPTER 5
LAZY ANT COLLECTIVES

The approach we took for persistification of tasks in lazy robots was inspired by biophysical collectives. We complement that study with a similar quest on how biological collective systems conserve energy and optimize efforts. We present studies on a collective fire ant system that provides a different insight into how heterogeneity in activity levels of individuals can be beneficial to the collective outcome. Sometimes, groups of interacting active particles, insects, or humans can form clusters that instead hinder the goals of the collective unlike the situations described in the previous chapters. In these cases, the development of robust strategies for the control of such clogs is essential, particularly in physically confined environments.

There are diverse examples in both living [96] and artificial [40, 97] active materials that spontaneously form clusters that persist for long time durations. But, there are certain tasks that demand a steady flow of agents, where such formations can be disadvantageous: Confined active systems such as pedestrian or vehicular traffic jams [98], competing bacterial biofilms [99], high-density migrating cells [100], jammed herds [101], and robot swarms [102] can produce high-density clogs that readily form glasslike arrests of flow [103]. In such systems, the ability to dissolve clusters and prevent their formation [103], particularly in the absence of global knowledge of the state of all elements, is crucial for uninterrupted flow.

Social insects perform many tasks that demand clog minimization and mitigation[104]. Substrate excavation specialists such as fire ants (Solenopsis Invicta sp.) cooperatively create nests of complex subterranean networks (Fig.5.1 A) consisting of tunnels in soil that support bidirectional traffic without lanes [105]. Laboratory experiments in [106] revealed that, in the early stages of nest construction, the few-millimeter-long ants construct vertical

tunnels approximately one body length in diameter [106]. These narrow tunnels benefit the climbing ants as they transport bulky pellets because close proximity to walls allows limbs, body parts, and antennae to aid slip recovery [107]. In addition to the benefits narrow tunnels provide for climbing and pellet transport [107, 106], we also claim that the ants benefit from narrow tunnels by expending less energy to dig wider tunnels to the same depth. Such benefits would be useful in the early stages of new nest construction (e.g., after the colony is flooded out) during which establishing the colony underground is critical. But although the structure of the tunnels seems to benefit individuals, physical-model experiments make it clear that excavation can suffer as a result of clogging during high-traffic conditions [108]. So, in this chapter, we explore how such high traffic situations are avoided in these collectives. For this, we present a series of experimental, computational, and robotic studies to show how counterintuitive behaviors like individual idleness and retreating help optimize tunnel density by limiting the severity and prevalence of clogs, thereby enabling rapid excavation by the collective.

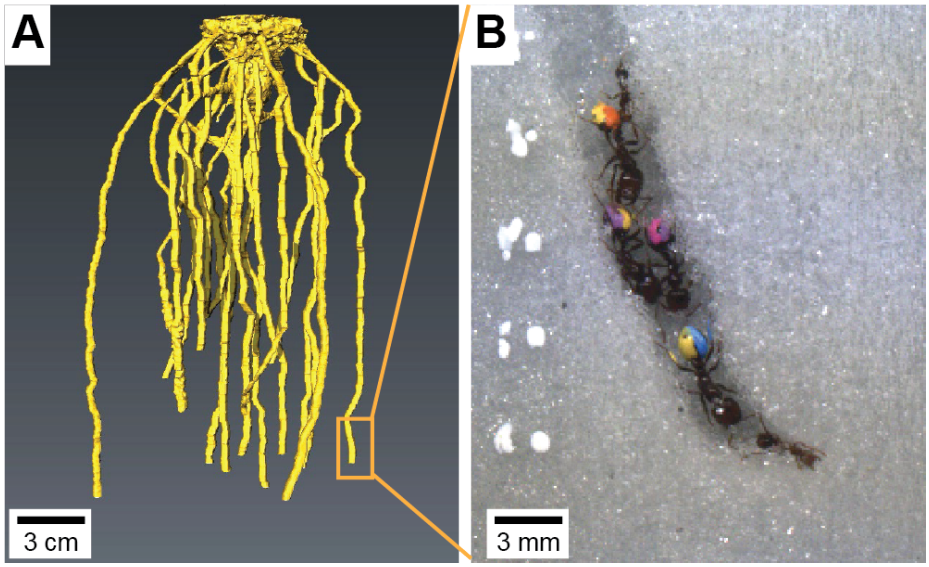

Figure 5.1: **Confined and crowded biological excavators.** (A) X-ray reconstruction of S. Invicta fire ant excavation in a large container (25 cm wide) filled with 240- to 270-m-diameter glass particles (supplementary materials). (B) Painted S. Invicta workers excavating a single tunnel along the wall of a transparent container with 0.25-mm-diameter wet glass particles.

5.1 Ant Experiments show inequality in workload distribution

Ten S. Invicta nests were collected during the spring, summer, and autumn of 2014, 2015, and 2016 at the Research and Education Garden of the University of Georgia, GA, USA, and the Chattahoochee-Oconee National Forest, GA, USA. Nest collection and colony extraction were performed according to methods found in [109]. Ants were housed in plastic bins for 23 months at an ambient room temperature of $23 \pm 3°$C with a relative humidity of 30 ± 2, and fed Vespula larvae and supplied with tap water twice a week.

[1]In laboratory settings, we monitored the activity of fire ants as they excavated a cohesive granular medium. Small groups of 30 ant workers from the laboratory-housed colonies were isolated in transparent containers containing particle-water mixtures (5.1B) with a soil moisture content, defined as the ratio of total water weight to total solid weight. The experiments were conducted for 48 hours in W=0.01 and W=0.1 wet soils (3 trials for each soil moisture). All the experiments were repeated for 3 different colonies. The abdomens of the workers were marked in different colors. A plastic insert separated ants from cohesive soil and featured a single entry point next to the transparent wall of the container. A small ($\sim 5mm$) indentation was made next to the transparent wall of the container to prompt excavation. Ants excavated for 48 hours, with individual ants entering and exiting the tunnel hundreds of times. Similar to the previous study [107], ants constructed narrow vertical tunnels through a stereotyped process of grain and multigrain (pellet) removal and transport, followed by tunnel ascent and substrate deposition upon exit [106]. The top portion of the container was used by the ants for excavated soil deposition. A camera mounted to a motorized linear stage tracked a small region of the tunnel face (Fig. 5.2A).

The container was fixed on the motorized stage with the camera precisely focused on the first 2 cm of the tunnel at a distance of approximately 3 ant body lengths. As the tunnel grew in length, the relative positions of the tunnel and the camera were adjusted such that the tip of the tunnel was always visible. The camera was streamed, during which real-time

[1]Experiments and simulations were done in collaboration with CRAB Lab member Daria Monaenkova

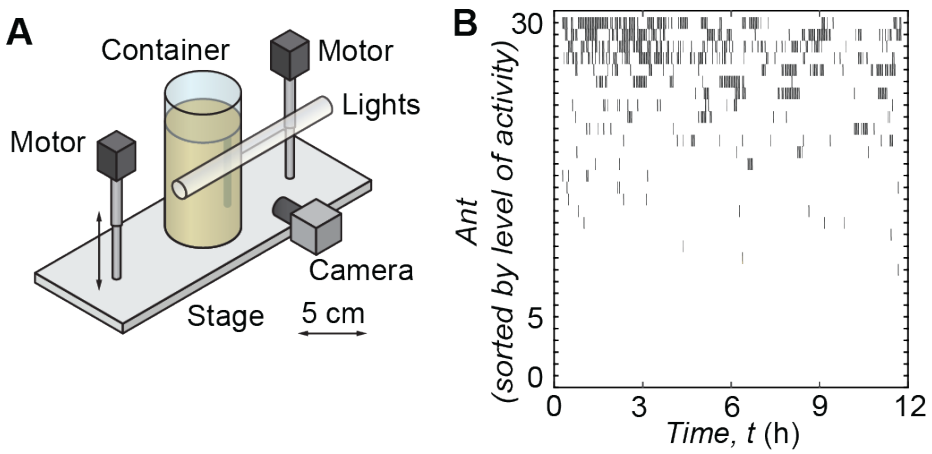

Figure 5.2: **Unequal workload distribution in fire ant nest excavation** Biological observations reveal workload inequality and reversal behaviors in ants. (A) Experimental apparatus to track ant excavation; container inner diameter is 5.21cm. (B) Visitation map derived from experimental data. Each point in the map indicates the presence of a particular ant (out of 30 ants) ordered from most active to least active (y-axis) in the tunnel at a time t. (moisture content of W = 0.1).

processing detected the presence of ants based on pixel intensity. Based on this detection of an ant in the camera's field of view, the camera was triggered to record 60 seconds of video at 15 fps. Work among excavators was characterized by manually counting the number of occurrences in which an ant visited the tunnel. Ants were classified as visitors if they appeared within the camera's view of the tunnel at any point within the duration of the experiment. Non-visitors were those ants that were never detected by the camera. Ants exhibited a variety of behavioral tasks during collective excavation. A large fraction (0.22 ± 0.1 for soil moisture content of 0.01 and 0.31 ± 0.13 for soil moisture content of 0.1) of ants never entered the tunnel to excavate during the 48-hour period of observation. As seen in Fig. 5.2B, ants that visited the tunnel face ("visiting" ants) varied in activity level.

We quantified this activity inequality among visitor ants using Lorenz curves[78]. Points on the Lorenz curves in Fig. 5.3B link the cumulative fraction of workers in the population to the cumulative share of activity by that fraction. The Gini coefficient (a measure of statistics dispersion) [78] derived from the shape of the curve reflects the inequality in the workload distribution within visiting group. In general, when the Gini coefficient is

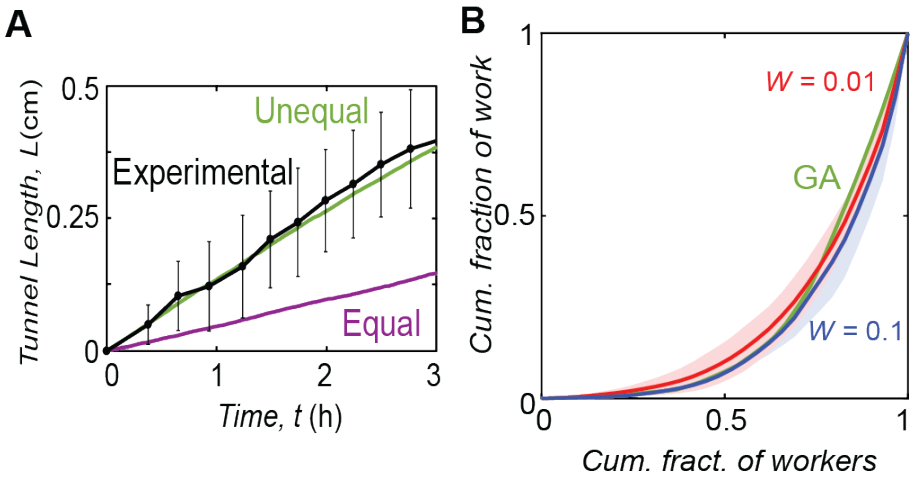

Figure 5.3: **Distribution of inequality and tunnel excavation efficiency.** (A) The growth of tunnel length over time. Shown are average experimental results ± standard deviation (SD)/2 for S. Invicta workers (black) and simulations for groups with equal (purple) and unequal (green) workload distribution. Error bars denote 1 SD in each direction. (B) Lorenz curves for workload distributions obtained in wet 0.25-mm-diameter glass particles with soil moisture content of 0.1 (blue) and 0.01 (red) and a CA model (green) whose excavation rate was optimized with a GA. Shaded areas correspond to the standard deviation from three experiments.

close to 0, the effort of the ants during the excavation is nearly equal. In contrast, a Gini coefficient close to 1 indicates highly unequal workload distribution with a few active diggers in the visiting group carrying out the bulk of the workload. To calculate the Lorenz curves and Gini coefficients of the 48-hour experiments, the only ants that were included were those that were detected as having visited at least once during those 48 hours. In all the experiments combined, Lorenz curves were characterized by a Gini coefficient, G = 0.75 ± 0.10 and displayed similar functional forms across a variety of experimental conditions (see Fig. 5.3B and 5.4A). We also recorded tunnel length over time (Fig. 5.3A) and compared it with simulations(explained in the next section) to highlight the efficacy of unequal workload distribution.

In the presence of competing tasks, like foraging or brood care, task allocation in ants can change depending on colony needs [110]. To investigate temporal variation in ant excavation workload, we divided 48-hour experiments into 12-hour epochs (time periods). To calculate the Lorenz curves and Gini coefficients for 12-hour epochs within

those 48-hour experiments, we only considered the ants that visited within those 12-hour time-frames. This ensured that the calculated workload distributions only ever considered the working population of that measured time-period. Please note again that visitors, who did not successfully dig and reversed without a pellet were also counted in the excavation effort because non-excavating visitors still expend energy in an excavation attempt and contribute to tunnel traffic. Although individual activity varied among epochs 5.4A and B, the cumulative workload distribution was independent of epoch [one-way analysis of variance (ANOVA) $F_{3,20} = 0.85, P = 0.48$] and soil moisture content (one-way ANOVA, $F_{1,23} = 2.54, P = 0.13$).

Similar workload inequality characteristics are observed from the first 3 hours, by which point the tunnel length has typically not yet exceeded 2 cm in length.

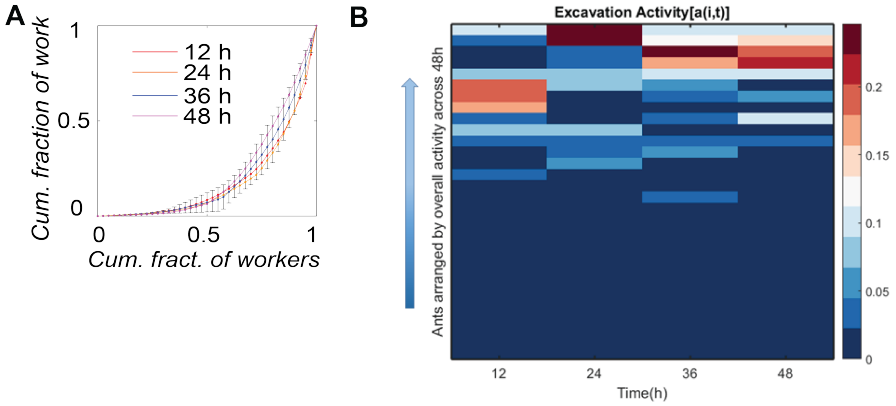

Figure 5.4: **Distribution of inequality across 12-hour epochs.** (A) Experimental Lorenz curves of ant workload distribution for individual 12-hour epochs of 48-hour trials. Error bars indicate standard deviation from multiple trials averaged over 6 trials (3 trials in 0.25 mm diameter glass particles at W=0.1 moisture content and 3 trials in W=0.01). (B) Dynamic activity pattern of individual ants over different time epochs. The ants are arranged by their overall activity for 48-hours ascending from the bottom upwards. Excavation activity, a(i,t) is the number of tunnel visits per 12-hour epochs for an ant i divided by the total number of tunnel visits within that epoch.

5.2 Unchanged workload distribution with removal of active diggers

To determine how the removal of the top 5 most active diggers from the colony affects the workload distribution and efficiency of tunnel construction, groups of 30 ants were set

to excavate the same cohesive granular media. The excavation process was recorded for 3 hours. The ants were removed from the container and set to rest for at least 12 hours. During this time, the recorded data was analyzed to determine the 5 excavators that most contributed to tunnel construction. These active excavators were removed from the group and the experiment was repeated for an additional 3 hours. Interestingly, a different set of excavators were activated during the second phase of the experiment and contributed to the bulk of the work (5.5A). The rates of tunnel construction and the Gini coefficients were measured and found to be comparable between the first (before removal) and the second (after removal) parts of the experiment (5.5B). The results were obtained in the experiments with three different colonies and averaged. Tunnel construction rates varied little between the two phases of the experiment. In fact, the individual growth rate increased slightly: 0.58 ± 0.2 mm/ant within the first part of the experiment versus 0.67 ± 0.3 mm/ant in the second part. The workload distribution also did not change and the Gini coefficient was 0.73 ± 0.15 for control (first phase of experiment) and 0.62 ± 0.06 for active removal (second phase). After the most active excavators from the first part were removed, several idle diggers increased their contribution to the excavation task. The contribution of the 5 most active excavators within the first and the second parts of the experiment was comparable: 74 ± 21 versus 74 ± 5 of all observations in the tunnel. The most active diggers of the second part of the experiment had contributed to only 10 ± 11.4 of total observations (546 ± 65.8) during the first part of the experiment. Thus, we show that individual ants were able to modify their behavior in response to the changing traffic dynamics of the tunnel.

5.3 Voluntary modulation of activity

Similar to the experiment above, we conducted another series of 2-day experiments where we again took a group of 30 ants and set them to excavate the same cohesive glass media. Experiments were recorded for 3 hours and then, the ants were removed from the container and set to rest for at least 12 hours. The top 5 excavators who contributed the most to

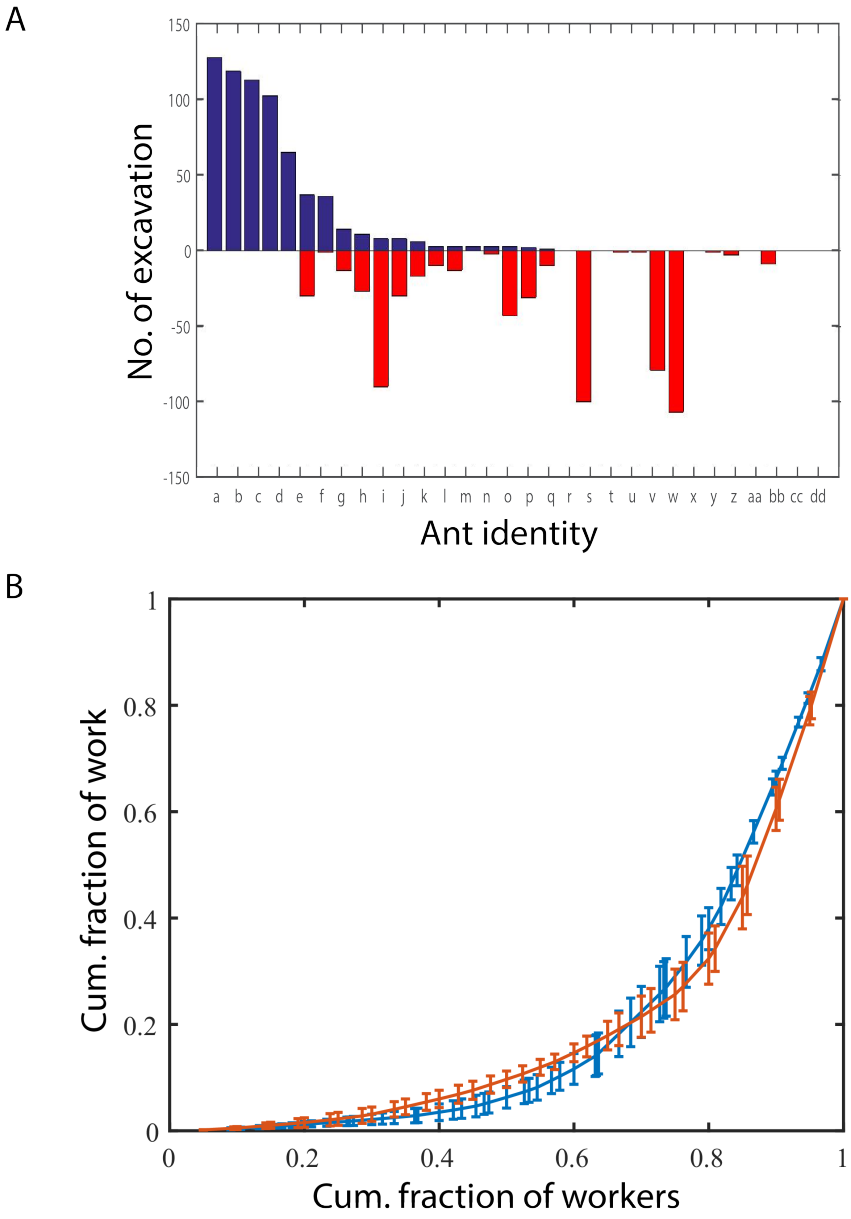

Figure 5.5: **Active Removal experiment**(A) Bar graph showing the number of trips made by each ant to the tunnel in the first half of the active removal series of experiments (blue) and second half of the experiments (red) after removal of the top 5 active diggers. (B) Lorenz curves displaying similarity in distribution of inequality in workload in both half of the experiments.

tunnel excavation were again noted and the experiment was repeated with the same set of 30 excavators the next day. Please note that the top excavators were not removed in these runs. The experiments were repeated over 3 colonies and the relevant metrics were averaged over the 3 experiments. Similar to the previous observations, both halves of the

experiments exhibited a Lorenz workload distribution (5.6B) and the Gini coefficient did not change significantly with 0.66 ± 0.1 for the first half of the experiment and 0.69 ± 0.15 for the repeat second half. However, the identity of the top 5 excavators changed and this change is again shown with the help of bar graphs in figure 5.6A. The tunnel construction rate was nearly identical in both parts of the experiments with 0.89 ± 0.1 mm/ant growth within the first part of the experiment and 0.78 ± 0.25 mm/ant in the second part of the experiment.

This highlights the fact that the inactivity in the ants is not genotypic, meaning every ant is capable of doing the maximum excavation per ant observed. They however, choose to modulate their activity to maintain a Lorenzian workload distribution similar to the kind seen in previous sections. We would like to note here that activity modulation was observed in the 12 hour distributions of workload as seen in 5.4A and B as well. The mechanisms behind the modulation remain unclear.

Given the consistency of the inequality in workload distribution in all these experiments, we hypothesize that variations in idleness (low activity levels) within a population may play an adaptive role in modulating the crowded conditions of confined tunnel traffic and aiding maximum traffic flow in tunnels and in turn, improve excavation efficiency.

5.4 Reversal Behavior in ants

Another useful behavior exhibited by the ants during tunnel excavation was reversal/retreat. Reversal behaviors were characterized by ants entering the tunnel and returning to the exit without carrying soil pellets. During the first 3 hours of the excavation, reversals occurred for $26 \pm 13\%$ of trips for soil moisture content of 0.01 and $18 \pm 3\%$ of trips for soil moisture content of 0.1. These events were often associated with local crowding at the excavation face (Fig. 5.7A) ($16 \pm 12\%$ of trips for soil moisture content of 0.01 and $10 \pm 2\%$ of observations for soil moisture content of 0.1). Reversal behaviors in crowded conditions also occur on foraging trails as seen in (18), and similar phenomena have been observed in

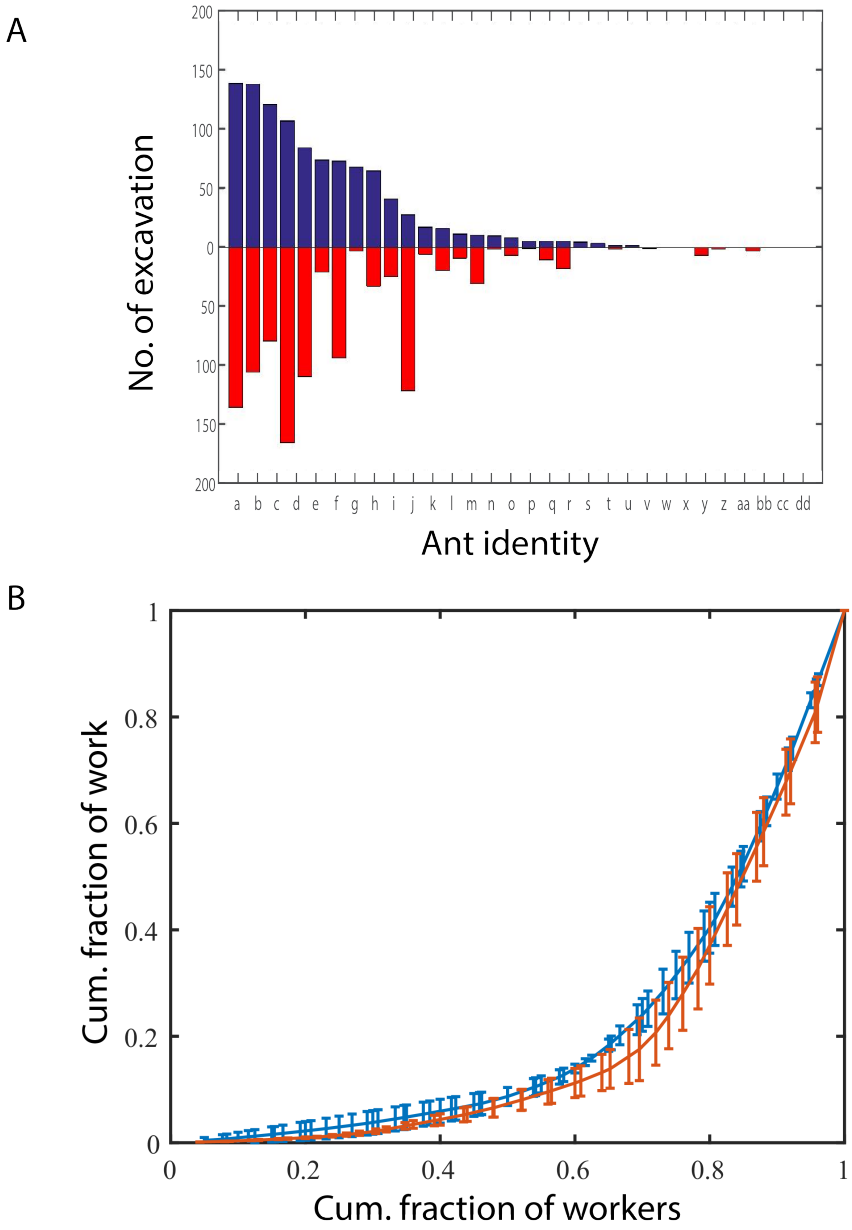

Figure 5.6: **Active Repeat experiment**(A) Bar graph showing the number of trips made by each ant to the tunnel in the first half (blue) and second half (red) of the active repeat experiments. (B) Lorenz curves displaying similarity in distribution of inequality in workload in both half of the experiments.

swarming bacteria [99]. The incidence of this seemingly unproductive behavior increased with increasing overall activity of ants (Fig. 5.7F), suggesting that this behavior serves as a feedback mechanism for mitigating clogs during excavation.

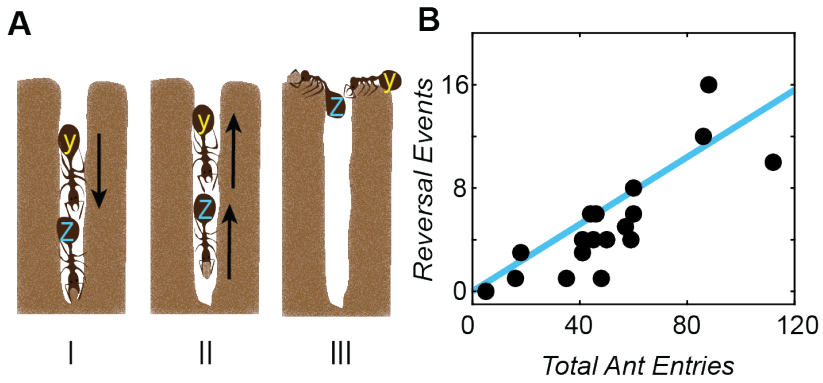

Figure 5.7: **Ant retreat with higher tunnel densities.** (A) Illustration of observed reversal behavior. (I) Ant Ys path to excavate is blocked by ant Z. (II) After Z collects a pellet, it reverses, (III) forcing Y to reverse without excavating. (B) Total number of reversal events vs total ant visitors for the first 3 hours of ant excavation. (moisture content of W = 0.1) Each data point represents total reversal events and total entries counted for 30 min segments collected from 3 experiments. Linear fit (blue line) with R2=0.69.

5.5 Optimal ant density in tunnels maximize excavation efficiency

To systematically examine the effects of idleness and individual retreating behaviors on excavation performance, a cellular automata (CA) excavation model (Fig. **??**A) was developed in collaboration with other members of the Goldman Lab. Such models are useful in elucidating the dynamics of biological and vehicular traffic [103, 111]. The model consists of a lattice (the tunnel) with a width of two cells [similar to S. Invicta tunnel widths (20)] where each lattice site can be occupied by soil, empty space, an ascending CA ant, and/or a descending CA ant as shown in Fig. 5.8. The CA ants can move, change directions, excavate, deposit a pellet, or rest. As seen in the biological experiments, activity for the workload distribution in the CA model was measured by counting instances when CA ants visited the tunnel within three body lengths (cells) of the excavation site.

We simulated the behavior of CA ants using both equal workload distributions (which we refer to as active CA ants) and unequal workload distributions (which we refer to as Lorenz CA ants) with identical reversal probabilities. In unequal workload distributions, individual CA ants were assigned individual entrance probabilities defined as the probabil-

ity that a CA ant will enter the tunnel. The initial entrance probability distribution for the 30 CA ants was taken from the biological distribution.

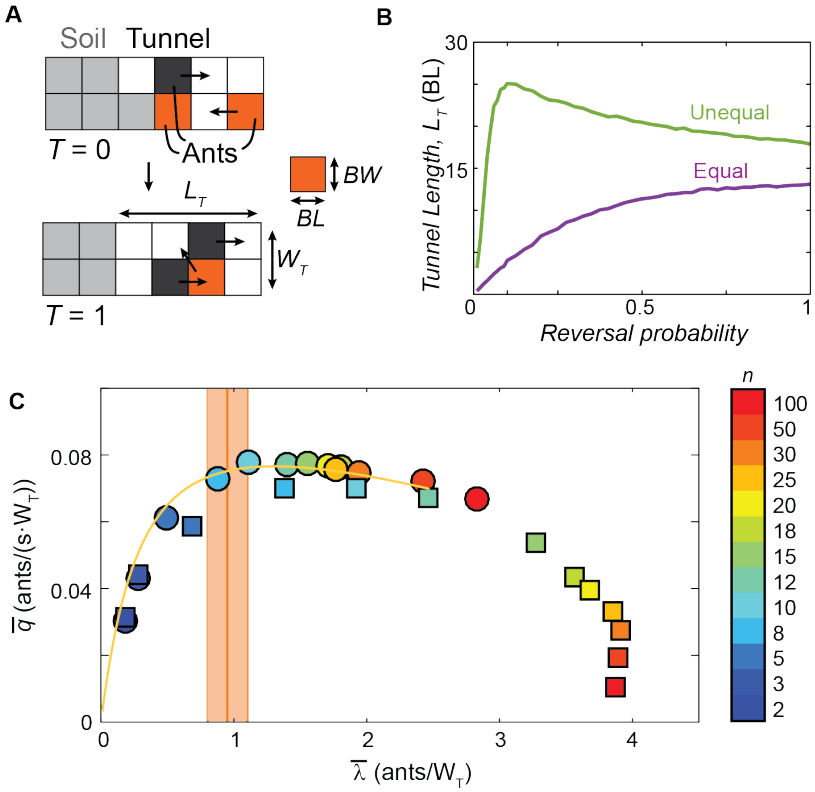

Figure 5.8: **Optimal traffic flow in narrow tunnels through workload inequality.** (A) Schematic showing the main components of the CA model. Cell colors denote soil (light gray), tunnel (white), ants moving toward the excavation site (orange), and ants exiting the tunnel (dark gray); T is the simulation time-step. (B) Excavated tunnel length after 24-hour simulation time versus reversal probability for equal and unequal (optimized for 30 CA ants) workload distributions. (C) Simulated traffic flow versus CA ant occupancy for groups of equally (squares) and unequally (circles) active ants. The color bar indicates the size, n, of the excavating group. Embedded shaded bar shows number of ants divided by time in seconds times tunnel width v/s number of ants divided by tunnel width, measured in excavator body widths from experiments. Experimental ant observations reveal an average occurrence around the density (orange-shaded region, where the orange centerline is the mean and the extents are one standard deviation away from the mean) that maximizes traffic flow.

During a time-step, if its path toward the excavation area was blocked, a CA ant would reverse direction toward the exit with a probability, R, of 0.34; R was set by the proportion of total reversal events observed for 0.01 soil moisture in the biological experiments. The CA model that used unequal workload distribution and reversals reproduced experimentally observed biological ant digging rates (5.3A).

We claim that the unequal workload distribution and reversals were linked to the uniform flow of CA ants in the tunnel. To clarify this, we measured the average flow rate of successful excavators, q, versus the average tunnel-width normalized occupancy of excavators, l (the ratio of average number of ants in the tunnel to tunnel width measured in ant body widths). To generate a wide range of average occupancies, we varied the population size of the CA system. The flow rate was optimal at an intermediate occupancy (5.8C). This nonmonotonic trend in q versus l is characteristic of traffic flow in various multiagent systems, including bridge-building army ants[112] and vehicle traffic [113, 114], and is referred to in traffic literature as the fundamental diagram [115]. Active ants, which do not modulate their workload distribution, increase tunnel occupancy with increasing population and thus exhibit optimal flow rates for only a few population sizes. By contrast, simulated ants that uses Lorenzian distribution of workload produced tunnel occupancies in the ideal range by generating increasingly unequal workload distributions for increasing CA ant population sizes. The CA model also revealed the importance of the reversal behavior in conjunction with unequal workload distributions. Although the active excavation could be improved by sufficient reversal probability, only a small amount of reversal was needed to increase the excavation performance in the unequal distribution as seen in 5.8B.

Of particular importance is the observation that fire ants produced tunnel densities in the ideal range shown by the simulations (Fig. 5.8C, orange-shaded region). The calculation of these densities from experiments is explained in the next section.

5.6 Calculation of tunnel-width normalized ant occupancy

The control experiments from the active removal experiments were used for calculating tunnel-width normalized ant occupancy, $\bar{\lambda}$ (average number of ants in the tunnel/tunnel width). Each frame in the video ($15fps * (60 * 60 * 3s) = 162000$ frames) was analyzed in MATLAB to identify each colored ant using image processing techniques as shown in 5.9B. The number of color blobs identified in each frame was representative of the number

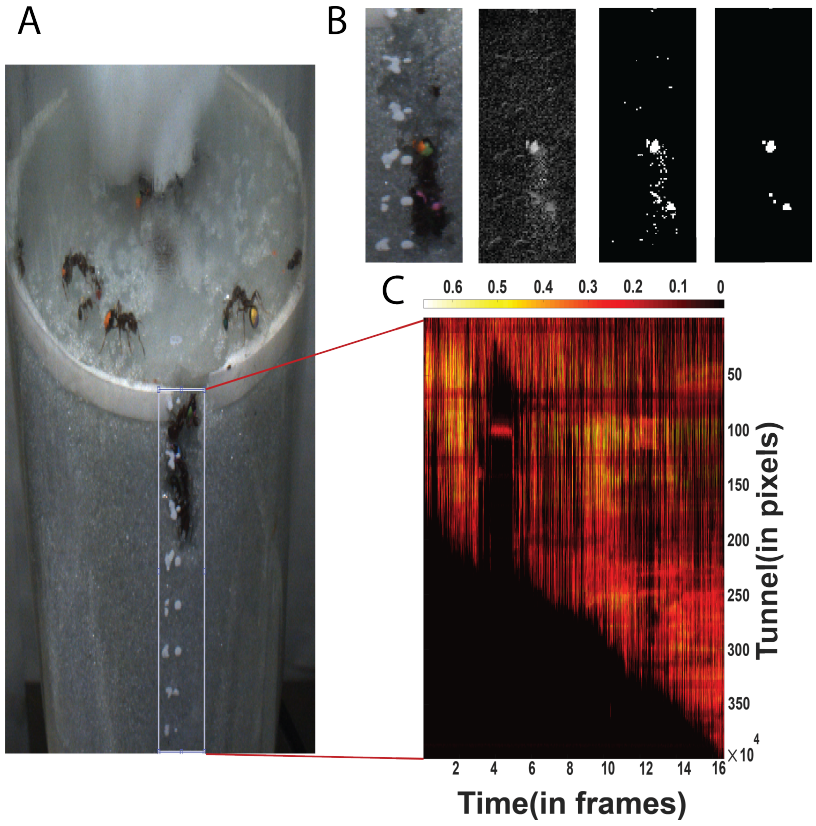

Figure 5.9: **Calculation of ant tunnel density and heatmap of traffic flow.** (A) Sample tunnel face created through excavation with defined region of interest (ROI) for density and flow analysis. (B) Image processing steps showing the color blob extraction for density estimates. (C) Heatmap of ant flow in the tunnel illustrating seamless flow and tunnel growth.

of visiting ants in that particular frame. The tunnel width was approximated to be 2 ant body widths (BW) following results from a previous study ([116]). The occupancy was then temporally averaged over 3 minute chunks ($15fps * (60 * 3s) = 2700$ frames) at 3 different time points in the experiment. This was repeated for 3 different experiments and the average experimental ant occupancy across these experiments is projected on the fundamental traffic diagram in Fig. 5.8C with shaded areas representing standard deviation from the 3 experiments.

Cluster Dissolution times show the importance of laziness and retreats

We characterized how cluster severity was affected by reversals and unequal workload distributions through an analysis of cluster formation. Clusters in 30-ant simulations were

identified at each simulation time point and categorized by the number of CA ants that comprised the cluster. Any group of ants that blocked the entire tunnel width was considered a cluster. We found a prevalence of large clusters for extremely low reversal probabilities in both equal (Fig. 5.10A) and unequal (Fig. 5.10B) workload distributions. A minimal increase in reversal probability reduced the prevalence of the largest clusters from forming. However, even accounting for higher reversal probabilities, equal workload distributions resulted in wider distribution of cluster sizes, whereas the optimized workload distribution produced a sharper concentration of small clusters, which were more easily dispersed (5.10C). Thus, cluster mitigation is most effective using both reversals and unequal work probabilities in combination.

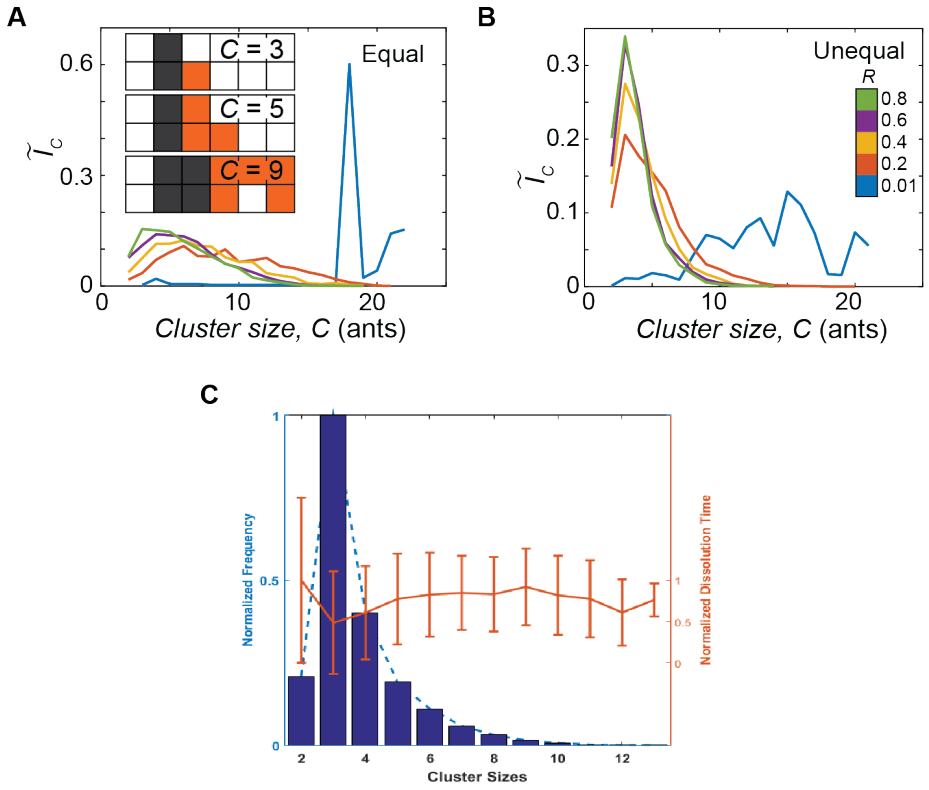

Figure 5.10: **Cluster size and frequency dynamics.** Proportional number of CA ant clusters $\tilde{I}_c = I_c/I_{total}$, of different sizes, C, measured over 24 hours for (A) equal and (B) unequal (optimized for 30 CA ants) workload distributions at different reversal probabilities (blue: 0.01, red: 0.2, yellow: 0.4, purple: 0.6, green: 0.8). (C) Cluster dissolution times as a function of cluster size overlaid on cluster frequency distribution plots. Sample illustrations for different cluster sizes in (A) inset.

5.7 Robotic explorations

We next used a system of excavating robots to test if the above theoretical strategies could improve traffic in confined experimental situations with more complex, unpredictable interactions. Because, presently, robot mobility in real-world environments is poor relative to biological systems and because real collisional interactions not modeled in CA are typically neglected in swarming robot studies [40], such robophysical [117] studies can aid robot design and control for real-world robot swarms, as well as suggest hypotheses for studies of ant traffic (18), adaptive behaviors, and morphological features for crowded excavation and movement. [2]Groups of roughly elliptical robots with similar aspect ratios to the biological ants were tasked with excavating a model cohesive granular medium of hollow plastic spheres containing loose magnets; this design allows clumps of media to be formed, analogous to the pellets of cohesive soil formed by the biological ants (13). The robots followed simple instructions triggered by onboard sensory feedback of the surrounding environment [108]. Previous work in swarm robotics [118] used similar decentralized strategies in conjunction with collision-avoidance schemes [40, 119] to produce emergent flocking behavior. By contrast, our robots detected collisions with push switches on their outer shell, which triggered navigation strategies such as steering away and readjusting to promote clog resolution. To challenge the robots, a tunnel (Fig. 5.11A) with a width of three robot widths (or 1.5 robot lengths) was constructed, which, combined with the oblong robot shape, forced a challenge of turning around in confined spaces. We tracked the positions of the robots in the main tunnel area (i.e., excluding the excavation site) to generate space-time overlap maps of robot positions (see Fig. 5.11, B to D), which give visual insight into robot flow during excavation. We first examined systematically how excavation performance changed as numbers of robots increased for our active protocol, which assigned equal work desire to all diggers: After soil deposition, each robot immediately returned to the tunnel to excavate. Despite constraints on maneuverability, sensing, and

[2]The alpha version of the robots was built by CRAB Lab member Vadim Linevich

morphology, the robophysical experiments demonstrated qualitatively similar performance to the ants and the computational and theoretical models. For example, measurement of the average flow rate, q, of successful excavators (which we quantify here as the number of deposits per minute) revealed that excavation performance increased with an increasing number of robots in the trial (N) until the system became sufficiently crowded (Fig. 5.11E).

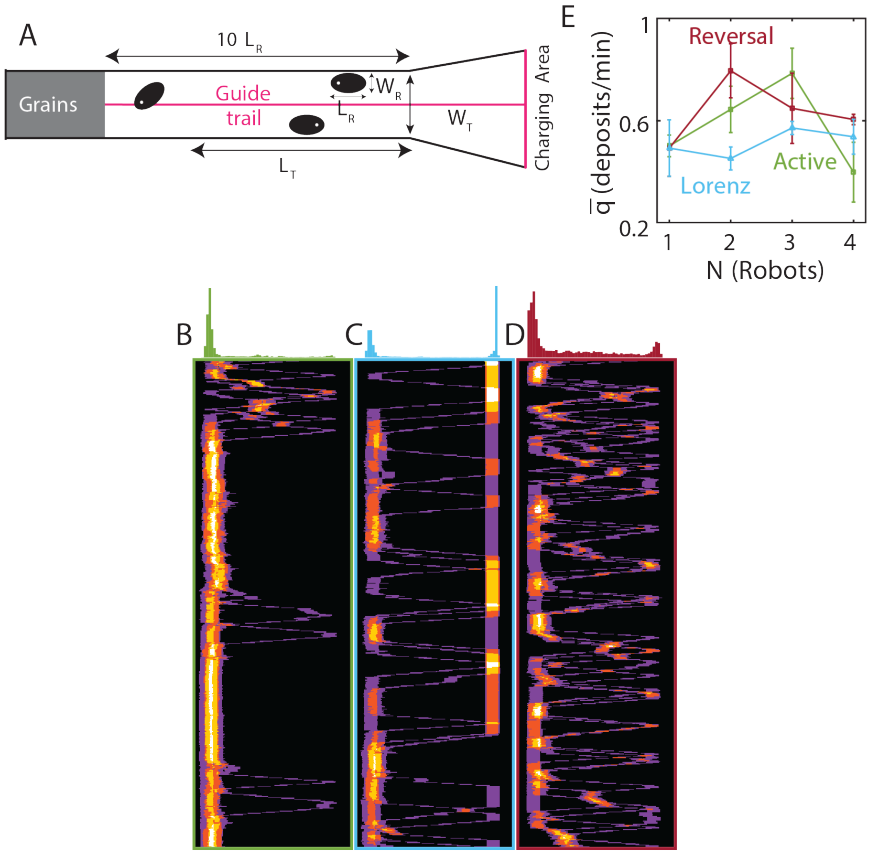

Figure 5.11: **Traffic flow and local dynamics during robot excavation** (A) Schematic of the excavation arena indicating the tunnel length excluding the excavation area (LT); robot width, (WR); robot length, (LR); and tunnel width, (WT). A pink centerline along the tunnel was monitored by the robots onboard cameras, enabling them to follow the tunnel path. (B to D) Experimental space-time overlap heat maps of robot positions (x-axis) for four-robot trials of (B) active digging, (C) Lorenz digging, and (D) reversal digging. Color indicates the number of robots occupying a particular space and time: one (purple), two (orange), three (yellow), and four (white) robots. Histograms above the graphs show the frequency of occurrence of clusters with two or more robots at different lateral positions. (E) Average flow rate, $\bar{q}$, SD measured in deposits per minute versus number of robots in the experiment, N, for active (green), Lorenz (light blue), and reversal (maroon) strategies.

To characterize how clustering led to performance degradation in the active protocol, we measured the frequency of cluster occurrences, denoted Ic. Here we defined clusters

as groups of robots of number Nc, whose center positions were within a robot length of each other (supplementary materials). Such clusters occurred most frequently at the excavation site (histograms in Fig. 5.11, B to D), yielding phase separation [120] in the system, whereby a portion of robots were jammed at high density, whereas others moved smoothly through the tunnel at low density. To discover how the strategies of idleness distributions and reversals affected clustering and traffic dynamics in the robots, we implemented two protocols inspired by the biological observations and theoretical models. Like the CA model, in the Lorenz protocol, we implemented an unequal probability to enter the tunnel derived from experimental ant workload inequalities. We also implemented a separate robot reversal protocol, which produced selective retreats, whereby the robots were programmed to immediately resume excavation after deposition but reversed after not successfully reaching the excavation site within a given time. These strategies led to different excavation performances as N increased; but most importantly, both strategies outperformed the active protocol at $N = 4$ (Fig. 5.11E).

In summary, this chapter elucidates a slightly contrasting scenario that benefits from individual activity differences. This scenario warrants that persistent clusters do not form and that a steady, persistent flow of agents is obtained. We show that one way to achieve persistification in this task-oriented active matter system is grounded in distributed inactivity, which in turn, is attained through probabilistic laziness and selective retreats.

CHAPTER 6
HIGH THROUGHPUT IMPLEMENTATION

Statistical physics-based simulations like the ones used in this thesis are useful in making accurate predictions only when done in large numbers. This is due to the presence of noise terms in the dynamics. This requirement of repeating simulations a large number of times often limits its applications in several fields. DEM simulations, in particular, model each and every interaction between particles, and the computational requirements grow exponentially with the number of particles. Ever since its inception in 1979 by Peter A. Cundall [121], these simulations have benefited several areas of fluid and molecular dynamics, but it's only now that we are starting to exploit the most out of these approaches because of accessible high throughput and high performance computational resources.

Regardless of the approaches discussed in Chapter 2, computational analysis and modeling play an integral part in most multi-agent robotics studies. The rapid production of cheaper processing units, GPUs specifically, has helped researchers make giant leaps in computational studies. However, there is still a non-uniform distribution of these resources across the globe due to a variety of reasons including cost and expertise.

As part of this thesis, we created a high throughput workflow for managing and running our simulations and post processing algorithms on the Open Science Grid (OSG) clusters [94, 95]. The Open Science Grid (OSG) is an NSF funded, open source platform of shared computational resources available for scholars of research and academic institutions of the United States at no cost. It has over 100 sites with computing and data storage resources across the country. Some remarkable scientific discoveries of the past decade like the 2017 Nobel Prize winning Laser Interferometer Gravitational-Wave Observatory (LIGO) project [122] leveraged OSG to estimate the statistical significance of gravitational wave candidate events.

This shared resource, however, is still used sparsely in the field of collective robotics. This thesis is an example of how the field of statistical explorations of collective behavior can benefit from the power of parallel execution of computational physics simulations over shared resources. The studies reported in this thesis consist of several thousand simulations each with a runtime averaging a day on a four core CPU. At the beginning of our project, we had a few desktop computers at our disposal, but using just those, our study would have taken 5+ years to finish. Fortunately, we were able to reduce the execution time of these simulations significantly by running large batches in parallel on the OSG clusters which had 1000x more cores than what we possessed. The OSG uses a job management tool named HTCondor [123]. It uses concepts like Directed acyclic graphs (DAG) to manage sequential computational workflows where sets of jobs are connected by completion dependencies. These DAGs make the entire workflow seamless and automated, simplify parameter sweeps and post processing analyses. Using the OSG, we managed to run simulation jobs totaling approximately 2.6 million hours of wall time in less than 1 year, reducing our initial time estimate by several orders of magnitude. More details about our workflows can be found in the Appendix section. A simple flowchart of the steps of execution is as shown below:

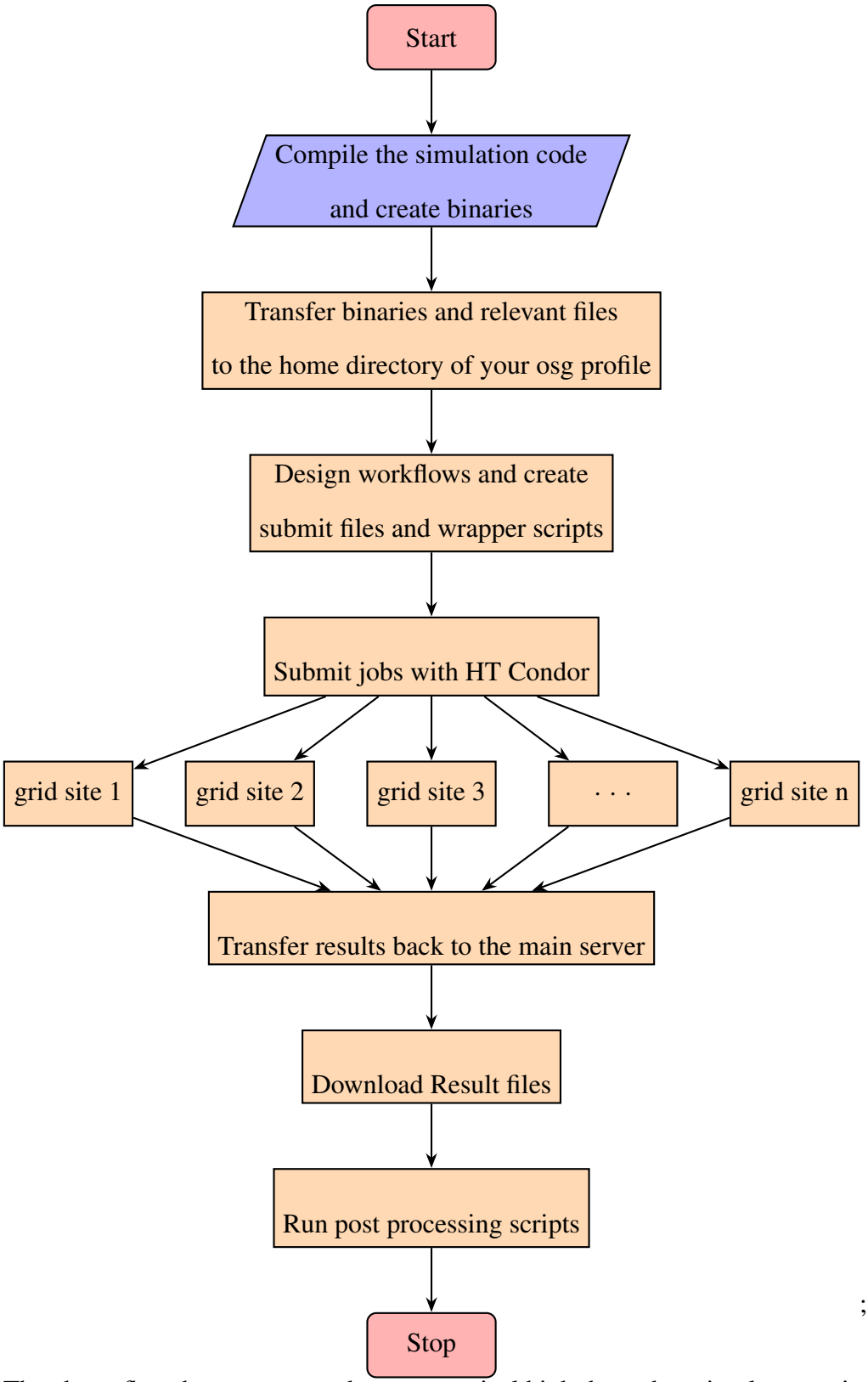

;

The above flowchart represents how any typical high throughput implementation looks like. However, due to the nature and scale of the OSG, there were a few checks that we

added to our workflows to make sure they ran seamlessly. First, since the OSG is a shared, distributed platform, the priority of execution for every user is unbiased, and changes over time in proportion to usage. The priority decreases with increased usage. Additionally, since the computing sites volunteer their computing resources, the host organizations are free to set the policy of job executions. Most sites assign higher priority to jobs of local users present at those sites, and therefore reserve the right to evict jobs of external users in a scenario that a local users requests computational resources. An eviction puts the job in a paused state and returns it to a running state once the queue clears, but due to the technicalities of the execution, all progress is lost and the job restarts from the initial iteration. Keeping this in mind, we took some extra measures to ensure we extracted the maximum successful execution out of our submissions.

While a job runs on the remote site, the output files are created locally and are transmitted back to the job submit site only when the job completes successfully. Another caveat of evictions in our case was that the execution of the post processing scripts required all jobs from the simulations to finish. Therefore, we often encountered situations where 99% of the jobs were completed but the post processing script was waiting for the unlucky 1% jobs to finish. These 1% jobs were usually the ones that had to restart due to evictions. We implemented a fairly common technique in the high throughput computation domain called "checkpointing" to overcome this challenge. Checkpointing periodically saves the progress of a job to the disk in a preset format. If a job is interrupted and restarted, it first checks for the presence of checkpoint files. On finding a checkpoint file, it resumes progress from that checkpoint. A snippet of the checkpointing code is added to the appendix to provide more clarity. This implementation helped us save significant time that would have been otherwise lost to failed jobs.

We also implemented a non-trivial approach to run our post processing codes which were written in MATLAB. Since MATLAB is a paid proprietary software, not all sites on OSG had them installed. In fact, the submit site that we were assigned by the OSG

administrators did not have MATLAB on it. The OSG team organizes a summer school every year, and I was selected to join the 2020 cohort. I was actively doing my simulations on the OSG by then and had the privilege to discuss some of my issues, specifically with regards to MATLAB, with one of the OSG core team members, Dr Tim Cartwright. I was given special access to the Centre of High Throughput Computation clusters of the University of Wisconsin-Madison for a year. We used those clusters to pre-package our MATLAB binaries and executables and transferred them to our OSG submit host for further execution. Technically, any system with MATLAB Runtime would work for compiling the binaries and executables. The ability to run the post processing scripts on the submit host where the result files were being collected saved us time and resources that would be otherwise spent on costly file transfer operations.

There is more room for improvement in enhancing the run times of the simulations. The immediate next step to optimizing the code is making it ready for high performance executions using libraries such as MPI to exploit the large-scale availability of multi-core CPUs at execution sites. Another potential direction of improvement is exploiting some of the more advanced features provided by HTCondor to generate sophisticated workflows that reduce the requirement of human intervention and are robust to events such as holds, evictions, or failures.

CHAPTER 7
CONCLUSIONS

Programming a group of robots for useful collective behavior is a research endeavor that has been a focus of researchers from various fields spanning control engineering to physics. Recently, a significant amount of effort has been invested in developing algorithms and schemes to control robot collectives. However, the scalability and feasibility of these algorithms are often impractical outside laboratory settings. Unpredictable natural settings outside the laboratory warrants sophisticated algorithms. Implementing such algorithms come with both hardware and software challenges which drive up the cost of building robotic systems that can work in natural settings. Nature is filled with examples of physical and biological systems that accomplish complex collective tasks in uncertain and unpredictable situations at ease and these systems can be used as inspiration to simplify such challenges and costs. These systems fall under the broad umbrella of active matter systems, and some of them have been rigorously studied and understood. Although the scale and reach of these systems are not always comparable to actual robotic systems, we argued and showed that the underlying governing principles can be translated into useful collective algorithms.

In this thesis, we developed and studied a dynamic collective aggregation algorithm where local robotic moves mimic the moves of a well studied SOPS algorithm which is inturn, inspired by a physical model of ferromagnetism called the Ising Model. We analyzed the resulting algorithm via discrete particle simulations, and translated the theoretical rules of movement on a robot via mechanics of an attractive exoskeleton housing loose magnets. We were interested in exploring the occurrence of phase change from "dispersed" to "aggregated" states as we changed one single parameter: the local attraction between robots a.k.a magnetization (F_M) (or λ in the theoretical setting). Our work led to the following results. We considered all $\lambda > 1$ and revealed bounds on the λ axis separating aggregated

and dispersed regimes in the SOPS through our theoretical analysis. This result highlights that the SOPS undergoes a phase change from dispersed to aggregated configurations when λ is increased above a threshold, even though all $\lambda > 1$ represent a system that has a bias towards gaining more neighbors. This finding thus, suggests that a distributed particle system can aggregate by having a sufficient bias towards moving to places with more neighbors. We predicted the formal relationship between size and perimeter of configurations in the aggregated and dispersed regimes which is that the aggregated configurations are densely and compactly packed. With the help of robotic experiments and simulations, we showed that there indeed is a phase change from "dispersed" to aggregated states as we increased the peripheral magnet strength (F_M), where F_M is a monotonic function of λ. The theory predicted P_{MC} should scale linearly with N_{MC} in dispersed steady states whereas P_{MC} should scale as $\mathcal{O}(\sqrt{N_{MC}})$ in aggregated steady states. Through experiments, we validated the theoretical predictions about this relationship between size and perimeter of the largest component to show that aggregated configurations are both large and compact. The experimental findings prove that a rudimentary approach of using a parameter that represents pairwise attractions between robots as a control knob can help shuffle between two functionally useful robotic configurations. Subsequent physical simulations showed that this phase change was scalable and observable in systems with different population sizes (N) of robots. Through robotic experiments, we were also able to show the utility of such a phase change in being able to accomplish a collective task of object clearing by simply increasing magnetization (F_M). Furthermore, with the help of physical simulations, we showed that an additional local input like "stress sensing" can be used to steer the collective across this phase change. Overall, this study provides an example of how algorithms based on the physical system model can be used for programming collective behavior in robots. We used one of many well studied physical models to guide our explorations. We hope that similar studies based on fundamental physics-based algorithms will benefit further this line of questioning. We next showed that for a simple and constrained artificial collective

system incapable of implementing complicated energy aware policies, distributed temporal inactivity can serve as a mechanism for energy conservation and task persistification. The simplicity of this finding makes it a great candidate for applications in systems where each individual is constrained in computation, memory, and energy. We demonstrated the applicability through simulations of a debris removal task performed by rudimentary simulated robots. In summary,

- We showed that for a system of fixed population size, a small percentage of active individuals can lead to a majority of the population to aggregate dynamically in the presence of stochastic chiral movement dynamics and short-range inter-particle attraction forces. This overall, suggests that some of the activity in a system where all individuals are active is redundant and strategies can be developed to exploit this redundancy for task persistification through activity modulation.

- We demonstrated that selective periodic hibernation of a fixed percentage of agents can lead to dynamically aggregated states for longer times. This demonstrates that a collective system with finite energy reserves can function for longer periods of time in comparison to run times provided by individual batteries by merely switching some robots to be inactive periodically to conserve energy.

- We reported the effectiveness of periodic hibernation of activity in carrying out a debris clearing task persistently and efficiently. These experiments show that by persistifying dynamic aggregation in robots through selective periodic activity modulation, one can fulfill tasks that depend on this behavior for long periods of time.

In a nutshell, this study suggests an approach to task persistification that doesn't require robots to utilize any sensing and communication protocol and shows the applicability of this finding with a relevant robotic task.

Finally, we studied the nest excavation behavior of fire ants and the usefulness of laziness and selective retreats in maintaining optimal flow of excavated materials in their nest

tunnels. To summarize:

- We showed that ants distribute workload unequally amongst excavators, and give up and retreat to avoid traffic jams while excavating their incipient nests. We represent this inequality in workload distribution by a popular tool from economics called the "Lorenz distribution" which is usually used to represent inequality in wealth distribution. This finding suggests that most of the work that goes into tunnel excavation is carried out by a few ants.

- We observed that the ant system evolves to a state of unequal workload distribution as an emergent process and that some ants are not biologically hardwired to be lazy through our 2-day experiments with a) active diggers removed and b) repeats where active diggers got swapped. This suggests that the few ants that do most of the work while excavating tunnels are not chosen based on their capabilities, but tasked based on some emergent mechanism to conserve energy and maximize throughput.

- We found that ants maintain the optimal tunnel density and traffic flow achievable for the width of the tunnel that they build. This was shown via a combination of experimental analysis and simulations. This shows the significance of the unequal distribution of workload that the ant system evolves towards. By evolving towards this distribution, ants can maintain the optimal density in tunnels that lead to maximum flow of excavated materials.

- We demonstrated the usefulness of laziness and retreats in mitigating jams through cluster analysis in simulations under various conditions. These analyses provide a more fundamental understanding of how the strategies implemented by the ant system help optimize traffic flow in the tunnels.

This study provides a good example of how natural systems tackle practical challenges to collective tasks under constraints. Task persistification through laziness and selective

retreat is a previously unexplored idea and we show the potential of using this in robotic task persistification through our other study. To conclude, although seemingly very different, both our robotic system and ants show that distributed inactivity is a straightforward and robust way to persistify tasks in collective systems where individuals have limited capabilities, or are constrained by other environmental conditions that limit their individual capabilities.

A few potential directions for further research and exploration would entail incorporating the activity modulation in other practical distributed settings on robots. For example, we could consider robots that turn off activity based on environmental cues instead of a timed alteration of activity. It will also be interesting to implement the findings in experiments with physical robots to complement the simulation findings, where we would surely gather more insight into which modulation policies are the most effective. Moreover, on a comparative scale, the overall reduction in average velocity of the system due to hibernation may have some similar characteristics with systems that utilize higher attraction forces between agents. There have been some preliminary discussions of the relationship between velocity and magnetization in Chapter 4, and this might be interesting to further explore with energy constraints in mind. For the fire ant studies, it will be interesting to further understand how the system emerges to the Lorenz workload distribution. There is some preliminary work currently in progress that is exploring this area.

On a broad level, this thesis conveyed the idea that a simple amalgamation of principles from biology, statistical physics, distributed computing, and robotics can give rise to the development of useful programming techniques for robot collectives. Such a principled approach can help develop simplified algorithms, tools, and analysis techniques that can be easily implemented, and are cost-effective. This is specifically relevant for new robotic systems where component capabilities are saturating, or components are microscopic and incapable of traditional computation. We show that interdisciplinary approaches can harness the full extent of useful features and weed out the unnecessary complexities of col-

lective algorithms to produce robust and persistent self organized behavior in a swarm of robots and hope this thesis will guide future studies governed by this idea of minimalism.

Appendices

APPENDIX A

BOBBOT DESIGN AND MANUFACTURING

Fig. A.1 depicts various cross-sectional views of a BOBbot's design and corresponding skeletal structure. Fig. A.2 shows the Printer Circuit Board (PCB) design and assembly. The force sensing circuitry shown in Fig. A.2 is present in the BOBbot hardware but was not used in this study. Table A.1 lists all components used in BOBbot manufacturing.

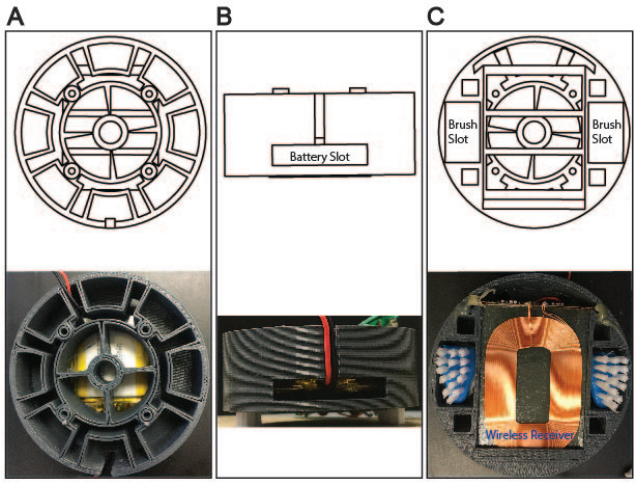

Figure A.1: **Cross-sectional views of the BOBbot mechanical design.** SolidWorks designs and assembled versions of (**A**) the BOBbot shell and magnet slots, (**B**) the battery slot, and (**C**) the brush slots and wireless QR charge receiver.

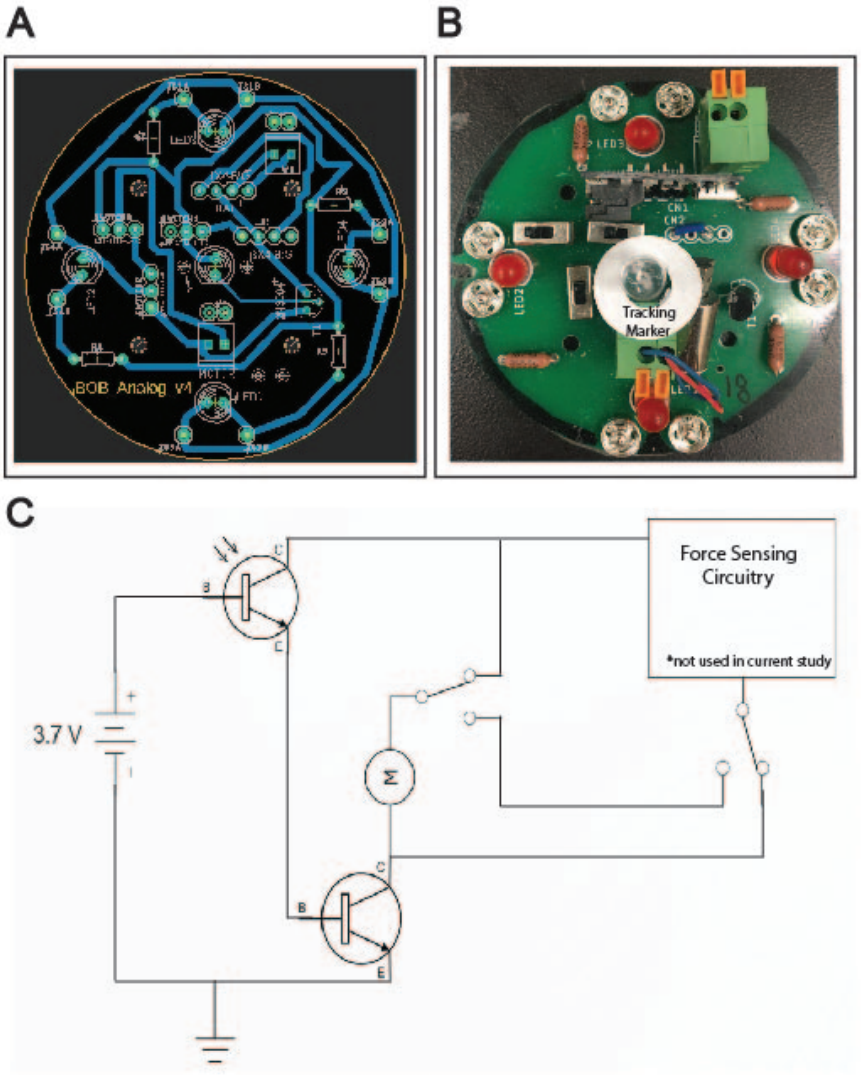

Figure A.2: **BOBbot circuitry.** (**A**) The analog PCB design, made in EagleCAD. (**B**) The printed PCB. (**C**) The force sensing circuitry, implemented in the PCB but unused in the present study.

Component	Manufacturer	Product Name
ERM Motor	BestTong	DC 3.7V 9500RPM Vibrating Coreless Brushed Motor
Brushes	Pienoy	Double-Headed Pet Toothbrush
Magnets	K&J Magnetics	S2 and S3
Battery	Adafruit Industries	Lithium Ion Polymer Battery 3.7V 500mAh
Battery Module	Adafruit Industries	Micro-Lipo Charger
Qi Transmitter	Adafruit Industries	Universal Qi Wireless Charging Transmitter
Qi Receiver	Adafruit Industries	Universal Qi Wireless Receiver Module
Red/Black Wiring	Adafruit Industries	Solid-Core Wire Spool
LED	KingSo	500pcs LED Diode Lights
Phototransistor	Adafruit Industries	Photo Transistor Light Sensor
Resistors	Vishay/Dale	Metal Film Resistor 1/10 Watt 50 Ohm 0.1% 50ppm
Transistors	ON Semiconductor	General Purpose Bipolar Transistor
Switches	Pololu	Mini Slide Switch 3-Pin, SPDT, 0.3A
Terminal Block	Pololu	Screwless Terminal Block: 2-Pin, 0.1” Pitch
Button Snaps	Adafruit Industries	Sewable Snaps, 5mm Diameter
Masking Tape	Daigger	DAI-T34-27-C Assorted Label Tape Pack
Jumper Cables	Anezus	700pcs Jumper Wire Kit Breadboard Wires

Table A.1: **List of BOBbot components.**

APPENDIX B

EXPERIMENTAL ARENA DESIGN

Fig. B.1 shows the design and details of the experimental platform.

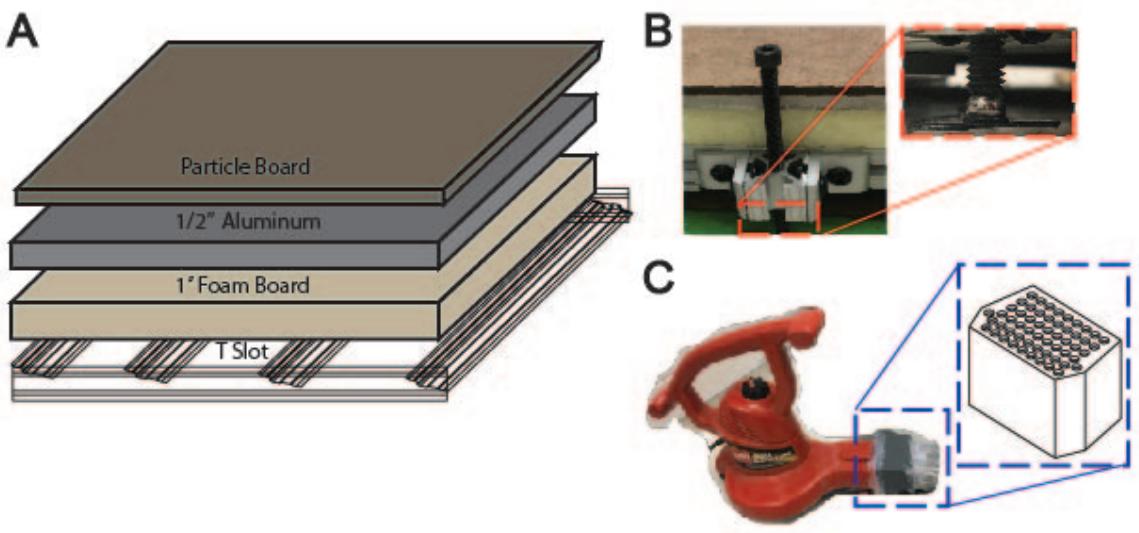

Figure B.1: **Experimental platform design and details.** (**A**) The experimental platform is composed of a T-slot base supporting a foam board, aluminum, and particle board layers. (**B**) Levelling screws in the T-slot framing allow for incline adjustment. (**C**) A leaf blower with a multi-pronged tygon tubing attachment provide airflow to the PVC pipe boundary to mitigate boundary effects.

APPENDIX C

CALIBRATION OF SIMULATIONS WITH EXPERIMENTS

The DEM simulation parameters (Table B.1) are calibrated to match the physical BOBbot experiments. Many parameters such as the mass and dimensions of each BOBbot are easily measured. However, other parameters are better calculated by conducting simple experiments. The first such experiment (Fig. B.2) calculates the magnetic force F_{M0} between two magnets when their BOBbots' shells are touching. The first magnet is placed in a BOBbot shell attached to a rigid stand; a second shell is then tethered beneath the first by placing the second magnet inside it. Thus, the second shell falls once its weight exceeds F_M. To leverage this insight, a cup is tethered to the second shell and BBs are added to the cup one-by-one until the second shell falls (Fig. B.2A). The weight of the shell, cup, and BBs are then measured to obtain a value of F_M that is precise up to 0.1 g, the weight of a single BB (Fig. B.2C).

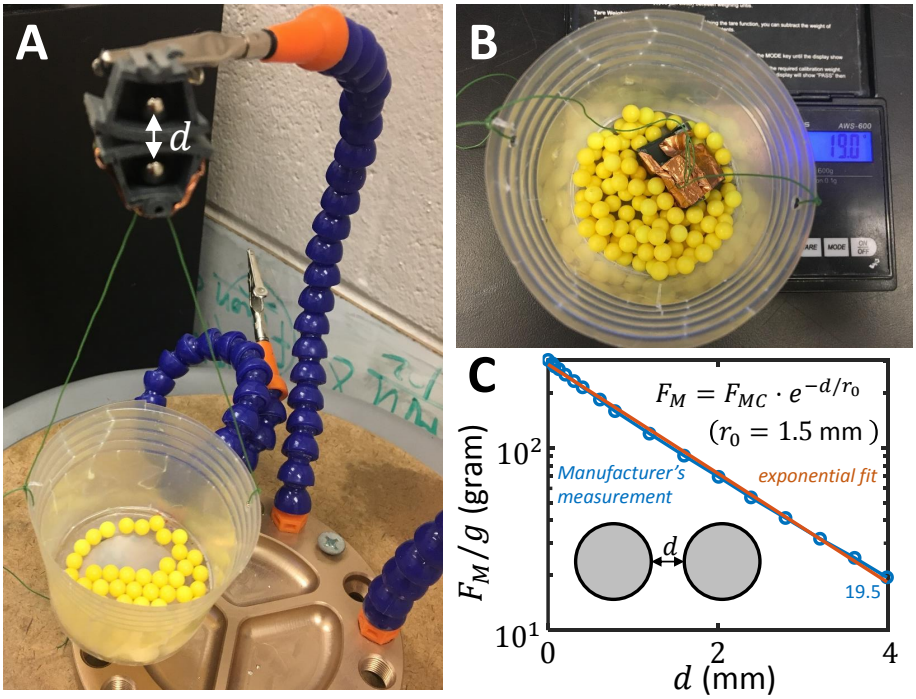

Figure C.1: **Calibration experiment for calculating magnet force F_M.** (**A**) The experimental setup for calculating F_M. (**B**) Measuring the weight of the tethered apparatus once it falls gives a close approximation of F_{M0}. (**C**) The magnetic force's decay with the separation d between two magnetic beads.

Each BOBbot's position $\vec{r}$ and orientation φ change at a constant rate subject to noise. A BOBbot's constant translational speed v_0 comes from the competing driving force $F_D\hat{u}$ and the translational drag $-\eta\dot{\vec{r}}$. Similarly, each BOBbot's constant rotational speed ω_0 comes from the competing driving torque τ_D and the rotational drag $-\eta_\varphi\dot{\varphi}$. The steady-state speeds therefore follow $v_0 = F_D/\eta$ and $\omega_0 = \tau_D/\eta_\varphi$. We again use simple experiments to determine the drive and drag. To measure the translational drag η, we compare a BOBbot's trajectory when it is on a 0° incline versus a tilted incline. In the former, the BOBbot circles regularly with some noise; in the latter, this regular circling is stretched towards the direction of gravity on the incline (Fig. S5, top). Using the known gravitational force on the BOBbot, we can calculate the translational drag force and coefficient η. We then simulate a BOBbot's motion using different translational drag coefficients; the one that produces the trajectory most closely matching those in the experiments is chosen as the simulation η (Fig. B.3).

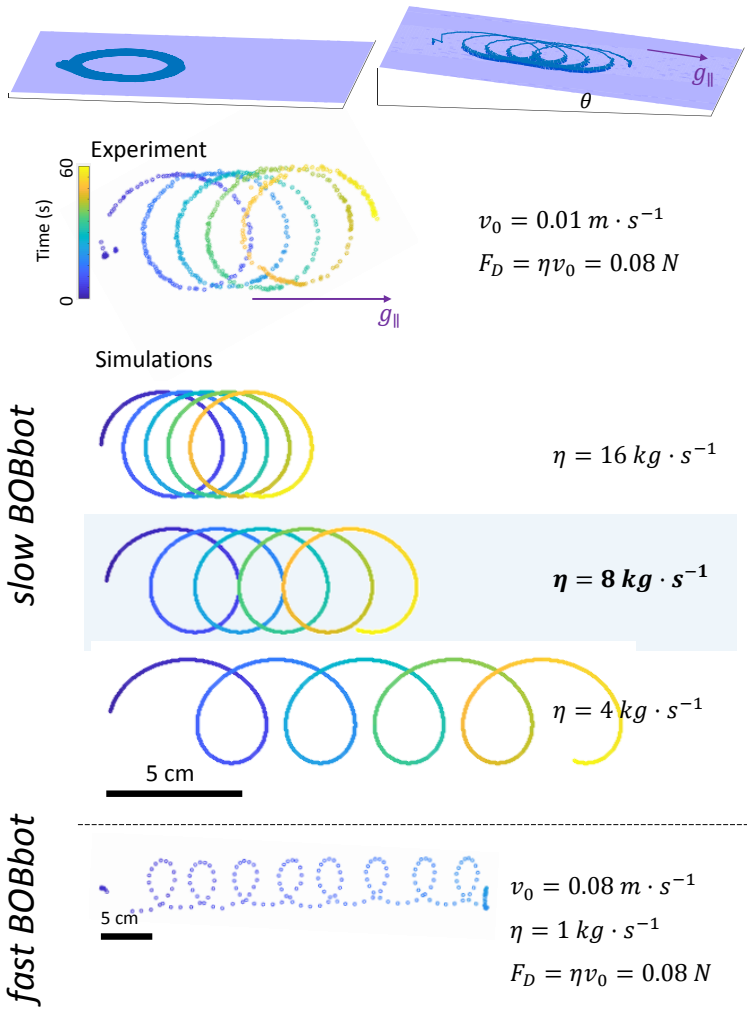

Figure C.2: **Calibration experiment for calculating translational drag coefficient η.** When a BOBbot is driven on a level plane, it circles regularly with some noise. When placed on a tilted incline, its trajectory is stretched towards the direction of gravity on the incline. Using this known force, we measure the drag force by simulating BOBbot trajectories on a tilted incline using different drag coefficients, comparing each trajectory's stretch to that of the experiment. The correct drag produces a close approximate of the experimental trajectory. We find that viscosity varies between BOBbots, implying that their speeds also vary. The first three trajectories are from a BOBbot with relatively slow velocity v_0; the last is from a fast BOBbot.

The measurement of the rotational drag η_φ exploits its balance with the driving torque. To measure the rotational torque exerted on a BOBbot, a very light rigid straw is attached across the diameter of a BOBbot (Fig. B.4). We then let the BOBbot use the straw to push objects at various arm lengths. For a given obstacle to push, the rotational torque is obtained by finding the largest torque of friction on an obstacle to balance. We decrease the

arm length from a large value to a point the BOBbots can just push the obstacle. Given the measured saturated angular velocity ω_0, the rotational drag can be inferred as $\eta_\varphi = \tau_D/\omega_0$.

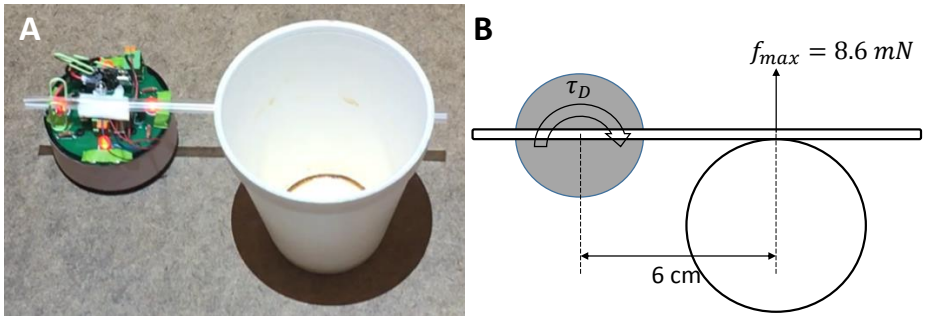

Figure C.3: **Calibration experiment for calculating rotational drag coefficient η_φ.** (**A**) The experimental setup and (**B**) the corresponding force diagram, where f_{max} denotes the largest frictional torque that the driving torque τ_D can balance.

Many of our preliminary experiments were adulterated by boundary effects that caused small groups of BOBbots to collect at the edges and corners of the arena, affecting steady state properties. We mitigate these affects using airflow-based boundary repulsion (Fig. B.5). To characterize these airflow effects, a BOBbot is placed close to the boundary and its trajectory is tracked with and without airflow. The corresponding simulation parameters are then chosen to match the average characteristics of these experimental trajectories. The airflow force profile is chosen to match the decay length observed in the example experiment (which is $R_A \approx 6 * R_0$). The resting speed of the bot used in this experiment is $v_0 = 3$ cm/s. Please note that the decay length chosen in the simulation runs throughout our study is $\sim 2 * R_0$.

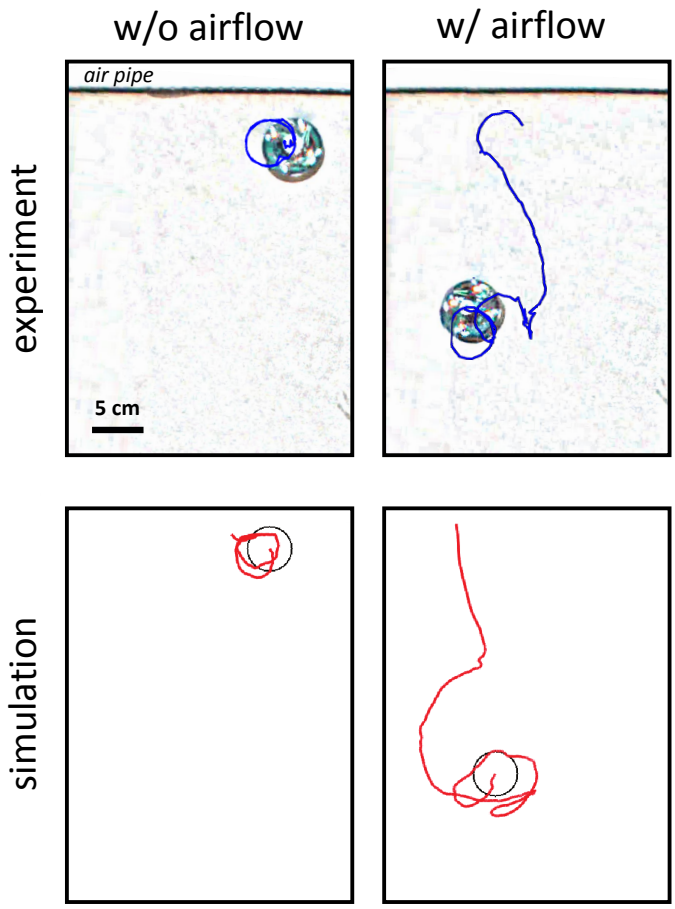

Figure C.4: **Boundary airflow effects in experiment and simulation.**

Table B.1 shows all the parameters used in the physical model, along with their experimental and calibrated simulation values.

Symbol	Description	Experiment	Simulation	Note
m	BOBbot mass	0.060 kg	0.060 kg	
R_0	BOBbot radius	0.030 m	0.030 m	
I	BOBbot moment of inertia	2.7e-5 kg·m^2	2.7e-5 kg·m^2	$= mR_0^2/2$
R_C	radius of the regular circular motion	0.025 ± 0.005 m	0.025 ± 0.005 m	
R_{B_0}	radius of the magnetic bead	2.3e-3 m	2.0e-3 m	
R_S	thickness of the magnet cavity shell	2.0e-3 m	2.0e-3 m	
R_B	effective radius of the magnetic bead	4.3e-3 m	4.0e-3 m	$= R_{B_0} + R_S$
v_0	Saturated speed	48.43 ± 20.16 mm/s	60.00 mm/s	$1 \leq v_0 \leq 70$ mm/s
ω_0	saturated angular velocity of the orbit	1.94 ± 0.81 rad/s	2.40 rad/s	$= v_0/R_C$
F_D	Translational drive	0.07 N	0.06 N	$= \eta v_0$
τ_D	rotational drive (torque)	0.0005 N·m	0.0007 N·m	$= \eta_\varphi \omega_0$
η	translational drag coefficient	$\sim$1 kg/s	1.0 kg/s	
η_φ	[l]rotational drag coefficient	$\leq$3e-4 N·m·s	3e-4 N·m·s	
F_{M0}	magnetic force on contact	0.003-0.035 kgf	0.003-0.035 kgf	
d_0	magnetic force decay length	0.0015 m	0.0015 m	$F_M(d) = F_{M0} \cdot e^{-d/d_0}$
μ	bot-bot friction coefficient	0.143	0.143	
μ_W	bot-wall friction coefficient		0.143	

Table C.1: **List of parameters used in physical simulations.**

APPENDIX D

OSG SUBMIT FILES AND CODE SNIPPETS

The OSG implementation of simulations were executed with the aid of a number of helper scripts as discussed below.

Main Implementation The main implementation of the workflow for simulations are done in a 3 step process starting with a iterative script that iterates over the parameters we want changed and creates a 'dag' file. Each line of a 'dag' file represented one instantiation of the simulation and is used by the condor submit file to process the workflow. An example code snippet of each of these file is shown below:

Compilation and execution file to be called by the iterative script

```
#!/bin/bash
#Compile the code
compile simulation.cpp
#Run and specify the arguments
./simulation $arguments$
```

An example iterative script

```
#!/bin/bash
for (loop over parameter 1 eg:fm)
do
  for (loop over parameter 2 eg:vel)
  do
    ...
    do
      ...
```

```
        do
          ...
          do
          #Specify a unique run name for the specific set of
          #parameters in a given run
          run_name="result_FM_${fm}_VEL_${vel}_N_${n}...Exp_${i}"
          #Append a line to the dag file with that unique
          #run name and associate the submit file with it
          echo "JOB ${run_name} simulation.sub" >> simulation.dag
          #Specify retry attempts if any
          echo "RETRY ${run_name} 1" >> simulation.dag
          #Add arguments to the submit line in dag file
          echo "VARS ${run_name} macromag=\"${FM}\" macrovel=\"
          ${vel}\"...macrojobname=\"${run_name}\"">>
          simulation.dag
          done
        done
      done
    done
done
```

An example submit file

```
#Specify OSG universe in which your submission will
#run
Universe = vanilla
#Add the file with compilation and execution line here
executable=simulation.sh
#Specify output, error and log files
```

```
output=log/simulation-$(macrojobname).out
err=log/simulation-$(macrojobname).err
log=log/simulation-$(macrojobname).log
#Specify arguments
arguments="$(macromag) $(macrovel) $(macroiter) $(macrotime)
$(macrosample) $(macroN) $(macroA) $(macroAP)"
#OSG specific output and input commands
transfer_output_files=result_FM_$(macromag)_VEL_$(macrovel)
_..._Exp_$(macroiter).dat
transfer_input_files=/home/simulation.cpp
should_transfer_files=YES
when_to_transfer_output=ON_EXIT_OR_EVICT
#Specify system requirements, storage and memory
Requirements=(HAS_MODULES =?= true) &&
(OSGVO_OS_STRING == "RHEL 7") && (OpSys == "LINUX")
+ProjectName = "osg.bobbot"
request_memory=2GB
request_disk=1GB
request_cpus=1
queue 1
```

MATLAB implementation MATLAB is a licensed software and is not readily available everywhere. We use the MATLAB compiler to compile our MATLAB programs as executables and pre package MATLAB binaries with our submission. Example pseudocodes are provided below to explain the workflow:

Setup environment for execution

```
#!/bin/sh
# Script for execution of deployed applications
```

```
# Sets up the MATLAB Runtime environment for the
#current $ARCH and executes
# the specified command.
# Unzip the MATLAB binary
tar -xzf r2015b.tar.gz
mkdir cache
export MCR_CACHE_ROOT=$PWD/cache
#Set up the environment and call the executable
#MATLABPostProcessing
exe_name=$0
exe_dir=`dirname "$0"`
echo "------------------------------------------"
if [ "x$1" = "x" ]; then
  echo Usage:
  echo    $0 \<deployedMCRroot\> args
else
  echo Setting up environment variables
  MCRROOT="$1"
  echo ---
  LD_LIBRARY_PATH=.:${MCRROOT}/runtime/glnxa64 ;
  LD_LIBRARY_PATH=${LD_LIBRARY_PATH}:${MCRROOT}/bin/glnxa64 ;
  LD_LIBRARY_PATH=${LD_LIBRARY_PATH}:${MCRROOT}/sys/os/glnxa64;
  LD_LIBRARY_PATH=${LD_LIBRARY_PATH}:${MCRROOT}
  /sys/opengl/lib/glnxa64;
  export LD_LIBRARY_PATH;
  echo LD_LIBRARY_PATH is ${LD_LIBRARY_PATH};
  shift 1
```

```
    args=
    while [ $# -gt 0 ]; do
        token=$1
        args="${args} \"${token}\""
        shift
    done
    eval "\"${exe_dir}/MATLABPostProcessing\"" $args
fi
exit
```

Submit File

```
#Specify OSG universe in which your submission will
#run
Universe = vanilla
#Specify executable, input files and the result file
#which needs to be processed as arguments
executable = wrapper_run_MATLABPostProcessing.sh
transfer_input_files = MATLABPostProcessing,
wrapper_MATLAB.sh, $(inputfile), r2015b.tar.gz
arguments = $(inputfile)
#Specify output, error and log files
Output = Log/job.$(inputfile).out
Error =  Log/job.$(inputfile).err
Log =    Log/job.$(inputfile).log
#Specify system requirements, storage and memory
requirements = OSGVO_OS_STRING == "RHEL 7" &&
Arch == "X86_64" && HAS_MODULES == True
request_cpus = 1
```

```
request_disk = 4GB
request_memory = 3GB
#Queue all the result files that was produced by
#simulations
queue inputfile matching result*
```

Wrapper script

```
./run_MATLABPostProcessing.sh v90 $1
```

Checkpointing As elucidated in Chapter 6, Checkpointing is a useful technique to ensure efficient utilization of resources in cases of job evictions. The following example code snippets show how this is done by modifying the C++ simulation program and our submit files.

Changes in the Simulation C++ file

```
// Check for file and find iteration number to resume from
if (exists_file(File_Name)==1) {
    //stream the file
        ifstream State_File(File_Name);
        if (State_File.is_open()) {
            // Extract the current state and line number
            //from where to resume
        }
        State_File.close();
} else {
// Initialize state files for starting anew
}
//checkpoint and exit
 if ((Simulation_Iteration % Checkpoint_Flag == 0) &&
```

```
 (Simulation_Iteration >0)) {
                    State_File.close();
                    exit(33);
}
```

Changes in submit file

```
#Specify OSG universe in which your submission will
#run
Universe = vanilla
#Add the file with compilation and execution line here
executable=simulation.sh
#Specify output, error and log files
output=log/simulation-$(macrojobname).out
err=log/simulation-$(macrojobname).err
log=log/simulation-$(macrojobname).log
#Specify arguments
arguments="$(macromag) $(macrovel) $(macroiter) $(macrotime)
$(macrosample) $(macroN) $(macroA) $(macroAP)"
#OSG specific output and input commands
transfer_output_files=result_FM_$(macromag)_VEL_$(macrovel)
_..._Exp_$(macroiter).dat
transfer_input_files=/home/simulation.cpp
should_transfer_files=YES
checkpoint_exit_code=33
#Specify system requirements, storage and memory
Requirements=(HAS_MODULES =?= true) &&
(OSGVO_OS_STRING == "RHEL 7") && (OpSys == "LINUX")
+ProjectName = "osg.bobbot"
```

```
request_memory=2GB
request_disk=1GB
request_cpus=1
queue 1
```

REFERENCES

[1] A. E. Magurran, "The adaptive significance of schooling as an anti-predator defence in fish," *Annales Zoologici Fennici*, vol. 27, no. 2, pp. 51–66, 1990.

[2] J. Prost, F. Jülicher, and J.-F. Joanny, "Active gel physics," *Nature physics*, vol. 11, no. 2, pp. 111–117, 2015.

[3] J. Brugués and D. Needleman, "Physical basis of spindle self-organization," *Proceedings of the National Academy of Sciences*, vol. 111, no. 52, pp. 18 496–18 500, 2014.

[4] N. J. Mlot, C. A. Tovey, and D. L. Hu, "Fire ants self-assemble into waterproof rafts to survive floods," *Proceedings of the National Academy of Sciences*, vol. 108, no. 19, pp. 7669–7673, 2011.

[5] J. Liu, A. Prindle, J. Humphries, M. Gabalda-Sagarra, M. Asally, D.-Y. D. Lee, S. Ly, J. Garcia-Ojalvo, and G. M. Süel, "Metabolic co-dependence gives rise to collective oscillations within biofilms," *Nature*, vol. 523, no. 7562, pp. 550–554, 2015.

[6] A. Prindle, J. Liu, M. Asally, S. Ly, J. Garcia-Ojalvo, and G. M. Süel, "Ion channels enable electrical communication in bacterial communities," *Nature*, vol. 527, no. 7576, pp. 59–63, 2015.

[7] E. Şahin, "Swarm robotics: From sources of inspiration to domains of application," in *Swarm Robotics*, 2005, pp. 10–20.

[8] M. Yim, W.-M. Shen, B. Salemi, D. Rus, M. Moll, H. Lipson, E. Klavins, and G. S. Chirikjian, "Modular self-reconfigurable robot systems [grand challenges of robotics]," *IEEE Robotics Automation Magazine*, vol. 14, no. 1, pp. 43–52, 2007.

[9] M. Rubenstein, A. Cornejo, and R. Nagpal, "Programmable self-assembly in a thousand-robot swarm," *Science*, vol. 345, no. 6198, pp. 795–799, 2014.

[10] D. Pickem, P. Glotfelter, L. Wang, M. Mote, A. Ames, E. Feron, and M. Egerstedt, "The robotarium: A remotely accessible swarm robotics research testbed," in *2017 IEEE International Conference on Robotics and Automation (ICRA)*, IEEE, 2017, pp. 1699–1706.

[11] F. Mondada, M. Bonani, X. Raemy, J. Pugh, C. Cianci, A. Klaptocz, S. Magnenat, J.-C. Zufferey, D. Floreano, and A. Martinoli, "The e-puck, a robot designed for education in engineering," in *Proceedings of the 9th conference on autonomous*

robot systems and competitions, IPCB: Instituto Politécnico de Castelo Branco, vol. 1, 2009, pp. 59–65.

[12] S. Kumar, *Fundamental limits to moore's law*, 2015. arXiv: 1511.05956.

[13] Y. Alapan, O. Yasa, B. Yigit, I. C. Yasa, P. Erkoc, and M. Sitti, "Microrobotics and microorganisms: Biohybrid autonomous cellular robots," *Annual Review of Control, Robotics, and Autonomous Systems*, vol. 2, pp. 205–230, 2019.

[14] P. Dario, R. Valleggi, M. C. Carrozza, M. C. Montesi, and M. Cocco, "Microactuators for microrobots: A critical survey," *Journal of Micromechanics and Microengineering*, vol. 2, no. 3, pp. 141–157, 1992.

[15] G. H. Lewes, *The principles of certitude. from the known to the unknown. matter and force. force and cause. the absolute in the correlations of feeling and motion. appendix: Imaginary geometry and the truth of axioms. lagrange and hegel: The speculative method. action at a distance*. Trübner & Company, 1875, vol. 2.

[16] S. Kivelson and S. A. Kivelson, "Defining emergence in physics," *Npj Quantum Materials*, vol. 1, no. 1, pp. 1–2, 2016.

[17] P. A. Corning, "The re-emergence of emergencei: A venerable concept in search of a theory," *Complexity*, vol. 7, no. 6, pp. 18–30, 2002.

[18] P. D. Manrique, M. Klein, Y. S. Li, C. Xu, P. M. Hui, and N. F. Johnson, "Getting closer to the goal by being less capable," *Science Advances*, vol. 5, no. 2, 2019.

[19] J Aguilar, D Monaenkova, V Linevich, W Savoie, B Dutta, H.-S. Kuan, M. Betterton, M. Goodisman, and D. Goldman, "Collective clog control: Optimizing traffic flow in confined biological and robophysical excavation," *Science*, vol. 361, no. 6403, pp. 672–677, 2018.

[20] S. J. Martin, R. R. Funch, P. R. Hanson, and E.-H. Yoo, "A vast 4,000-year-old spatial pattern of termite mounds," *Current biology*, vol. 28, no. 22, R1292–R1293, 2018.

[21] W. R. Tschinkel, *The fire ants*. Belknap Press, 2013.

[22] M. Kastner, "Existence and order of the phase transition of the ising model with fixed magnetization," *Journal of statistical physics*, vol. 109, no. 1, pp. 133–142, 2002.

[23] Y. Meng and Y. Jin, *Bio-inspired self-organizing robotic systems*. Springer-Verlag Berlin Heidelberg, 2011.

[24] K. Vulinec, "Collective security: Aggregation by insects as a defense," *Insect defenses*, pp. 251–288, 1990.

[25] S. A. Ocko and L Mahadevan, "Collective thermoregulation in bee clusters," *Journal of The Royal Society Interface*, vol. 11, no. 91, p. 20 131 033, 2014.

[26] T. Schmickl and K. Crailsheim, "A navigation algorithm for swarm robotics inspired by slime mold aggregation," in *International Workshop on Swarm Robotics*, Springer, 2006, pp. 1–13.

[27] F. Arvin, K. Samsudin, A. R. Ramli, and M. Bekravi, "Imitation of honeybee aggregation with collective behavior of swarm robots," *International Journal of Computational Intelligence Systems*, vol. 4, no. 4, pp. 739–748, 2011.

[28] R. Jeanson, C. Rivault, J.-L. Deneubourg, S. Blanco, R. Fournier, C. Jost, and G. Theraulaz, "Self-organized aggregation in cockroaches," *Animal Behaviour*, vol. 69, no. 1, pp. 169–180, 2005.

[29] S. S. Ding, L. J. Schumacher, A. E. Javer, R. G. Endres, and A. E. Brown, "Shared behavioral mechanisms underlie c. elegans aggregation and swarming," *ELife*, vol. 8, e43318, 2019.

[30] M. Bodi, R. Thenius, M. Szopek, T. Schmickl, and K. Crailsheim, "Interaction of robot swarms using the honeybee-inspired control algorithm beeclust," *Mathematical and Computer Modelling of Dynamical Systems*, vol. 18, no. 1, pp. 87–100, 2012.

[31] O. Soysal and E. Şahin, "Probabilistic aggregation strategies in swarm robotic systems," in *Proceedings 2005 IEEE Swarm Intelligence Symposium*, ser. SIS 2005, 2005, pp. 325–332.

[32] S. Garnier, J. Gautrais, M. Asadpour, C. Jost, and G. Theraulaz, "Self-organized aggregation triggers collective decision making in a group of cockroach-like robots," *Adaptive Behavior*, vol. 17, no. 2, pp. 109–133, 2009.

[33] N. Correll and A. Martinoli, "Modeling and designing self-organized aggregation in a swarm of miniature robots," *I. J. Robotic Res.*, vol. 30, pp. 615–626, Apr. 2011.

[34] M. Mesbahi and M. Egerstedt, *Graph theoretic methods in multiagent networks*. Princeton University Press, 2010.

[35] F. Rossi, S. Bandyopadhyay, M. Wolf, and M. Pavone, "Review of multi-agent algorithms for collective behavior: A structural taxonomy," *IFAC-PapersOnLine*, vol. 51, no. 12, pp. 112 –117, 2018, IFAC Workshop on Networked Autonomous Air Space Systems NAASS 2018.

[36] A. Barel, R. Manor, and A. M. Bruckstein, *Come together: Multi-agent geometric consensus (gathering, rendezvous, clustering, aggregation)*, 2019. arXiv: 1902.01455 [cs.MA].

[37] S. Martini, M. Egerstedt, and A. Bicchi, "Controllability decompositions of networked systems through quotient graphs," in *2008 47th IEEE Conference on Decision and Control*, IEEE, 2008, pp. 5244–5249.

[38] M. Egerstedt, S. Martini, M. Cao, K. Camlibel, and A. Bicchi, "Interacting with networks: How does structure relate to controllability in single-leader, consensus networks?" *IEEE control systems magazine*, vol. 32, no. 4, pp. 66–73, 2012.

[39] Z. Qiu, S. Liu, and L. Xie, "Distributed constrained optimal consensus of multi-agent systems," *Automatica*, vol. 68, pp. 209 –215, 2016.

[40] M. Brambilla, E. Ferrante, M. Birattari, and M. Dorigo, "Swarm robotics: A review from the swarm engineering perspective," *Swarm Intelligence*, vol. 7, no. 1, pp. 1–41, 2013.

[41] G. Dudek, M. R. Jenkin, E. Milios, and D. Wilkes, "A taxonomy for multi-agent robotics," *Autonomous Robots*, vol. 3, no. 4, pp. 375–397, 1996.

[42] L. Bayindir, "A review of swarm robotics tasks," *Neurocomputing*, vol. 172, pp. 292–321, 2016.

[43] D. Angluin, J. Aspnes, D. Eisenstat, and E. Ruppert, "The computational power of population protocols," *Distributed Computing*, vol. 20, no. 4, pp. 279–304, 2007.

[44] P. Flocchini, G. Prencipe, and N. Santoro, Eds., *Distributed computing by mobile entities*. Switzerland: Springer International Publishing, 2019.

[45] B. Piranda and J. Bourgeois, "Designing a quasi-spherical module for a huge modular robot to create programmable matter," *Autonomous Robots*, vol. 42, no. 8, pp. 1619–1633, 2018.

[46] G. Caprari, P. Balmer, R. Piguet, and R. Siegwart, "The autonomous micro robot" alice": A platform for scientific and commercial applications," in *MHA'98. Proceedings of the 1998 International Symposium on Micromechatronics and Human Science.-Creation of New Industry-(Cat. No. 98TH8388)*, IEEE, 1998, pp. 231–235.

[47] S. English, J. Gough, A. Johnson, R. Spanton, J. Sun, R. Crowder, and K.-P. Zauner, "Strategies for maintaining large robot communities," 2008.

[48] S. Kernbach, R. Thenius, O. Kernbach, and T. Schmickl, "Re-embodiment of honeybee aggregation behavior in an artificial micro-robotic system," *Adaptive Behavior*, vol. 17, no. 3, pp. 237–259, 2009.

[49] J. McLurkin, A. J. Lynch, S. Rixner, T. W. Barr, A. Chou, K. Foster, and S. Bilstein, "A low-cost multi-robot system for research, teaching, and outreach," in *Distributed Autonomous Robotic Systems*, Springer, 2013, pp. 597–609.

[50] N. Farrow, J. Klingner, D. Reishus, and N. Correll, "Miniature six-channel range and bearing system: Algorithm, analysis and experimental validation," in *2014 IEEE International Conference on Robotics and Automation (ICRA)*, IEEE, 2014, pp. 6180–6185.

[51] J. McLurkin, J. Smith, J. Frankel, D. Sotkowitz, D. Blau, and B. Schmidt, "Speaking swarmish: Human-robot interface design for large swarms of autonomous mobile robots.," in *AAAI spring symposium: To boldly go where no human-robot team has gone before*, Palo Alto, CA, vol. 72, 2006.

[52] F. Mondada, L. M. Gambardella, D. Floreano, S. Nolfi, J.-L. Deneuborg, and M. Dorigo, "The cooperation of swarm-bots: Physical interactions in collective robotics," *IEEE Robotics & Automation Magazine*, vol. 12, no. 2, pp. 21–28, 2005.

[53] D. Pickem, M. Lee, and M. Egerstedt, "The gritsbot in its natural habitat-a multi-robot testbed," in *2015 IEEE International conference on robotics and automation (ICRA)*, IEEE, 2015, pp. 4062–4067.

[54] H. Xie, M. Sun, X. Fan, Z. Lin, W. Chen, L. Wang, L. Dong, and Q. He, "Reconfigurable magnetic microrobot swarm: Multimode transformation, locomotion, and manipulation," *Science Robotics*, vol. 4, no. 28, eaav8006, 2019.

[55] D. H. Wolpert, "The stochastic thermodynamics of computation," *Journal of Physics A: Mathematical and Theoretical*, vol. 52, no. 19, p. 193 001, 2019.

[56] C. Bechinger, R. Di Leonardo, H. Löwen, C. Reichhardt, G. Volpe, and G. Volpe, "Active particles in complex and crowded environments," *Reviews of Modern Physics*, vol. 88, no. 4, p. 045 006, 2016.

[57] T. Vissers, A. van Blaaderen, and A. Imhof, "Band formation in mixtures of oppositely charged colloids driven by an ac electric field," *Physical review letters*, vol. 106, no. 22, p. 228 303, 2011.

[58] M. E. Leunissen, C. G. Christova, A.-P. Hynninen, C. P. Royall, A. I. Campbell, A. Imhof, M. Dijkstra, R. Van Roij, and A. Van Blaaderen, "Ionic colloidal crystals of oppositely charged particles," *Nature*, vol. 437, no. 7056, pp. 235–240, 2005.

[59] M. Sapozhnikov, Y. V. Tolmachev, I. Aranson, and W.-K. Kwok, "Dynamic self-assembly and patterns in electrostatically driven granular media," *Physical review letters*, vol. 90, no. 11, p. 114 301, 2003.

[60] A. Zöttl and H. Stark, "Emergent behavior in active colloids," *Journal of Physics: Condensed Matter*, vol. 28, no. 25, p. 253 001, 2016.

[61] J. Elgeti, R. G. Winkler, and G. Gompper, "Physics of microswimmerssingle particle motion and collective behavior: A review," *Reports on progress in physics*, vol. 78, no. 5, p. 056 601, 2015.

[62] I. S. Aranson, "Active colloids," *Physics-Uspekhi*, vol. 56, no. 1, p. 79, 2013.

[63] M. E. Cates and J. Tailleur, "Motility-induced phase separation," *Annu. Rev. Condens. Matter Phys.*, vol. 6, no. 1, pp. 219–244, 2015.

[64] S. Mayya, G. Notomista, D. Shell, S. Hutchinson, and M. Egerstedt, "Non-uniform robot densities in vibration driven swarms using phase separation theory," in *2019 IEEE/RSJ International Conference on Intelligent Robots and Systems (IROS)*, IEEE, 2019, pp. 4106–4112.

[65] G. S. Redner, C. G. Wagner, A. Baskaran, and M. F. Hagan, "Classical nucleation theory description of active colloid assembly," *Physical review letters*, vol. 117, no. 14, p. 148 002, 2016.

[66] É. Fodor, C. Nardini, M. E. Cates, J. Tailleur, P. Visco, and F. van Wijland, "How far from equilibrium is active matter?" *Physical review letters*, vol. 117, no. 3, p. 038 103, 2016.

[67] C. Liu, T. Xu, L.-P. Xu, and X. Zhang, "Controllable swarming and assembly of micro/nanomachines," *Micromachines*, vol. 9, no. 1, p. 10, 2018.

[68] V. Sridhar, B.-W. Park, and M. Sitti, "Light-driven janus hollow mesoporous TiO2Au microswimmers," *Advanced Functional Materials*, vol. 28, no. 25, p. 1 704 902, 2018.

[69] X. Dong and M. Sitti, "Controlling two-dimensional collective formation and cooperative behavior of magnetic microrobot swarms," *The International Journal of Robotics Research*, vol. 0, no. 0, p. 0 278 364 920 903 107, 2020.

[70] N. Fatès, "Solving the decentralised gathering problem with a reactiondiffusionchemotaxis scheme," *Swarm Intelligence*, vol. 4, no. 2, pp. 91–115, 2010.

[71] N. Fatès and N. Vlassopoulos, "A robust aggregation method for quasi-blind robots in an active environment," in *ICSI 2011*, 2011.

[72] M. Gauci, J. Chen, W. Li, T. J. Dodd, and R. Groß, "Self-organized aggregation without computation," *International Journal of Robotics Research*, vol. 33, no. 8, pp. 1145–1161, 2014.

[73] A. Özdemir, M. Gauci, S. Bonnet, and R. Groß, "Finding consensus without computation," *IEEE Robotics and Automation Letters*, vol. 3, no. 3, pp. 1346–1353, 2018.

[74] A. Özdemir, M. Gauci, A. Kolling, M. D. Hall, and R. Groß, "Spatial coverage without computation," in *2019 IEEE International Conference on Robotics and Automation*, ser. ICRA 2019, In Press, IEEE, 2019, pp. 1346–1353.

[75] J. Derenick, N. Michael, and V. Kumar, "Energy-aware coverage control with docking for robot teams," in *2011 IEEE/RSJ International Conference on Intelligent Robots and Systems*, IEEE, 2011, pp. 3667–3672.

[76] N. Kamra and N. Ayanian, "A mixed integer programming model for timed deliveries in multirobot systems," in *2015 IEEE International Conference on Automation Science and Engineering (CASE)*, IEEE, 2015, pp. 612–617.

[77] G. Notomista and M. Egerstedt, "Persistification of robotic tasks," *IEEE Transactions on Control Systems Technology*, 2020.

[78] P. Tenczar, C. C. Lutz, V. D. Rao, N. Goldenfeld, and G. E. Robinson, "Automated monitoring reveals extreme interindividual variation and plasticity in honeybee foraging activity levels," *Animal Behaviour*, vol. 95, pp. 41–48, 2014.

[79] J. Stenhammar, R. Wittkowski, D. Marenduzzo, and M. E. Cates, "Activity-induced phase separation and self-assembly in mixtures of active and passive particles," *Physical review letters*, vol. 114, no. 1, p. 018 301, 2015.

[80] S. Cannon, J. J. Daymude, D. Randall, and A. W. Richa, "A Markov chain algorithm for compression in self-organizing particle systems," in *Proceedings of the 2016 ACM Symposium on Principles of Distributed Computing*, ser. PODC '16, New York, NY, USA: ACM, 2016, pp. 279–288.

[81] S. Cannon, J. J. Daymude, C. Gökmen, D. Randall, and A. W. Richa, "A local stochastic algorithm for separation in heterogeneous self-organizing particle systems," in *Approximation, Randomization, and Combinatorial Optimization. Algorithms and Techniques (APPROX/RANDOM 2019)*, 2019, 54:1–54:22.

[82] S. Li, B. Dutta, S. Cannon, J. J. Daymude, R. Avinery, E. Aydin, A. W. Richa, D. I. Goldman, and D. Randall, *Programming active cohesive granular matter with mechanically induced phase changes*, 2021. arXiv: 2009.05710 [cond-mat.soft].

[83] N. Metropolis, A. W. Rosenbluth, M. N. Rosenbluth, A. H. Teller, and E. Teller, "Equation of state calculations by fast computing machines," *Journal of Chemical Physics*, vol. 21, pp. 1087–1092, 1953.

[84] S. Jahanshahi, H. Löwen, and B. Ten Hagen, "Brownian motion of a circle swimmer in a harmonic trap," *Physical Review E*, vol. 95, no. 2, p. 022 606, 2017.

[85] A. A. Middleton and N. S. Wingreen, "Collective transport in arrays of small metallic dots," *Physical Review Letters*, vol. 71, no. 19, 3198–? 1993.

[86] D. S. Fisher, "Collective transport in random media: From superconductors to earthquakes," *Physics Reports*, vol. 301, no. 1–3, pp. 113–150, 1998.

[87] O. Feinerman, I. Pinkoviezky, A. Gelblum, E. Fonio, and N. S. Gov, "The physics of cooperative transport in groups of ants," *Nature Physics*, vol. 14, pp. 683–693, 2018.

[88] S. L. Smith, M. Schwager, and D. Rus, "Persistent robotic tasks: Monitoring and sweeping in changing environments," *IEEE Transactions on Robotics*, vol. 28, no. 2, pp. 410–426, 2011.

[89] L. Liu and N. Michael, "Energy-aware aerial vehicle deployment via bipartite graph matching," in *2014 International Conference on Unmanned Aircraft Systems (ICUAS)*, IEEE, 2014, pp. 189–194.

[90] N. Mathew, S. L. Smith, and S. L. Waslander, "Multirobot rendezvous planning for recharging in persistent tasks," *IEEE Transactions on Robotics*, vol. 31, no. 1, pp. 128–142, 2015.

[91] S. Mayya, G. Notomista, D. Shell, S. Hutchinson, and M. Egerstedt, "Non-uniform robot densities in vibration driven swarms using phase separation theory," in *2019 IEEE/RSJ International Conference on Intelligent Robots and Systems (IROS)*, 2019, pp. 4106–4112.

[92] S. Li, R. Batra, D. Brown, H.-D. Chang, N. Ranganathan, C. Hoberman, D. Rus, and H. Lipson, "Particle robotics based on statistical mechanics of loosely coupled components," *Nature*, vol. 567, no. 7748, pp. 361–365, 2019.

[93] B. Yigit, Y. Alapan, and M. Sitti, "Programmable collective behavior in dynamically self-assembled mobile microrobotic swarms," *Advanced Science*, vol. 6, no. 6, p. 1 801 837, 2019.

[94] R. Pordes, D. Petravick, B. Kramer, D. Olson, M. Livny, A. Roy, P. Avery, K. Blackburn, T. Wenaus, F. Würthwein, I. Foster, R. Gardner, M. Wilde, A. Blatecky,

J. McGee, and R. Quick, "The open science grid," in *J. Phys. Conf. Ser.*, ser. 78, vol. 78, 2007, p. 012 057.

[95] I. Sfiligoi, D. C. Bradley, B. Holzman, P. Mhashilkar, S. Padhi, and F. Wurthwein, "The pilot way to grid resources using glideinwms," in *2009 WRI World Congress on Computer Science and Information Engineering*, ser. 2, vol. 2, 2009, pp. 428–432.

[96] A. Okubo, "Dynamical aspects of animal grouping: Swarms, schools, flocks, and herds," *Advances in biophysics*, vol. 22, pp. 1–94, 1986.

[97] M. C. Marchetti, J.-F. Joanny, S. Ramaswamy, T. B. Liverpool, J. Prost, M. Rao, and R. A. Simha, "Hydrodynamics of soft active matter," *Reviews of Modern Physics*, vol. 85, no. 3, p. 1143, 2013.

[98] D. Helbing, "Traffic and related self-driven many-particle systems," *Reviews of modern physics*, vol. 73, no. 4, p. 1067, 2001.

[99] N. C. Darnton, L. Turner, S. Rojevsky, and H. C. Berg, "Dynamics of bacterial swarming," *Biophysical journal*, vol. 98, no. 10, pp. 2082–2090, 2010.

[100] E. Méhes and T. Vicsek, "Collective motion of cells: From experiments to models," *Integrative biology*, vol. 6, no. 9, pp. 831–854, 2014.

[101] A Garcimartín, J. Pastor, L. Ferrer, J. Ramos, C Martín-Gómez, and I Zuriguel, "Flow and clogging of a sheep herd passing through a bottleneck," *Physical Review E*, vol. 91, no. 2, p. 022 808, 2015.

[102] L Giomi, N Hawley-Weld, and L Mahadevan, "Swarming, swirling and stasis in sequestered bristle-bots," *Proceedings of the Royal Society A: Mathematical, Physical and Engineering Sciences*, vol. 469, no. 2151, p. 20 120 637, 2013.

[103] N. Gravish, G. Gold, A. Zangwill, M. A. Goodisman, and D. I. Goldman, "Glass-like dynamics in confined and congested ant traffic," *Soft matter*, vol. 11, no. 33, pp. 6552–6561, 2015.

[104] D. M. Gordon, "The organization of work in social insect colonies," *Nature*, vol. 380, no. 6570, pp. 121–124, 1996.

[105] D Cassill, W. R. Tschinkel, and S. B. Vinson, "Nest complexity, group size and brood rearing in the fire ant, solenopsis invicta," *Insectes Sociaux*, vol. 49, no. 2, pp. 158–163, 2002.

[106] D. Monaenkova, N. Gravish, G. Rodriguez, R. Kutner, M. A. Goodisman, and D. I. Goldman, "Behavioral and mechanical determinants of collective subsurface

nest excavation," *Journal of Experimental Biology*, vol. 218, no. 9, pp. 1295–1305, 2015.

[107] N. Gravish, D. Monaenkova, M. A. Goodisman, and D. I. Goldman, "Climbing, falling, and jamming during ant locomotion in confined environments," *Proceedings of the National Academy of Sciences*, vol. 110, no. 24, pp. 9746–9751, 2013.

[108] V. Linevich, D. Monaenkova, and D. I. Goldman, "Robophysical study of excavation in confined environments," *Artificial Life and Robotics*, vol. 21, no. 4, pp. 460–465, 2016.

[109] D. P. Jouvenaz, G. E. Allen, W. A. Banks, and D. P. Wojcik, "A survey for pathogens of fire ants, solenopsis spp., in the southeastern united states," *The Florida Entomologist*, vol. 60, no. 4, pp. 275–279, 1977.

[110] E. J. Robinson, O. Feinerman, and N. R. Franks, "Flexible task allocation and the organization of work in ants," *Proceedings of the Royal Society B: Biological Sciences*, vol. 276, no. 1677, pp. 4373–4380, 2009.

[111] A. John, A. Schadschneider, D. Chowdhury, and K. Nishinari, "Collective effects in traffic on bi-directional ant trails," *Journal of theoretical biology*, vol. 231, no. 2, pp. 279–285, 2004.

[112] C. R. Reid, M. J. Lutz, S. Powell, A. B. Kao, I. D. Couzin, and S. Garnier, "Army ants dynamically adjust living bridges in response to a cost–benefit trade-off," *Proceedings of the National Academy of Sciences*, vol. 112, no. 49, pp. 15 113–15 118, 2015.

[113] C. Gershenson and D. Helbing, "When slower is faster," *Complexity*, vol. 21, no. 2, pp. 9–15, 2015.

[114] K. Nagel and M. Schreckenberg, "A cellular automaton model for freeway traffic," *Journal de physique I*, vol. 2, no. 12, pp. 2221–2229, 1992.

[115] R Kuhne, "Traffic patterns in unstable traffic flow on freeways. highway capacity and level of service. proceedings of the international symposium on highway capacity, karlsruhe, germany, 24-27 july 1991," 1991.

[116] N. Gravish, M. Garcia, N. Mazouchova, L. Levy, P. B. Umbanhowar, M. A. Goodisman, and D. I. Goldman, "Effects of worker size on the dynamics of fire ant tunnel construction," *Journal of the Royal Society Interface*, vol. 9, no. 77, pp. 3312–3322, 2012.

[117] J. Aguilar, T. Zhang, F. Qian, M. Kingsbury, B. McInroe, N. Mazouchova, C. Li, R. Maladen, C. Gong, M. Travers, *et al.*, "A review on locomotion robophysics:

The study of movement at the intersection of robotics, soft matter and dynamical systems," *Reports on Progress in Physics*, vol. 79, no. 11, p. 110 001, 2016.

[118] J.-A. Meyer, H. L. Roitblat, S. W. Wilson, and S. W. Wilson, *From animals to animats 2: Proceedings of the second international conference on simulation of adaptive behavior*. MIT Press, 1993, vol. 2.

[119] U. Borrmann, L. Wang, A. D. Ames, and M. Egerstedt, "Control barrier certificates for safe swarm behavior," *IFAC-PapersOnLine*, vol. 48, no. 27, pp. 68–73, 2015.

[120] G. S. Redner, M. F. Hagan, and A. Baskaran, "Structure and dynamics of a phase-separating active colloidal fluid," *Physical review letters*, vol. 110, no. 5, p. 055 701, 2013.

[121] P. A. Cundall and O. D. Strack, "A discrete numerical model for granular assemblies," *Geotechnique*, vol. 29, no. 1, pp. 47–65, 1979.

[122] D. Weitzel, B. Bockelman, D. A. Brown, P. Couvares, F. Würthwein, and E. F. Hernandez, "Data access for ligo on the osg," in *Proceedings of the Practice and Experience in Advanced Research Computing 2017 on Sustainability, Success and Impact*, 2017, pp. 1–6.

[123] D. Thain, T. Tannenbaum, and M. Livny, "Distributed computing in practice: The condor experience," *Concurrency and computation: Practice and experience*, vol. 17, no. 2-4, pp. 323–356, 2005.

VITA

Bahnisikha Dutta received her Bachelors degree in Electronics and Communication Engineering from SRM University at Chennai, India in 2013. After that, she joined the Bioengineering Masters program at Georgia Tech in 2014 and graduated in 2016 from the program, following which she enrolled for a PhD in ECE. Her research interests are highly interdisciplinary in nature and she worked in collaboration with a group of diverse faculties from areas of Engineering, Computer Science, Biology and Physics.